J. Mech. Phys. Solids 193 (2024) 105888

Contents lists available at ScienceDirect

Journal of the Mechanics and Physics of Solids

journal homepage: www.elsevier.com/locate/jmps

Nonlinear mechanics of phase-change-induced accretion

Satya Prakash Pradhan [a], Arash Yavari [a,b,*]

[a] School of Civil and Environmental Engineering, Georgia Institute of Technology, Atlanta, GA 30332, USA
[b] The George W. Woodruff School of Mechanical Engineering, Georgia Institute of Technology, Atlanta, GA 30332, USA

ARTICLE INFO

Dedicated to Professor Marcelo Epstein on the occasion of his 80th birthday.

Keywords:
Accretion
Ablation
Surface growth
Nonlinear elasticity
Thermoelasticity
Phase change
Solidification
Stefan's problem

ABSTRACT

In this paper, we formulate a continuum theory of solidification within the context of finite-strain coupled thermoelasticity. We aim to fill a gap in the existing literature, as the existing studies on solidification typically decouple the thermal problem (the classical Stefan's problem) from the elasticity problem, and often limit themselves to linear elasticity with small strains. Treating solidification as an accretion problem, with the growth velocity correlated with the jump in the heat flux across the boundary, it presents an initial boundary-value problem (IBVP) over a domain whose boundary location is a priori unknown. This IBVP is solved numerically for the specific example of radially inward solidification in a spherical container. Several parametric studies are conducted to compare the numerical results with the rigid cases in the literature and gain insights into the role of elastic deformations in solidification.

1. Introduction

Various types of phase changes are observed in our surroundings, ranging from the freezing of seas (Stefan, 1891) and the polymerization of proteins within living cells (Fedosejevs and Schneider, 2022; Jiang et al., 2015) to the ongoing solidification process in the Earth's core (Buffett et al., 1992, 1996, 1993; Labrosse et al., 1997, 2007). In engineering, phase transitions are highly relevant in various contexts, including concrete solidification (Bažant et al., 1997), the shape memory effect observed in polymers and alloys (Zarek et al., 2016; Elahinia et al., 2016), cryopreservation (Mazur, 1970; Coussy, 2005), as well as the applications of phase change materials in thermal energy storage and photonics (Pielichowska and Pielichowski, 2014; Wuttig et al., 2017). Several theoretical studies comprehensively categorize all such phase transition phenomena that are observed in Nature (Landau, 1936; Jaeger, 1998; Binder, 1987; Stanley, 1971). Without going into too much detail, we specify that in this work our focus is on the liquid-to-solid phase transition, which is classified as a first-order phase transition. These transitions are characterized by a finite discontinuity in the first derivative of the free energy with respect to a specific thermodynamic variable. In the case of solidification, this discontinuity manifests as a change in density, which can be heuristically related to the derivative of free energy with respect to pressure. Such transitions involve the release of latent heat while the temperature remains constant. This latent heat release causes a jump in the heat flux across the moving boundary, which is typically known as Stefan's condition.

The term *Stefan's problem* broadly refers to the family of mathematical models describing physical processes involving heat transfer, diffusion, and latent heat, which feature a moving boundary with an *a priori* unknown location. The earliest known work in this field was a study conducted by Lamé and Clapeyron (1831) on the cooling of a half-space filled with a homogeneous liquid at its solidification temperature. They demonstrated that the thickness of the solidified crust is proportional to the square root of time. However, it was when Stefan (1891) published his work on the formation of ice in polar seas that this type of problem caught the

* Corresponding author at: School of Civil and Environmental Engineering, Georgia Institute of Technology, Atlanta, GA 30332, USA.
E-mail address: arash.yavari@ce.gatech.edu (A. Yavari).

https://doi.org/10.1016/j.jmps.2024.105888
Received 18 April 2024; Received in revised form 21 July 2024; Accepted 28 September 2024
Available online 4 October 2024

attention of many researchers, and the field was named after him. The history of what is now known as Stefan's problem has been meticulously compiled in several texts (Rubinšteĭn, 1971; Rubinstein, 1979; Danilyuk, 1985; Vuik, 1993; Visintin, 2008; Gupta, 2017), all of which provide extensive and comprehensive bibliographies on the subject matter. Therefore, we do not attempt to provide a historical survey here.

Over the past century, research on Stefan-type problems has predominantly fallen into the following categories: mathematical modeling of natural and engineering processes involving moving interfaces (Horvay, 1962; Chambre, 1956; Crank and Gupta, 1972), investigations into the existence and uniqueness of solutions (Rubinstein, 1947; Evans et al., 1951; Douglas, 1957; Oleĭnik, 1960), development of efficient numerical techniques for solutions of problems with an unknown moving boundary (Lotkin, 1960; Melamed, 1958; Budak et al., 1965; Fasano and Primicerio, 1979), and generalizations such as extensions to higher dimensions.

Motivation of this study. Solidification plays a vital role in several manufacturing processes that constitute the backbone of modern-day industries, such as traditional casting (Kou, 2015), injection molding (Isayev and Crouthamel, 1984; Yang and Zhiwei, 2009), selective laser sintering (Mercelis and Kruth, 2006), vat photopolymerization (Deore et al., 2021; Bachmann et al., 2021), and ice-templating (Shao et al., 2020). However, within the setting of fully nonlinear and coupled thermoelasticity, there is a scarcity of studies addressing the mathematical modeling of deformations and stresses during the solidification process. Such modeling is important for the design and analysis of manufacturing processes involving solidification, where molten materials cool to ambient temperatures. The substantial temperature drop in this process can result in severe part distortion and the development of high residual stresses. It is equally important to obtain the continuous evolution of thermal stresses and deformations throughout the manufacturing process to assess the potential occurrence of mechanical instabilities and failures (DebRoy et al., 2018). Residual stresses play a vital role, as they dictate how manufactured components respond to external stimuli, including service loads (Withers and Bhadeshia, 2001b). Excessive residual and thermal stresses can give rise to issues such as layer delamination during deposition and the formation of cracks as the part cools down (DebRoy et al., 2018). Moreover, thermal contraction can distort parts made through these processes, affecting their geometric tolerance (Klingbeil et al., 2002). While many methods exist for measuring thermal stresses during fabrication or residual stresses post-fabrication, they typically measure the values at specific locations due to the cost and time constraints (Withers and Bhadeshia, 2001a). Thus, understanding the continuous evolution of thermal stresses and residual stress distribution, whether through numerical or analytical tools (Mukherjee et al., 2017b), is critical for designing manufacturing processes to mitigate geometric inaccuracies, instabilities, and failures (Mukherjee et al., 2017a).

The aim of the present work is to analyze stress and deformation during solidification and their residual effects in a nonlinear thermoelastic framework. As new layers are deposited onto the surface of a solidifying body, it gives rise to an accretion problem. Accretion (or boundary growth (Epstein, 2010)) refers to the growth of a deformable body through the addition of material points on its boundary. Drawing inspiration from Eckart (1948) and Kondo (1949), a natural approach to modeling accreting bodies is to treat them as time-dependent Riemannian manifolds. The Riemannian metric for the new material points depends on the state of deformation at that point during the accretion process. If the source of anelasticity in the problem is time-independent, the metric at each point remains constant after attachment. However, in the case of thermoelastic accretion, this metric is temperature-dependent and therefore evolves with time at each material point. The geometric theory of accretion was initially formulated by Sozio and Yavari (2017) for surface growth in cylindrical and spherical bodies. Several theoretical results related to accretion boundary-value problems were discussed in (Sozio and Yavari, 2019). This theory was later extended by Pradhan and Yavari (2023) to include ablation, which refers to the removal of material points from the boundary. Accretion of circular cylindrical bars under finite extension and torsion has been explored in studies by Yavari et al. (2023) and Yavari and Pradhan (2022). Further, Sozio et al. (2020) formulated a thermoelastic accretion boundary-value problem using the geometric theory of thermoelasticity proposed by Ozakin and Yavari (2010) and Sadik and Yavari (2017a). In their work, Sozio et al. (2020) modeled the effects of heat conduction and thermal expansion in an infinite cylinder and a 2D block undergoing accretion through the addition of hot molten layers. However, the effect of phase transition was not taken into consideration, and the accretion surface velocity was assumed to be externally controlled. In this paper, we model accretion induced by solidification as a Stefan's problem, where the accretion velocity is a priori unknown. We take into account the effects of latent heat released during solidification, and the accretion velocity is related to the heat flux through Stefan's condition.

Existing literature. One of the earliest studies of solidification that focused on mechanical stresses was conducted by Rongved (1954), who examined the residual stresses generated during the quenching of glass spheres. He modeled the viscoelastic behavior of glass similar to that of a Maxwell material with temperature-dependent viscosity and provided an explicit solution for transient thermal stresses in a compressible sphere. Weiner and Boley (1963) studied the one-dimensional growth of an elastic/perfectly-plastic slab that started solidifying as the surface temperature of a molten liquid pool at one end was dropped below the melting point. The liquid melt was assumed to be at a fixed temperature initially. The time evolution and spatial variation of temperature in both phases were considered. They utilized Neumann's solution (Carslaw and Jaeger, 1959, p. 283) for the temperature field and the location of the moving boundary in one-dimensional phase change problems. The slab was assumed to have vanishing stress at the moving interface and was constrained against bending. Their problem was inspired by the early stages of solidification during the metal casting process where temperatures are close to the melting point. Their findings revealed that plastic flow can initiate right from the beginning on both the casting and solidification surfaces. Moreover, they observed that the stresses at the casting surface were compressive.

Chambre (1956) conducted one of the earliest studies on the dynamics of liquid-to-solid phase change, considering the density changes induced during solidification. He considered the convective motion in the fluid near the interface, arising from the large density jumps across it, and modeled it using the incompressible Navier–Stokes equations at constant pressure. Further, he assumed

the solid to be rigid and have infinite thermal conductivity so that it remained at the constant solidification temperature throughout the process. However, in the present work, we neglect inertial effects in both the solid and the liquid phases, while still considering a moderate density change across the solidification interface.

Tien and Koump (1969) studied the thermal stresses developed during the solidification of an elastic beam with a temperature-dependent Young's modulus. Richmond and Tien (1971) considered a nonlinear viscoelastic model with a temperature-dependent Young's modulus and viscosity to study the early stages of solidification inside a rectangular mold with a uniform non-steady surface temperature and pressure. In particular, they computed the stresses and deformations in the solidifying skin for slow cooling processes and calculated the time required for the formation of air gap between the mold and the skin. O'Neill (1983) used a boundary integral element method to study moving boundaries in phase change heat transfer problems. The analysis was limited to problems with a very low Stefan's number, meaning that the heat capacity effects were negligible compared to the latent heat effects. In such cases, the temperature profiles within the individual phases remain relatively constant over time. They investigated the radial freezing around a pipe with a thin initial frozen layer surrounded by the unfrozen liquid initially at the freezing temperature. The temperature history of the surface of the pipe was considered to be known and was assumed to decrease with time. They examined the evolution of the freezing front radius until it became considerably large compared to the pipe radius. They compared their numerical solution with the semi-analytical solution for phase change around an annulus with an infinitesimally small radius. Although the semi-analytical solution considered the transient heat equation in both phases while the numerical solution considered the steady state heat equation only in the frozen state, there was still good agreement between the two. They also studied the radial ablation of a pre-existing frozen layer around the same pipe, melting due to a specified impinging surface flux. Furthermore, they studied radially-asymmetric freezing around a cold pipe passing eccentrically through a drum containing fluid and compared their numerical solution with experimental results. However, they did not consider stresses due to solidification and heat transfer.

Heinlein et al. (1986) investigated solidification stresses generated during 1D solidification of aluminum bars using the boundary element method. An aluminum bar is assumed to be solidifying as it is chilled at one end where the temperature is given as a function of time. The other end of the bar is the moving solidification front, which is exposed to the hydrostatic pressure exerted by the liquid aluminum. They solved the 1D transient heat equation by modifying the boundary integrals prescribed in (O'Neill, 1983). For the elastic analysis, they worked in the setting of small strains and linear elasticity theory. They assumed an additive decomposition of the total strain into elastic, thermal and other non-elastic strains. Zabaras and Mukherjee (1987) analyzed the motion of the phase-change interface in 2D problems. They considered the inward solidification of a liquid melt initially at its melting temperature inside a square cavity whose surface is suddenly cooled down and maintained at a colder temperature. They used the boundary element method to solve the transient heat equation. Zabaras et al. (1990) studied the evolution of deformations and thermal stresses induced during radially inward solidification of a hypoelastic–viscoplastic circular cylinder. They used finite elements that continuously move and deform to analyze boundary-value problems with an evolving domain. They assumed an additive decomposition of the strain rate into elastic and non-elastic components with a hydrostatic state of stress at the solidification interface. Zabaras et al. (1991) examined the residual stresses generated during axially-symmetric solidification of cylinders for different cooling conditions using the same FEM formulation.

Inspired by applications in cryobiology, Rubinsky et al. (1980) and Rabin and Steif (1998) examined the stresses generated during inward freezing of a sphere. The stresses induced due to the freezing of water in a biological material can be a source of damage in an organ. Rubinsky et al. (1980) considered a homogeneous spherical organ, initially near its freezing temperature, which is frozen by the application of a constant cooling rate on its outer surface. They modeled ice as a perfectly elastic medium and computed the temperature and stress distributions. Rabin and Steif (1998) considered an inviscid liquid initially at its solidification temperature occupying a spherical domain whose outer surface is subsequently cooled and forcibly maintained at a fixed temperature. They regarded the frozen portion as an elastic/perfectly-plastic material, and conducted parametric studies to examine the mechanical stresses within the solid and the hydrostatic pressure within the fluid as the freezing front advances. They showed that in materials with physical properties resembling water, the stresses arising from thermal expansion in the solid state were notably lower in comparison to the stresses resulting from volumetric expansion during phase transition. They demonstrated that following the completion of the freezing process, a substantial portion of the frozen region is occupied by a plastic zone. They concluded that the potential for tissue destruction was inevitable, regardless of the speed at which the freezing process was conducted, as long as there was a substantial expansion associated with phase transition.

Chan and Tan (2006) conducted experiments to study the solidification of *n*−hexadecane inside a sphere by keeping the surface temperature constant. They observed that the solidification front starts to propagate inward in a spherically-symmetric fashion. Later, the phase-change interface loses its spherical symmetry and develops some irregularity/eccentricity as the shrinkage in the solidified material causes the formation of voids. The rate of solidification is very high initially and reduces subsequently. However, they did not consider stresses generated during the process. Numerous studies have explored the inward solidification of a spherical liquid domain initially at its freezing temperature (Pedroso and Domoto, 1973a; Riley et al., 1974; Stewartson and Waechter, 1976; Soward, 1980). However, their main focus was to improve the approximation of the temperature profile as the phase change interface neared the center of the sphere. Another example of such a study is the asymptotic analysis conducted by McCue et al. (2003) who investigated the 2D inward solidification of a melt within a rectangular domain at its fusion temperature. For a large Stefan's number, they computed the time required for complete solidification and observed that the phase change interface forms an exact ellipse as it approaches the center. In none of these studies, mechanical stresses were taken into account in their analyses. Pedroso and Domoto (1973b) studied the stresses generated during the inward solidification of spheres. The state of stress at the freezing front was assumed to be hydrostatic, determined by the corresponding pressure in the fluid, and the stress inside the solid was modeled using linear isotropic thermoelasticity equations. They showed that the solid is residually stressed after the inner liquid pressure

and outer tractions were removed. They also investigated the effects of different liquid compressibility, freezing temperature, and liquid pressure.

Abeyaratne and Knowles (1993) investigated solid–solid phase transitions in a one-dimensional domain by deriving a kinetic relation for the motion of the phase-change interface that allowed them to be influenced by local stress states. This kinetic equation related the interface velocity to the thermodynamic driving force using the second law of thermodynamics. They also analyzed the onset of thermally or mechanically induced phase transitions in thermoelastic solids via a nucleation criterion. Hodge and Papadopoulos (2010) considered the configurations of an accreting body at discrete instances of time and analyzed the deformation map between these instances. This map was decomposed multiplicatively into elastic and anelastic parts for each incremental step, and the theory was applied to study deformations in 1D examples. They also mentioned the idea of an evolving reference configuration, though their theory treated this evolution to be discrete in time. This idea was separately formulated in a much more general setting by Yavari (2010) in the context of bulk growth, modeling the reference configuration as a Riemannian manifold with a time-dependent metric.

Tomassetti et al. (2016) studied accretion–ablation induced by diffusion. They considered a thick permeable spherical shell that has grown on the surface of a rigid spherical substrate. The spherical shell is surrounded by a fluid medium with free particles that diffuse into the permeable shell to reach the surface of the spherical substrate where they polymerize and attach to the spherical shell. As this accretion occurs at the fixed inner boundary some of the particles on the outer boundary are ablated out into the fluid medium. Accretion and ablation are governed by the following factors: strain energy of the solid shell, external mechanical power, and the difference in chemical potential of the particles when they are free as compared to when they are attached to the solid shell. The driving force—a measure of deviation from thermodynamic equilibrium—is assumed to have a linear relationship with the flux of particles at the accretion–ablation boundaries. The accretion–ablation rates are thermodynamically determined in terms of the chemical potential of the particles and strain energy density of the shell. They studied accretion–ablation in a treadmilling regime and simply considered the steady state solution of the diffusion equation. A more general analysis would take into account the time-evolution of particle flux and stresses in the solid due to transient diffusion.

Inspired by Brown and Goodman (1963), Zurlo and Truskinovsky (2017) studied accretion by analyzing the incremental deformation and stress and their accumulation over time. The deformation increment is the velocity of a point integrated over time, and the Cauchy stress increment is the stress rate of the point integrated over time. The balance of linear momentum in this incremental theory requires the time derivative of the Cauchy stress to be divergence-free in the absence of body forces. They studied accretion in hollow cylindrical tubes manufactured by winding infinitesimally thin layers under extremely small tangential loads and analyzed the conditions under which a single cut renders a residually-stressed tube stress-free. Further, Zurlo and Truskinovsky (2018) calculated growth-induced inelastic strain in 1D examples, such as a growing bar attached to a Winkler foundation. The formulation of Zurlo and Truskinovsky (2017, 2018) was based on linear elasticity, which was subsequently generalized to finite deformations in (Truskinovsky and Zurlo, 2019). Truskinovsky and Zurlo (2019) studied stress distributions in various examples of radial accretion. These included a hollow sphere where the outer growth surface is exposed to controlled pressure, and the cases of outward and inward accretion through a rigid spherical surface. They also modeled 2D disks manufactured by winding infinitesimally-thin layers through accretion, and illustrated the 3D shapes that alleviate the residual stresses in such structures.

Ganghoffer and Goda (2018) studied accretion in the framework of irreversible thermodynamics and configurational forces. They distinguished between accretion and surface growth: simple material deposition on a boundary is referred to as pure accretion, while pure surface growth involves isolated growth on a particular surface, where material points in the layer are not conserved as the layer regenerates within itself, causing incompatibility with other layers. They identified the driving forces incorporating mechanical, chemical, and thermal effects for both accretion and surface growth phenomena. Inspired by fluid-structure interactions, Naghibzadeh et al. (2021) studied accretion in a Eulerian framework, bypassing the explicit identification of a reference configuration. They worked with an evolution equation for the elastic part of the deformation gradient (i.e., $\overset{e}{\mathbf{F}}$ in $\mathbf{F} = \overset{e}{\mathbf{F}}\overset{a}{\mathbf{F}}$), which was their sole kinematic descriptor besides the velocity field. However, $\overset{a}{\mathbf{F}}$ was assumed to be constant over time for a given particle. Later, in (Naghibzadeh et al., 2022), they recovered several results of Sozio and Yavari (2017) and extended their theory to include ablation.

Abeyaratne et al. (2022a) studied the stability of a pre-stressed elastic half space accreting due to steady-state diffusion of free particles from the other half space. They reported that such surface growth of a half space with surface tension is not always stable if the accretion interface is traction-free. Abeyaratne et al. (2022b) examined the stability of a similar prestressed elastic half space accreting by diffusion, while the other half space containing the free particles is assumed to be compliant and provide some resistance to growth.

Fekry (2023) examined the evolution of stresses in a thermoviscoelastic cylinder manufactured via the process of selective laser melting. He modeled the process of additive manufacturing as the accretion of discrete layers on the cylindrical boundary. Furthermore, Lychev and Fekry (2023a,b) studied the evolution of temperature and stress, as well as residual stresses and distortions in a thermoelastic cylindrical bar manufactured by lateral sintering. In the context of small strains and temperature gradients, they formulated discrete accretion as a recursive problem in terms of strain and stress increments. However, the effects of latent heat during solidification was not considered in these works.

Rejovitzky et al. (2015) formulated a continuum theory to study the stresses generated during the deposition of solid electrolyte interphase layers, which play a significant role in the degradation of Li-ion batteries. Based on the experimental results of Smith et al. (2011), they assumed the thickness of the accumulated layer to be proportional to the square root of time, thus avoiding the complexity of obtaining it through the use of the diffusion equation and reaction kinetics. They modeled the electrolyte as a linear elastic material with a small Young's modulus and vanishing Poisson's ratio. The state of the attaching layers at the time

of deposition was considered as the stress-free reference configuration for the points within it. The deformation gradient of the attaching layer, relative to this configuration, was then decomposed multiplicatively into growth and elastic parts, with the growth part corresponding to the inelastic deformation induced within each layer during attachment. They demonstrated the capability of their formulation by simulating the evolution of Cauchy stress in the deposited layers during charging and discharging cycles on deformable spheroidal anodes.

Polymerization is an example where phase transformation occurs as the result of an exothermic reaction converting a partially cured gel to fully cured polymer. Kumar et al. (2021) provided analytical estimates for the velocity of the reaction front propagating steadily in a 1D adiabatic domain. Kumar et al. (2022) studied the evolution of mechanical stresses and large deformations that are induced due to phase transformation by polymerization. Their thermo-chemo-mechanical model involves a coupled system of the following equations: the balance of linear momentum, the transient heat equation and the reaction kinetics, where the unknowns are the deformation field, the temperature field, and the degree of cure. The reaction kinetics are assumed to be unaffected by mechanical deformations based on experimental observations. Since the polymerization reaction is extremely exothermic and fast, no mechanical effects on the reaction kinetics were observed. However, a clear thermo-mechanical coupling is evident in their formulation. They considered the example of a 2D adiabatic domain and observed that the reaction interface travels at an almost constant speed. Li and Cohen (2024) examined the propagation of reaction fronts in the process of polymerization, where a minimal energy input transforms monomers at a soft gel-like state to a stiffer solid polymer. They used the same polymer as Kumar et al. (2022), but cured to a higher degree in its initial state, making the front speed more sensitive to deformations and heat loss. In a slender one-dimensional body under axial load, they studied the influence of mechanical properties on the propagation of the reaction front, considering the effects of thermal expansion and density changes resulting from the reaction. Using both experimental and theoretical analyses, they demonstrated that the propagation of the reaction front can be quenched by the application of mechanical loads, establishing a clear thermo-mechanical coupling. In particular, they observed that below a critical applied load, the reaction front moves at an almost constant speed, but slows down abruptly above this critical load.

Problem overview. In this paper, we consider the solid and liquid phases as homogeneous, isotropic, compressible, hyperelastic materials that are rigid heat conductors. We neglect the inertial effects in both phases. Additionally, we do not account for the influence of pressure on the phase change temperature. To be specific, our study focuses on the inward solidification of a liquid inclusion initially at its solidification temperature, trapped within a deformable solid body that is being externally cooled, with both phases composed of the same material. For such problems, we calculate the evolution of deformation, stresses, and temperature field inside the solid, as well as the location of the phase change front as it progresses inward. We consider the solidification process until the radius of the inclusion reaches a certain small value. This is because surface stresses are known to dominate when the inclusion size decreases beyond a certain limit (Bico et al., 2018). Since surface stresses have not been considered in this work, the numerical solutions corresponding to very small liquid inclusions would be physically irrelevant. Furthermore, in materials where the liquid phase is denser than the solid phase near the melting point, the pressure in the liquid inclusion induced by compressive stresses significantly increases as the phase change front approaches the center of the sphere. Therefore, the accretion process is terminated with a certain time margin prior to achieving full solidification. Finally, the resulting body is detached from the rigid container, drained of any remaining liquid, and then cooled to an ambient temperature. The residual stresses and distortions are subsequently computed for this configuration.

This paper is organized as follows. First, the general theory of thermoelastic accretion is described in Section 2. The balance laws—including the conservation of mass, linear and angular momenta, the heat equation, and Stefan's condition—are discussed in Section 3. In Section 4, radially inward solidification in a cold rigid container is modeled as a thermoelastic accretion problem with an unknown accretion velocity, and the numerical results for the corresponding non-dimensionalized moving boundary-value problem are discussed in detail. Conclusions are given in Section 5

2. Thermoelastic accretion induced by phase change

This section provides a concise overview of nonlinear thermoelasticity, the mechanics of accretion and the application of Stefan's condition in solidification problems. For a thorough analysis of geometric thermoelasticity, see (Ozakin and Yavari, 2010; Sadik and Yavari, 2017a). In-depth insights into accretion mechanics are available in (Sozio and Yavari, 2019). For a comprehensive understanding of the Stefan's problem the reader is referred to the texts by Rubinšteĭn (1971) and Gupta (2017).

Consider the phase transition of a finite quantity of liquid undergoing cooling and solidification, either within a rigid container or as an inclusion within a deformable solid. As the liquid solidifies and attaches to the surface of the container or the deformable solid, the solid grows via accretion. In other words, the solid undergoes accretion and the adjacent liquid undergoes ablation, while the set of material points in the solid–liquid system as a whole remains conserved.

Let $\mathcal{S}$ denote the three-dimensional ambient Euclidean space, with $\mathbf{g}$ representing its standard flat metric.[1] Both the solid and liquid phases assume their respective deformed configurations endowed with this ambient Euclidean metric. Those parts of the

[1] $\mathbf{g}$ is a symmetric second-order tensor field on $\mathcal{S}$. An explicit representation of $\mathbf{g}$ depends on the local coordinate chart. At a point $x \in \mathcal{S}$, and in a local chart $\{x^a\}$, $\{\frac{\partial}{\partial x^a}\}$ is a coordinate basis for the tangent space $T_x\mathcal{S}$. The corresponding basis for the cotangent space $T_x^*\mathcal{S}$ is $\{dx^a\}$. With respect to this coordinate chart, the metric has the following representation: $\mathbf{g} = g_{ab}\, dx^a \otimes dx^b$. This representation is independent of whether the metric is flat. If a Cartesian coordinate system is chosen for the ambient space, then $\mathbf{g} = \delta_{ab}\, dx^a \otimes dx^b = dx^1 \otimes dx^1 + dx^2 \otimes dx^2 + dx^3 \otimes dx^3$. As another example, if cylindrical coordinates $\{r, \theta, z\}$ are considered, then $\mathbf{g} = dr \otimes dr + r^2\, d\theta \otimes d\theta + dz \otimes dz$.

solid–liquid (pair) composite body which remain unaffected by phase transformation are equipped with a temperature-dependent metric, which is flat at the initial temperature. The individual reference configurations of the solid and liquid phases evolve as material points are transferred from one phase to the other. The material metric for an accreting layer is a priori an unknown field and is determined by its temperature and state of deformation at the time of attachment.

2.1. The solidifying body

Consider a solid body $\mathcal{B}_0$ with a liquid inclusion $\mathcal{L}_0$, both initially stress-free.[2] The initial solid–liquid body $\mathcal{Z} = \mathcal{B}_0 \cup \mathcal{L}_0$ inherits a flat metric from the ambient Euclidean space. Assume that solidification (accretion) begins at $t = 0$. Let $\mathcal{M} \supset \mathcal{Z}$ denote the ambient material space, which is any connected and orientable three-dimensional manifold embeddable in $\mathbb{R}^3$ that includes $\mathcal{Z}$. Let the map $\tau : \mathcal{L}_0 \to [0, \infty)$ assign a time of solidification (attachment) to every fluid point. The accreting solid and the ablating fluid are identified with their respective time-dependent material manifolds $\mathcal{B}_t$ and $\mathcal{L}_t$ (Fig. 1).[3] They are defined as follows

$$\mathcal{B}_t = \mathcal{B}_0 \cup \tau^{-1}[0,t], \qquad \mathcal{L}_t = \mathcal{L}_0 \setminus \tau^{-1}[0,t). \tag{2.1}$$

Note that $\mathcal{B}_t \sqcup \mathcal{L}_t = \mathcal{B}_0 \sqcup \mathcal{L}_0$, although $(\mathcal{B}_t, \mathcal{L}_t) \neq (\mathcal{B}_0, \mathcal{L}_0)$. It is assumed that the differential $\mathrm{d}\tau$ never vanishes, i.e., at any moment during the solidification process, a smooth surface is being solidified. Let $\Omega_t \subset \partial\mathcal{B}_t$ be the accretion surface where the solidifying material is about to attach. The level sets $\Omega_t = \tau^{-1}(t)$ are assumed to be 2−manifolds, which are diffeomorphic to each other for all $t \geq 0$. This assumption ensures the existence of a material motion $\Phi : \Omega_0 \times [0, t_e] \to \mathcal{M}$, which is a diffeomorphism such that $\Phi(\Omega_0, t) = \Omega_t$, where t_e is the time at which solidification ends. The assumption $d\tau \neq 0$ implies that the solidified body is a union of smooth surfaces. Each surface has a unique time of attachment and that implies existence of a diffeomorphism Φ. The deformation map $\varphi_t : \mathcal{Z} \to \mathcal{S}$ is assumed to be a homeomorphism for each t, with the restrictions $\varphi_t|_{\mathcal{B}_t}$ and $\varphi_t|_{\mathcal{L}_t}$ being C^1 on the respective solid and liquid domains.

2.2. Kinematics of accretion

The kinematic quantities described in this subsection are specialized for the accreting domain (i.e., the solid portion $\mathcal{B}_t$ in this case) but are identical for the ablating domain (i.e., the liquid portion $\mathcal{L}_t$ in this case). The only difference is that for the ablating domain, the initial material metric is known; it is the flat Euclidean metric. In the case of melting, the liquid domain would be accreting, and the formalism presented in this subsection would directly apply to the liquid.

For an accreting solid, the deformation map $\varphi_t : \mathcal{B}_t \to \mathcal{S}$ is a C^1 homeomorphism for each t. The so-called deformation gradient $\mathbf{F}_t = T\varphi_t$ ($T\varphi_t$ is the derivative of the deformation mapping (Marsden and Hughes, 1983), and sometimes the notation $d\varphi_t$ is used instead) is a two-point tensor $\mathbf{F}_t : T_X\mathcal{B}_t \to T_x\mathcal{C}_t$, where $x = \varphi_t(X)$ and $\mathcal{C}_t = \varphi_t(\mathcal{B}_t)$.[4] The material and spatial velocity fields are defined as $\mathbf{V}(X,t) = \frac{\partial}{\partial t}\varphi(X,t)$ and $\mathbf{v}_t = \mathbf{V}_t \circ \varphi_t^{-1}$, respectively. More specifically, the material and spatial velocities of the solid and fluid particles are defined as

$$\mathbf{V}^{\mathrm{s}}(X,t) = \frac{\partial}{\partial t}\varphi^{\mathrm{s}}(X,t), \quad \mathbf{v}^{\mathrm{s}}_t = \mathbf{V}^{\mathrm{s}}_t \circ (\varphi^{\mathrm{s}}_t)^{-1}, \qquad \mathbf{V}^{\mathrm{f}}(X,t) = \frac{\partial}{\partial t}\varphi^{\mathrm{f}}(X,t), \quad \mathbf{v}^{\mathrm{f}}_t = \mathbf{V}^{\mathrm{f}}_t \circ (\varphi^{\mathrm{f}}_t)^{-1}, \tag{2.3}$$

where $\varphi^{\mathrm{s}} = \varphi|_{\mathcal{B}_t}$ and $\varphi^{\mathrm{f}} = \varphi|_{\mathcal{L}_t}$. Note that the deformation gradient $\mathbf{F}_t$ and the spatial velocity $\mathbf{v}_t$, defined separately for the liquid and for the solid, are not necessarily continuous across the solidification interface. Similarly, the material and spatial acceleration fields are defined as $\mathbf{A}(X,t) = \frac{\partial}{\partial t}\mathbf{V}(X,t)$ and $\mathbf{A}_t = \mathbf{a}_t \circ \varphi_t^{-1}$, respectively.[5]

The map $\bar{\varphi}(X) = \varphi(X, \tau(X))$ records the placement of X at its time of attachment. In general, $\bar{\varphi} : \mathcal{L}_0 \to \mathcal{S}$ is not injective. Moreover, the *frozen deformation gradient* $\bar{\mathbf{F}}(X) = \mathbf{F}_{\tau(X)}(X)$, which captures the deformation gradient at the time of attachment, is not the tangent of an embedding, in general. Even when $\bar{\varphi}$ is an embedding, $T\bar{\varphi}$ is not equal to $\bar{\mathbf{F}}$. In fact $T\bar{\varphi} = \bar{\mathbf{F}} + \bar{\mathbf{V}} \otimes d\tau$ (Sozio and Yavari, 2019). While $\bar{\mathbf{F}}$ is compatible within each individual layer Ω_t,[6] it is incompatible, in general. The incompatibility of $\bar{\mathbf{F}}$ (and more precisely of the accretion tensor $\mathbf{Q}$ that explicitly depends on $\bar{\mathbf{F}}$) is the fundamental reason behind the existence of local anelastic distortions in accreting bodies, and hence the presence of residual stresses.

---

[2] The effect of gravity is neglected, and hence, there is no pressure caused by the self-weight of the liquid.

[3] It should be emphasized that working with only a single attachment map implies that we are not considering ablation (melting).

[4] Let $\{X^A\}$ and $\{x^a\}$ be local coordinate charts on $\mathcal{B}_t$ and $\mathcal{C}_t \subset \mathcal{S}$, respectively. The deformation gradient is represented as

$$\mathbf{F} = \frac{\partial \varphi^a}{\partial X^A}\frac{\partial}{\partial x^a} \otimes dX^A. \tag{2.2}$$

We use the flexible notations $\varphi_t(X) = \varphi(X,t)$ and $\mathbf{F}_t(X) = \mathbf{F}(X,t)$. Note that $\left\{\frac{\partial}{\partial x^a}\right\}$ and $\{dX^A\}$ form the bases for $T_x\mathcal{C}_t$ and $T^*_X\mathcal{B}_t$, respectively. It should be emphasized that the term "deformation gradient" is misleading as $\mathbf{F}$ is not a gradient as it is metric independent. However, this term is commonly used in the literature, and we have chosen to use it in this paper as well.

[5] In components, $A^a = \frac{\partial V^a}{\partial t} + \gamma^a{}_{bc}V^bV^c$ and $a^a = \frac{\partial v^a}{\partial t} + \frac{\partial v^a}{\partial x^b}v^b + \gamma^a{}_{bc}v^bv^c$. Here, $\gamma^a{}_{bc}$ denote the Christoffel symbols for the Levi-Civita connection $\nabla^{\mathbf{g}}$, i.e., $\nabla^{\mathbf{g}}_{\frac{\partial}{\partial x^b}}\frac{\partial}{\partial x^c} = \gamma^a{}_{bc}\frac{\partial}{\partial x^a}$. Similarly, the Christoffel symbols of $\nabla^{\mathbf{G}}$ are denoted as $\Gamma^A{}_{BC}$, i.e., $\nabla^{\mathbf{G}}_{\frac{\partial}{\partial X^B}}\frac{\partial}{\partial X^C} = \Gamma^A{}_{BC}\frac{\partial}{\partial X^A}$.

[6] Recall that each layer Ω_t is a smooth surface.

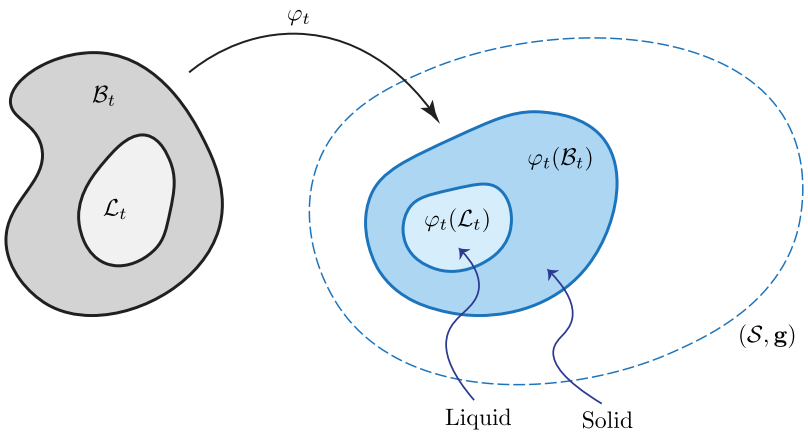

Fig. 1. Motion of an elastic solid with a liquid inclusion.

Let $\omega_t = \varphi_t(\Omega_t)$ denote the accretion surface in the deformed configuration. The growth (accretion) velocity $\mathbf{u}_t$ is a vector field that describes the velocity at which new material is being added onto ω_t, i.e., $-\mathbf{u}_t$ is the velocity of accreting particles relative to ω_t just before attachment.[7] The material growth velocity, denoted as $\mathbf{U}_t$, is a vector field that characterizes the time evolution of the layers Ω_t within the material ambient space. The vector field $\mathbf{U}_t$ is not uniquely determined and can be selected from an equivalence class of material growth velocities that correspond to isometric material manifolds. Let $\mathbf{w}_t$ and $\mathbf{W}_t$ be the spatial and referential depictions of the total velocity of the accretion surface ω_t, i.e., $\mathbf{W}_t \circ \varphi_t = \mathbf{w}_t$. It can be shown that $\mathbf{W}_t = \bar{\mathbf{F}}\mathbf{U}_t + \mathbf{V}_t$, where the term $\bar{\mathbf{F}}\mathbf{U}_t$ accounts for the influence of accretion.

The accretion-induced anelasticity is modeled by the accretion tensor $\mathbf{Q}$, which is a time-independent two-point tensor, defined as

$$\mathbf{Q}(X) = \bar{\mathbf{F}}(X) + \left[\mathbf{u}_{\tau(X)}(\bar{\varphi}(X)) - \bar{\mathbf{F}}(X)\mathbf{U}_{\tau(X)}(X)\right] \otimes \mathrm{d}\tau(X), \qquad X \in \mathcal{L}_0\,. \tag{2.4}$$

Since $\langle d\tau, \mathbf{U}\rangle = 1$, it follows that $\mathbf{QU} = \mathbf{u}$. Although the accretion tensor $\mathbf{Q}$ is compatible within each individual layer, it is not the tangent map of any embedding. For more details, see Sozio and Yavari (2019).

Remark 2.1. Let us consider a foliation chart[8] $\{\Xi^1, \Xi^2, \tau\}$ induced by the time of attachment map τ in the ambient material manifold $\mathcal{M}$ and a local chart $\{x^1, x^2, x^3\}$ in the ambient Euclidean manifold $\mathcal{S}$. The accretion tensor has the following representation with respect to the frames $\left\{\frac{\partial}{\partial \Xi^1}, \frac{\partial}{\partial \Xi^2}, \frac{\partial}{\partial \tau}\right\}$ and $\left\{\frac{\partial}{\partial x^1}, \frac{\partial}{\partial x^2}, \frac{\partial}{\partial x^3}\right\}$ (Sozio and Yavari, 2019)

$$\left[Q^i{}_J\right] = \begin{bmatrix} \frac{\partial \bar{\varphi}^1}{\partial \Xi^1} & \frac{\partial \bar{\varphi}^1}{\partial \Xi^2} & u^1_\tau \circ \bar{\varphi} \\ \frac{\partial \bar{\varphi}^2}{\partial \Xi^1} & \frac{\partial \bar{\varphi}^2}{\partial \Xi^2} & u^2_\tau \circ \bar{\varphi} \\ \frac{\partial \bar{\varphi}^3}{\partial \Xi^1} & \frac{\partial \bar{\varphi}^3}{\partial \Xi^2} & u^3_\tau \circ \bar{\varphi} \end{bmatrix}. \tag{2.5}$$

2.3. Material metric for thermoelastic accretion

Consider a time-dependent material manifold $(\mathcal{B}_t, \mathbf{G})$, where the metric $\mathbf{G}$ measures distances corresponding to the relaxed state, taking into account the thermal history of the body. In geometric thermoelasticity, the metric $\mathbf{G}$ is a function of temperature $T(X,t)$, and is given as (Sadik and Yavari, 2017a; Sozio et al., 2020)

$$\mathbf{G}(X,T) = e^{\boldsymbol{\omega}^\star(X,T)}\mathbf{G}_0(X)\, e^{\boldsymbol{\omega}(X,T)}\,, \tag{2.6}$$

[7] For an observer in the solid phase, solidification is an accretion process. A liquid particle that is about to solidify has velocity $-\mathbf{u}_t$ relative to the solidification surface ω_t. This implies that $-\mathbf{u}_t = \mathbf{v}^{\mathrm{f}}_t\big|_{\omega_t} - \mathbf{w}$, and hence $\mathbf{u}_t = \mathbf{w}_t - \mathbf{v}^{\mathrm{f}}_t\big|_{\omega_t}$, where $\mathbf{w}_t$ is the velocity of the solidification surface. Note that $\mathbf{W}_t(X) = \mathbf{F}^{\mathrm{s}}(X, \tau(X))\mathbf{U}_t(X) + \mathbf{V}^{\mathrm{s}}_t(X)$, and hence, $\mathbf{w}_t = \bar{\mathbf{F}}\mathbf{U}_t \circ \varphi_t + \mathbf{v}^{\mathrm{s}}_t$. Thus, $\mathbf{u}_t = \bar{\mathbf{F}}\mathbf{U}_t \circ \varphi_t + \mathbf{v}^{\mathrm{s}}_t\big|_{\omega_t} - \mathbf{v}^{\mathrm{f}}_t\big|_{\omega_t}$.

[8] Let $\mathcal{M}$ be a 3-dimensional manifold. A 2-foliation, or a foliation of codimension 1, is an atlas of charts $(\mathcal{U}_a, \Xi_a)$ where a belongs to some index set $\mathcal{I}$, such that $\Xi_a(\mathcal{U}_a) = V_a \times I_a$ with $V_a \subset \mathbb{R}^2$ and $I_a \subset \mathbb{R}$ being open sets. The charts Ξ_a are referred to as foliation charts. Under this condition, $\mathcal{M}$ is partitioned into a collection $\{\Omega_t\}_{t\in\mathbb{R}}$ of embedded submanifolds of dimension 2, known as the leaves of the foliation (Camacho and Neto, 2013).

where $\boldsymbol{\omega}$ is a $\binom{1}{1}$-tensor characterizing thermal expansion properties in the solid and $\mathbf{G}_0$ is a temperature-independent metric.[9] The volumetric coefficient of thermal expansion $\beta(X,T)$ is given by

$$\beta(X,T) = \frac{\partial}{\partial T}\,\mathrm{tr}\,\boldsymbol{\omega}(X,T)\,. \tag{2.9}$$

For a time-independent reference temperature field $T_0(X)$, it is assumed that $\boldsymbol{\omega}\big(X,T_0(X)\big)=\mathbf{0}$, and hence $\mathbf{G}\big(X,T_0(X)\big)=\mathbf{G}_0(X)$. In the thermally accreted part of the body, $T_0(X)$ is assumed to be the temperature of the attached material at its time of attachment. However, in the initial body $\mathcal{B}_0$, $T_0(X)$ represents the initial temperature. The material metric $\mathbf{G}\big(X,T_0(X)\big)$ for the accreted portion is calculated by pulling back the Euclidean ambient metric $\mathbf{g}$ via the accretion tensor $\mathbf{Q}$:

$$\mathbf{G}\big(X,T_0(X)\big) = \mathbf{Q}^{\star}(X)\,\mathbf{g}\big(\bar{\varphi}(X)\big)\mathbf{Q}(X)\,. \tag{2.10}$$

The temperature-dependent material metric is therefore given by

$$\mathbf{G}(X,T) = e^{\boldsymbol{\omega}^{\star}(X,T)}\mathbf{Q}^{\star}(X)\,\mathbf{g}\big(\bar{\varphi}(X)\big)\mathbf{Q}(X)e^{\boldsymbol{\omega}(X,T)}\,. \tag{2.11}$$

Let $\mathrm{d}v$ and $\mathrm{d}V$ denote the spatial and material volume elements, respectively. They are related via the Jacobian as $\mathrm{d}v = J\,\mathrm{d}V$, where

$$J = \sqrt{\frac{\det\mathbf{g}}{\det\mathbf{G}}}\,\det\mathbf{F} = \sqrt{\frac{\det\mathbf{g}}{\det\mathbf{g}\circ\bar{\varphi}}}\,\frac{\det\mathbf{F}}{\det\mathbf{Q}}\,e^{-\mathrm{tr}\,\boldsymbol{\omega}}\,. \tag{2.12}$$

Remark 2.2. For a thermally isotropic and homogeneous body, (2.6) is simplified as

$$\mathbf{G}(X,T) = e^{2\omega(T)}\mathbf{G}_0(X)\,, \tag{2.13}$$

where the scalar $\omega(T)$ is related to the coefficient of thermal expansion $\alpha(T)$ as

$$\omega(T(X)) = \int_{T_0(X)}^{T(X)} \alpha(\eta)\,\mathrm{d}\eta\,. \tag{2.14}$$

The volumetric coefficient of thermal expansion in dimension three is $\beta = 3\alpha$.

Remark 2.3. Let $\mathbf{n}_\tau$ and $\mathbf{N}_\tau$ denote the unit normals to ω_τ and Ω_τ, with respect to the metrics $\mathbf{g}$ and $\mathbf{G}$, respectively. The growth (accretion) velocities in the deformed and material configurations can be decomposed as follows

$$\mathbf{u} = \mathbf{u}^{\parallel} + \mathbf{u}^{\perp} = \mathbf{u}^{\parallel} + u^n\,\mathbf{n}\,, \qquad \mathbf{U} = \mathbf{U}^{\parallel} + \mathbf{U}^{\perp} = \mathbf{U}^{\parallel} + U^N\,\mathbf{N}\,, \tag{2.15}$$

where $\langle\!\langle \mathbf{u}^{\parallel},\mathbf{n}\rangle\!\rangle_{\mathbf{g}} = \langle\!\langle \mathbf{U}^{\parallel},\mathbf{N}\rangle\!\rangle_{\mathbf{G}} = 0$. Moreover, $\mathbf{Q}\mathbf{U}^{\parallel} = \mathbf{u}^{\parallel}$, $\mathbf{Q}\mathbf{N} = \mathbf{n}$ and $U^N = u^n\circ\varphi > 0$ (Sozio and Yavari, 2019).

3. Balance laws

The balance laws for the solid and liquid domains are presented here in a generic manner, without any distinction between the phases.

3.1. Conservation of mass

Let the material and spatial mass densities be denoted by $\rho(X,t)$ and $\varrho(x,t)$, respectively. Let $\rho_0(X)$ represent the material mass density corresponding to the metric $\mathbf{G}_0$. The mass of a sub-body $\mathcal{U}\subset\mathcal{P}_t$ is calculated as

$$\int_{\varphi_t(\mathcal{U})} \varrho\,\mathrm{d}v = \int_{\mathcal{U}} \rho\,\mathrm{d}V = \int_{\mathcal{U}} \rho_0 \mathrm{d}V_0\,, \tag{3.1}$$

where $\mathrm{d}V_0$ is the volume element corresponding to the stress-free material metric, and is related to $\mathrm{d}V$ as $\mathrm{d}V = \sqrt{\frac{\det\mathbf{G}}{\det\mathbf{G}_0}}\,\mathrm{d}V_0$. The mass densities are related as $J\varrho = \rho$ and $\rho_0\sqrt{\det\mathbf{G}_0} = \rho\sqrt{\det\mathbf{G}}$, i.e.,

$$J(X,t)\,\varrho\big(\varphi(X,t),t\big) = \rho(X,t) = e^{-\mathrm{tr}\,\boldsymbol{\omega}(X,T(X,t))}\rho_0(X)\,. \tag{3.2}$$

[9] The adjoint of deformation gradient $\mathbf{F}^{\star}(X,t) : T^*_{x}C_t \to T^*_{X}\mathcal{B}_t$ is defined such that

$$\langle\boldsymbol{\alpha},\mathbf{F}\mathbf{W}\rangle = \langle\mathbf{F}^{\star}\boldsymbol{\alpha},\mathbf{W}\rangle\,,\quad \forall\,\mathbf{W}\in T_X\mathcal{B}_t\,,\ \boldsymbol{\alpha}\in T^*_xC_t\,, \tag{2.7}$$

where $\langle\,.\,,.\,\rangle$ is the natural paring of 1-forms in $T^*_xC_t$ with vectors in T_xC_t, i.e., $\langle\boldsymbol{\alpha},\mathbf{w}\rangle = \alpha_a\,u^a$. $\mathbf{F}^{\star}$ is a $\binom{1}{1}$-tensor with the following coordinate representation

$$\mathbf{F}^{\star} = \frac{\partial\varphi^a}{\partial X^A}\,dX^A\otimes\frac{\partial}{\partial x^a}\,. \tag{2.8}$$

.

The material mass continuity equation is written as[10]

$$\dot{\rho} + \frac{1}{2}\rho \operatorname{tr}_{\mathbf{G}} \dot{\mathbf{G}} = 0\,, \tag{3.3}$$

while the spatial mass continuity equation reads[11]

$$\dot{\rho} + \rho \operatorname{div}_{\mathbf{g}} \mathbf{v} = \rho_{,t} + \operatorname{div}_{\mathbf{g}}(\rho \mathbf{v}) = 0\,. \tag{3.4}$$

Here, $\dot{(\,)} = \frac{\partial}{\partial t}\Big|_X (\,)$ represents the material time derivative, while $(\,)_{,t}$ represents the partial derivative $\frac{\partial}{\partial t}\Big|_x (\,)$.

3.2. Stress and strain tensors

The right and left Cauchy–Green strains are defined as $\mathbf{C} = \mathbf{F}^{\mathsf{T}}\mathbf{F}$ and $\mathbf{b} = \mathbf{F}\mathbf{F}^{\mathsf{T}}$, respectively.[12] In components

$$C^A{}_B = G^{AM} F^a{}_M \, g_{ab} F^b{}_B\,, \qquad b^a{}_b = F^a{}_A G^{AB} F^c{}_B \, g_{cb}\,. \tag{3.6}$$

Further, their inverses are denoted by $\mathbf{B} = \mathbf{C}^{-1}$ and $\mathbf{c} = \mathbf{b}^{-1}$, respectively. Note that $\mathbf{C}^\flat$ is the pull-back of the spatial metric $\mathbf{g}$ via the deformation map φ (i.e. $\mathbf{C}^\flat = \varphi^*\mathbf{g}$) and $\mathbf{c}^\flat$ is the push-forward of the material metric $\mathbf{G}$ via φ (i.e. $\mathbf{c}^\flat = \varphi_*\mathbf{G}$).[13] Moreover, $\mathbf{b}^\sharp = \varphi_*(\mathbf{G}^\sharp)$ and $\mathbf{B}^\sharp = \varphi^*(\mathbf{g}^\sharp)$.[14] In components

$$C_{AB} = g_{ab} F^a{}_A F^b{}_B\,, \quad c_{ab} = G_{AB} F^{-A}{}_a F^{-B}{}_b\,, \quad B^{AB} = g^{ab} F^{-A}{}_a F^{-B}{}_b\,, \quad b^{ab} = G^{AB} F^a{}_A F^b{}_B\,, \tag{3.9}$$

where $F^{-A}{}_a$ are the components of $\mathbf{F}^{-1}$. The principal invariants of the right Cauchy–Green strain read

$$I_1 = \operatorname{tr} \mathbf{C} = \operatorname{tr}_{\mathbf{G}} \mathbf{C}^\flat\,, \qquad I_2 = \frac{1}{2}\left(I_1^2 - \operatorname{tr} \mathbf{C}^2\right)\,, \qquad I_3 = \det \mathbf{C} = \frac{\det \mathbf{C}^\flat}{\det \mathbf{G}}\,. \tag{3.10}$$

With respect to a coordinate chart $\{X^A\}$, $I_1 = C^A{}_A$ and $I_2 = \frac{1}{2}\left(I_1^2 - C^A{}_B C^B{}_A\right)$. Note that $\sqrt{I_3} = J = \sqrt{\frac{\det \mathbf{g}}{\det \mathbf{G}}}\det \mathbf{F}$. The constitutive model for hyperelastic materials is given by a free energy density function $W = \tilde{W}(X, T, \mathbf{F}, \mathbf{g}, \mathbf{G}) = \hat{W}(X, T, \mathbf{C}^\flat, \mathbf{G})$,[15] per unit undeformed volume, i.e., volume calculated using the metric $\mathbf{G}$. The Cauchy stress tensor $\boldsymbol{\sigma}$, the first Piola–Kirchhoff stress tensor $\mathbf{P}$, and the second Piola–Kirchhoff stress tensor $\mathbf{S}$ are related to the free energy function as[16]

$$\boldsymbol{\sigma} = \frac{2}{J}\frac{\partial \tilde{W}}{\partial \mathbf{g}}\,, \qquad \mathbf{P} = \mathbf{g}^\sharp \frac{\partial \tilde{W}}{\partial \mathbf{F}}\,, \qquad \mathbf{S} = 2\frac{\partial \hat{W}}{\partial \mathbf{C}^\flat}\,. \tag{3.12}$$

---

[10] For a material tensor field $\mathbf{K}$ with components K_{AB}, $\operatorname{tr}_{\mathbf{G}} \mathbf{K} = K_{AB} G^{AB} = \mathbf{G}^\sharp : \mathbf{K}^\flat$. Similarly, for a spatial tensor field $\mathbf{k}$ with components k_{ab}, $\operatorname{tr}_{\mathbf{g}} \mathbf{k} = k_{ab} g^{ab} = \mathbf{g}^\sharp : \mathbf{k}^\flat$.

[11] Note that $\operatorname{div}_{\mathbf{g}} \mathbf{v} = \operatorname{tr}_{\mathbf{g}} \nabla^{\mathbf{g}} \mathbf{v}$, where $\nabla^{\mathbf{g}}$ is the Levi-Civita connection corresponding to the metric $\mathbf{g}$. In a coordinate chart $\{x^a\}$, $\operatorname{div}_{\mathbf{g}} \mathbf{v} = v^a{}_{|a} = v^a{}_{,a} + \gamma^a{}_{ab} v^b$, where $\gamma^a{}_{bc} = \frac{1}{2} g^{ak}\left(g_{kb,c} + g_{kc,b} - g_{bc,k}\right)$ are the Christoffel symbols corresponding to the metric $\mathbf{g}$.

[12] The transpose of the deformation gradient $\mathbf{F}^{\mathsf{T}}(X,t) : T_x\mathcal{C}_t \to T_X\mathcal{B}$ is defined such that

$$\langle\!\langle \mathbf{F}\mathbf{W}, \mathbf{w} \rangle\!\rangle_{\mathbf{g}} = \langle\!\langle \mathbf{W}, \mathbf{F}^{\mathsf{T}}\mathbf{w} \rangle\!\rangle_{\mathbf{G}}\,, \quad \forall\, \mathbf{W} \in T_X\mathcal{B}_t\,,\ \mathbf{w} \in T_x\mathcal{C}_t\,. \tag{3.5}$$

In components, $\left(F^{\mathsf{T}}\right)^A{}_a = G^{AB} F^b{}_B \, g_{ba}$. Thus, $\mathbf{F}^\star$ and $\mathbf{F}^{\mathsf{T}}$ are related as $\mathbf{F}^{\mathsf{T}} = \mathbf{G}^\sharp \mathbf{F}^\star \mathbf{g}$.

[13] Given a diffeomorphism (a differentiable map with differentiable inverse) $\varphi : \mathcal{B} \to \mathcal{C}$, a tensor field $\mathbf{K}$ on $\mathcal{B}$ has a unique corresponding natural tensor field $\mathbf{k} = \varphi_*\mathbf{K}$—the push-forward of the tensor field $\mathbf{K}$ by the map φ. Similarly, a tensor field $\mathbf{l}$ on $\mathcal{C}$, has a unique corresponding tensor field $\mathbf{L} = \varphi^*\mathbf{l}$ on $\mathcal{B}$—its pull-back by the map φ.

[14] Here, the musical symbols $^\flat$ and $^\sharp$ denote the flat and sharp operators that lower and raise tensor indices, respectively. Recall that a Riemannian metric induces natural isomorphisms between the tangent space and the cotangent space, namely the flat operator that maps a vector $\mathbf{u}$ to its corresponding covector (1-form) $\mathbf{u}^\flat$:

$$\begin{aligned} &\flat : T_x\mathcal{C} \longrightarrow T_x^*\mathcal{C} \\ &\mathbf{u} = u^a \frac{\partial}{\partial x^a} \longmapsto \mathbf{u}^\flat = g_{ab}\, u^b \, dx^a\,, \end{aligned} \tag{3.7}$$

and the sharp operator that maps a covector (1-form) $\boldsymbol{\alpha}$ to its corresponding vector $\boldsymbol{\alpha}^\sharp$:

$$\begin{aligned} &\sharp : T_x^*\mathcal{C} \longrightarrow T_x\mathcal{C} \\ &\boldsymbol{\alpha} = \omega_a \, dx^a \longmapsto \boldsymbol{\alpha}^\sharp = g^{ab}\alpha_b \frac{\partial}{\partial x^a}\,. \end{aligned} \tag{3.8}$$

.

[15] Free energy (a scalar) depends on $\mathbf{F}$ (a two-point tensor). To make a scalar out of a two-point tensor, one would need metrics of both the reference and current configurations (Marsden and Hughes, 1983).

[16] The relationship between stress and strain measures in hyperelasticity are obtained either using a Coleman and Noll (1963) argument, which gives $(3.12)_2$ (or $(3.12)_3$) or covariance of energy balance (Marsden and Hughes, 1983; Yavari et al., 2006) that gives the Doyle–Ericksen formula $(3.12)_1$. Let us start with the Doyle–Ericksen formula and recall that $\mathbf{C}^\flat = \mathbf{F}^*\mathbf{g} = \mathbf{F}^\star \mathbf{g}\, \mathbf{F}$, and hence

$$\frac{\partial \tilde{W}}{\partial \mathbf{g}} = \frac{\partial \hat{W}}{\partial \mathbf{C}^\flat} : \frac{\partial \mathbf{C}^\flat}{\partial \mathbf{g}} = \mathbf{F}\frac{\partial \hat{W}}{\partial \mathbf{C}^\flat}\mathbf{F}^\star\,. \tag{3.11}$$

Knowing that $\mathbf{S} = J\mathbf{F}^{-1}\mathbf{P}\mathbf{F}^{-\star}$, one obtains $(3.12)_3$.

In components[17]

$$\sigma^{ab} = \frac{2}{J}\frac{\partial \tilde{W}}{\partial g_{ab}}, \qquad P^{aA} = g^{ab}\frac{\partial \tilde{W}}{\partial F^{b}{}_{A}}, \qquad S^{AB} = 2\frac{\partial \hat{W}}{\partial C_{AB}}. \tag{3.13}$$

Note that $\mathbf{P} = J\boldsymbol{\sigma}\mathbf{F}^{-\star}$ and $\mathbf{S} = \mathbf{F}^{-1}\mathbf{P}$.

Remark 3.1. The free energy function for an isotropic hyperelastic solid is a function of the principal invariants of $\mathbf{C}$, i.e., $W = \check{W}(X, T, I_1, I_2, I_3)$, and the Cauchy stress is represented as (Doyle and Ericksen, 1956; Simo and Marsden, 1984)

$$\boldsymbol{\sigma} = \frac{2}{\sqrt{I_3}}\left[\left(I_2\frac{\partial \check{W}}{\partial I_2} + I_3\frac{\partial \check{W}}{\partial I_3}\right)\mathbf{g}^{\sharp} + \frac{\partial \check{W}}{\partial I_1}\mathbf{b}^{\sharp} - I_3\frac{\partial \check{W}}{\partial I_2}\mathbf{c}^{\sharp}\right]. \tag{3.14}$$

Remark 3.2. The free energy function for hyperelastic fluids has the functional form $W = \check{W}(X, T, J)$, where $\check{W}$ is a smooth, strictly convex function of J that tends to infinity as J approaches 0 (Podio-Guidugli et al., 1985). Thus, the Cauchy, the first and the second Piola–Kirchhoff stress tensors are written as

$$\boldsymbol{\sigma} = \frac{\partial \check{W}}{\partial J}\mathbf{g}^{\sharp}, \qquad \mathbf{P} = J\frac{\partial \check{W}}{\partial J}\mathbf{g}^{\sharp}\mathbf{F}^{-\star}, \qquad \mathbf{S} = J\frac{\partial \check{W}}{\partial J}\mathbf{F}^{-1}\mathbf{g}^{\sharp}\mathbf{F}^{-\star}. \tag{3.15}$$

Note that one must have $\frac{\partial \check{W}}{\partial J} < 0$, as hydrostatic stresses are compressive in fluids.

The free energy function for homogeneous materials is independent of X, i.e., $W = \hat{W}(T, \mathbf{C}^{\flat}, \mathbf{G})$ for hyperelastic solids and $W = \check{W}(T, J)$ for hyperelastic fluids.

3.3. Balance of linear and angular momenta

The localized forms of the balance of linear momentum in terms of the Cauchy and the first Piola–Kirchhoff stress read[18]

$$\mathrm{div}_{\mathbf{g}}\,\boldsymbol{\sigma} + \varrho\,\mathbf{b} = \varrho\,\mathbf{a}, \qquad \mathrm{Div}\,\mathbf{P} + \rho\,\mathbf{B} = \rho\,\mathbf{A}, \tag{3.17}$$

where $\mathbf{b}$ is the spatial body force (per unit mass), while $\mathbf{B}$ is body force referred in material coordinates, i.e., $\mathbf{B}(X, t) = \mathbf{b}(\varphi_t(X), t)$. In components

$$\sigma^{ij}{}_{|j} + \varrho\,b^i = \varrho\,a^i, \qquad P^{iI}{}_{|I} + \rho\,B^i = \rho\,A^i. \tag{3.18}$$

The balance of angular momentum in local form reads

$$\sigma^{ij} = \sigma^{ji}, \qquad P^{iJ}F^{j}{}_{J} = P^{jJ}F^{i}{}_{J}. \tag{3.19}$$

Note that for slow accretion, the inertial effects can be disregarded.

Let $\mathbf{t}$ be the spatial traction field. Consider a material surface element $\mathrm{d}A$ with unit normal $\mathbf{N}$, which gets mapped to the element $\mathrm{d}a$ with unit normal $\mathbf{n}$ in the deformed configuration. The traction is related to the Cauchy stress as $\mathbf{t} = \boldsymbol{\sigma}\mathbf{n}^{\flat} = \langle\!\langle \boldsymbol{\sigma}, \mathbf{n}\rangle\!\rangle_{\mathbf{g}}$. The material traction field is denoted by $\mathbf{T}$ and is related to the first Piola–Kirchhoff stress as $\mathbf{T} = \mathbf{P}\mathbf{N}^{\flat} = \langle\!\langle \mathbf{P}, \mathbf{N}\rangle\!\rangle_{\mathbf{G}}$.[19] Note that $\mathbf{t}\,\mathrm{d}a = \boldsymbol{\sigma}\mathbf{n}^{\flat}\,\mathrm{d}a = J\boldsymbol{\sigma}\mathbf{F}^{-\star}\mathbf{N}^{\flat}\,\mathrm{d}A = \mathbf{P}\mathbf{N}^{\flat}\,\mathrm{d}A = \mathbf{T}\,\mathrm{d}A$.[20] Therefore, the force on the surface element in consideration is $\mathbf{t}\,\mathrm{d}a = \mathbf{T}\,\mathrm{d}A$.

3.4. The heat equation

Let $\mathcal{T}(x, t)$ be the temperature field defined with respect to the current configuration and let $T(X, t)$ be the temperature field defined with respect to the reference configuration. Since $x = \varphi(X, t)$, it follows that $T(X, t) = \mathcal{T}(\varphi(X, t), t)$, i.e., $T_t = \mathcal{T}_t \circ \varphi_t$, or equivalently, $T_t = \varphi_t^*\mathcal{T}_t$. Recall that $\mathrm{d}\mathcal{T} = \frac{\partial \mathcal{T}}{\partial x^a}\mathrm{d}x^a$, and $\mathrm{d}T = \frac{\partial T}{\partial X^A}\mathrm{d}X^A$. Note that $\mathrm{d}\mathcal{T}$ is a 1-form in the Euclidean ambient manifold with components $(\mathrm{d}\mathcal{T})_a = \frac{\partial \mathcal{T}}{\partial x^a}$, while $\mathrm{d}T$ is a 1-form in the material manifold with components $(\mathrm{d}T)_A = \frac{\partial T}{\partial X^A}$ related to $\mathrm{d}\mathcal{T}$ via pull back, i.e., $\mathrm{d}T = \varphi_t^*\mathrm{d}\mathcal{T}$. Thus

$$\frac{\partial T}{\partial X^A} = \frac{\partial \mathcal{T}}{\partial x^a}\frac{\partial x^a}{\partial X^A} = F^{a}{}_{A}(\mathrm{d}\mathcal{T})_a = (\varphi_t^*\mathrm{d}\mathcal{T})_A. \tag{3.20}$$

---

[17] In the standard notation of nonlinear elasticity, one simply writes $\mathbf{P} = \frac{\partial \check{W}}{\partial \mathbf{F}}$, which has components $P_a{}^A$. When this two-point tensor acts on a unit normal vector $\mathbf{N}$ in the reference configuration, it gives a co-vector in the current configuration $\mathbf{t}^{\flat}$—the traction co-vector. The corresponding two-point tensor $\mathbf{g}^{\sharp}\frac{\partial \check{W}}{\partial \mathbf{F}}$ acting on the same unit vector $\mathbf{N}$ gives the corresponding vector $\mathbf{t}$—the traction vector. In the standard notation of nonlinear elasticity, either Cartesian coordinates are used, or the physical components of tensor fields are implicitly assumed. In the presence of eigenstrains (sources of residual stresses), a global reference configuration would have a non-trivial geometry, and it is important to ensure that the tensorial character of all the physical fields is clearly understood.

[18] In coordinates

$$\left(\mathrm{div}_{\mathbf{g}}\boldsymbol{\sigma}\right)^a = \sigma^{ab}{}_{|b} = \frac{\partial \sigma^{ab}}{\partial x^b} + \sigma^{ac}\gamma^{b}{}_{cb} + \sigma^{cb}\gamma^{a}{}_{cb}, \qquad \left(\mathrm{Div}\,\mathbf{P}\right)^a = P^{aA}{}_{|A} = \frac{\partial P^{aA}}{\partial X^A} + P^{aB}\Gamma^{A}{}_{BA} + F^{b}{}_{A}P^{cA}\gamma^{a}{}_{cb}, \tag{3.16}$$

where $\gamma^{a}{}_{bc} = \frac{1}{2}g^{ak}\left(g_{kb,c} + g_{kc,b} - g_{bc,k}\right)$ and $\Gamma^{A}{}_{BC} = \frac{1}{2}G^{AM}\left(G_{MB,C} + G_{MC,B} - G_{BC,M}\right)$. Note that Div depends on both the metrics $\mathbf{g}$ and $\mathbf{G}$ through the Christoffel coefficients $\Gamma^{A}{}_{BC}$ and $\gamma^{a}{}_{bc}$.

[19] Note that $n_b = g_{bc}n^c$ and $N_B = G_{BC}N^C$. Thus, $t^a = \sigma^{ab}n_b = \sigma^{ab}g_{bc}\,n^c$ and $T^a = P^{aA}N_A = P^{aA}G_{AB}\,N^B$.

[20] The Nanson's formula $\mathbf{n}^{\flat}da = J\mathbf{F}^{-\star}\mathbf{N}^{\flat}dA$ has been used here. In components, the 1-forms $n_b\mathrm{d}a$ and $N_B\mathrm{d}A$ are related as $n_b\mathrm{d}a = JF^{-B}{}_{b}N_B\mathrm{d}A$.

Let $\mathbf{h}(x,t)$ denote the heat flux in the current configuration. Note that $\langle\!\langle \mathbf{h}, \mathbf{n} \rangle\!\rangle_{\mathbf{g}} \mathrm{d}a$ is interpreted as the flux through the surface element $\mathrm{d}a$ with unit normal $\mathbf{n}$ ($\mathrm{d}a$ is the area 2-form).

The material heat flux vector $\mathbf{H}$ is defined via the Piola transform as

$$\mathbf{H}(X,t) = J(X,t)\,\mathbf{F}^{-1}(X,t)\,\mathbf{h}(\varphi(X,t),t)\,. \tag{3.21}$$

In components,

$$H^A = J\,F^{-A}{}_a\,h^a\,. \tag{3.22}$$

Let $\mathbf{N}$ denote unit normal to the material surface element $\mathrm{d}A$, which gets mapped to the deformed element $\mathrm{d}a$. Using (3.22) and Nanson's formula, it is implied that $H^B N_B\,\mathrm{d}A = J F^{-B}{}_b\,h^b N_B\,\mathrm{d}A = h^b n_b\,\mathrm{d}a$, i.e., $\langle\!\langle \mathbf{H}, \mathbf{N} \rangle\!\rangle_{\mathbf{G}}\,\mathrm{d}A = \langle\!\langle \mathbf{h}, \mathbf{n} \rangle\!\rangle_{\mathbf{g}}\,\mathrm{d}a$. Thus, $\langle\!\langle \mathbf{H}, \mathbf{N} \rangle\!\rangle_{\mathbf{G}}$ is interpreted as the heat flux per unit undeformed area.

The generalized Fourier's law of thermal conduction in the deformed configuration reads

$$\mathbf{h} = -\mathbf{k}\,\mathrm{d}\mathcal{T}\,, \tag{3.23}$$

where the $\binom{2}{0}$-tensor $\mathbf{k}$ represents the spatial thermal conductivity. In components, $h^a = -k^{ab}\frac{\partial \mathcal{T}}{\partial x^b}$. The Fourier's law in the reference configuration is written as

$$\mathbf{H} = -\mathbf{K}\,\mathrm{d}T\,, \quad \text{or} \qquad H^A = -K^{AB}\frac{\partial T}{\partial X^B}\,, \tag{3.24}$$

where $\mathbf{K}$ denotes the material thermal conductivity. Note that the material and spatial thermal conductivity tensors are related as $\mathbf{K} = J\varphi_t^*\mathbf{k}$.[21] In components, $K^{AB} = J F^{-A}{}_a\,k^{ab}F^{-B}{}_b$. Furthermore, upon substituting $(3.24)_1$ into the reduced form of the Clausius–Duhem inequality $\langle \mathrm{d}T, \mathbf{H}\rangle \leq 0$, it can be deduced that $\mathbf{K}$ is a positive semi-definite tensor. The spatial heat equation reads

$$\varrho\, c_E \dot{\mathcal{T}} + \mathrm{div}_{\mathbf{g}}\,\mathbf{h} = \mathcal{T}\mathbf{m} : \mathbf{d} + r\,, \tag{3.26}$$

where c_E is the specific heat capacity at constant strain, $\mathbf{m}$ is the spatial thermal stress coefficient, $\mathbf{d} = \frac{1}{2}\pounds_{\mathbf{v}}\mathbf{g}$ denotes the rate of deformation tensor and r represents a heat source (per unit deformed volume) term. The heat equation is a consequence of the first law of thermodynamics, as shown in detail in Appendix A.2. Equivalently, the material heat equation is written as

$$\rho\, c_E\, \dot{T} + \mathrm{Div}_{\mathbf{G}}\,\mathbf{H} = T\,\mathbf{M} : \mathbf{D} + R\,, \tag{3.27}$$

where $\mathbf{M}$ is the material thermal stress coefficient, $\mathbf{D} = \frac{1}{2}\dot{\mathbf{C}}^\flat$ denotes the material rate of deformation tensor and R represents a heat source (per unit undeformed volume) term, see Appendix A.1. The material and spatial thermal stress coefficients are related as $\mathbf{M} = J\varphi_t{}^*\mathbf{m}$ (see Appendix A.2). Note that the term $\mathcal{T}\mathbf{m} : \mathbf{d}$ (or equivalently, $T\mathbf{M} : \mathbf{D}$) can be omitted if there is no thermoelastic coupling in the material under consideration.[22] In the absence of heat sources, the spatial heat equation for a rigid heat conductor is written as

$$\varrho\, c_E\, \dot{\mathcal{T}} = \mathrm{div}_{\mathbf{g}}(\mathbf{k}\,\mathrm{d}\mathcal{T})\,, \tag{3.28}$$

or, in components, $\varrho\, c_E \dot{\mathcal{T}} = \left(k^{ab}\frac{\partial \mathcal{T}}{\partial x^b}\right)_{|a}$. The equivalent material heat equation is written as

$$\rho\, c_E\, \dot{T} = \mathrm{Div}_{\mathbf{G}}\,(\mathbf{K}\,\mathrm{d}T)\,. \tag{3.29}$$

In components, $\rho\, c_E\, \dot{T} = \left(K^{AB}\frac{\partial T}{\partial X^B}\right)_{|A}$. The heat flux in thermally isotropic solids has the following representation

$$\mathbf{H} = \left(\phi_{-1}\mathbf{B}^\sharp + \phi_0\mathbf{G}^\sharp + \phi_1\mathbf{C}^\sharp\right)\,\mathrm{d}T\,, \tag{3.30}$$

where $\phi_k = \hat{\phi}_k(X, T, \mathrm{d}T, \mathbf{C}^\flat, \mathbf{G})$, $k = -1, 0, 1$, are scalar response functions (Truesdell and Noll, 2004). We consider the model $\mathbf{H} = -K\mathbf{G}^\sharp \mathrm{d}T$ for our numerical examples, where $K = K(T)$ denotes the heat conduction coefficient.[23] Further, $D = \frac{K}{c_E\rho}$ is the traditional thermal diffusivity.

[21] Using (3.22), (3.20) and (3.23), it is implied that

$$H^A = -J\,F^{-A}{}_a\,k^{ab}\frac{\partial \mathcal{T}}{\partial x^b} = -J\,F^{-A}{}_a\,k^{ab}\frac{\partial T}{\partial X^B}F^{-B}{}_b\,. \tag{3.25}$$

Hence, it can be inferred from (3.24) and $(3.25)_2$ that $K^{AB} = J\,F^{-A}{}_a\,k^{ab}F^{-B}{}_b$.

[22] A classic illustration of thermoelastic coupling is the *Gough–Joule effect*, observed in vulcanized rubber, where the temperature of a rubber band changes during adiabatic stretching (Gough, 1805; Joule, 1859).

[23] Note that $\mathrm{grad}_{\mathbf{G}}\,T = \mathbf{G}^\sharp \mathrm{d}T$.

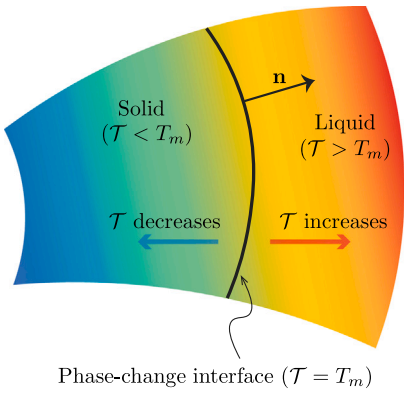

Fig. 2. The interface between the (cold) solid and (hot) liquid phases forms an isothermal surface at the solidification temperature T_m. The unit normal $\mathbf{n}$ to the phase-change interface is assumed to point from solid to liquid.

3.5. Stefan's condition

Let $\Gamma_t \subset \partial\mathcal{B}_t$ and $\gamma_t = \varphi_t(\Gamma_t)$. Let $\overset{+}{\mathbf{h}}$ and $\overset{-}{\mathbf{h}}$ denote the heat flux per unit area on the opposite sides of the interface γ_t in the current configuration. In the absence of any phase change or heat source/sink, the jump in the normal heat flux across γ_t vanishes, i.e.,

$$\langle\!\langle \overset{+}{\mathbf{h}} - \overset{-}{\mathbf{h}}, \mathbf{n} \rangle\!\rangle_{\mathbf{g}} = 0 \quad \text{on } \gamma_t\,, \tag{3.31}$$

where $\mathbf{n}$ is the outward unit normal to γ_t.

When γ_t is the solidification interface between the (cold) solid and (hot) liquid phases, it forms an isothermal surface at the melting point T_m (Fig. 2). Let $\mathbf{n}$ be the unit normal to γ_t, pointing from solid to liquid, and let υ be an arbitrary subset of γ_t. Let $\mathbf{h}_S$ and $\mathbf{h}_L$ be the heat flux in the solid and liquid phases, respectively, in the current configuration. As one moves into the liquid phase from the solidification interface, $\mathcal{T}$ increases, implying that $\mathbf{h}_L$ points towards the solid (Fig. 3). Hence, $q_{\text{in}} = -\int_\upsilon \langle\!\langle \mathbf{h}_L, \mathbf{n} \rangle\!\rangle_{\mathbf{g}}\, \mathrm{d}a$ represents the rate of normal heat inflow into the subset υ on the interface from the liquid via conduction. There is a decrease in $\mathcal{T}$ as one moves from the phase change interface into the solid, indicating that $\mathbf{h}_S$ also points into the solid. Thus, the rate of heat flowing out normally from the subset υ on the interface into the solid is $q_{\text{out}} = -\int_\upsilon \langle\!\langle \mathbf{h}_S, \mathbf{n} \rangle\!\rangle_{\mathbf{g}}\, \mathrm{d}a$. The rate of mass solidified on the subset υ of the interface is represented by the integral $\int_\upsilon \rho u^n \mathrm{d}a$ (Sozio and Yavari, 2019). As solidification is exothermic, the rate of heat released in the process is expressed as $q_{\text{exo}} = l \int_\upsilon \rho u^n \mathrm{d}a$, where l is the specific latent heat of solidification. The heat flowing into the solid consists of two components: the heat released during solidification and the heat transferred from the surrounding liquid medium (Rubinšteĭn, 1971; Gupta, 2017). In terms of heat flow per unit time, $q_{\text{out}} = q_{\text{exo}} + q_{\text{in}}$ (Fig. 3), i.e.,

$$-\int_\upsilon \langle\!\langle \mathbf{h}_S, \mathbf{n} \rangle\!\rangle_{\mathbf{g}}\, \mathrm{d}a = l \int_\upsilon \varrho\, J u^n \mathrm{d}a - \int_\upsilon \langle\!\langle \mathbf{h}_L, \mathbf{n} \rangle\!\rangle_{\mathbf{g}}\, \mathrm{d}a\,, \tag{3.32}$$

where $\upsilon \subset \gamma_t$ is an arbitrary subset. The localized Stefan's condition therefore reads

$$\langle\!\langle \mathbf{h}_S - \mathbf{h}_L, \mathbf{n} \rangle\!\rangle_{\mathbf{g}} + l\varrho\, J u^n = 0 \qquad \text{on } \gamma_t\,, \tag{3.33}$$

where $\varrho\, J u^n = \rho\, U^N$ represents the mass accreted, per unit area, per unit time. The localized Stefan's condition in the reference configuration is expressed as

$$\langle\!\langle \mathbf{H}_S - \mathbf{H}_L, \mathbf{N} \rangle\!\rangle_{\mathbf{G}} + l\rho\, U^N = 0 \qquad \text{on } \Gamma_t\,. \tag{3.34}$$

Note that if the liquid is initially at the solidification temperature, there is no heat flux in the liquid phase, i.e., $\mathbf{h}_L = \mathbf{0}$. In this case, Stefan's condition is simplified as

$$-\langle\!\langle \mathbf{H}_S, \mathbf{N} \rangle\!\rangle_{\mathbf{G}} = l\rho\, U^N \qquad \text{on } \Gamma_t\,, \quad \text{or} \qquad -\langle\!\langle \mathbf{h}_S, \mathbf{n} \rangle\!\rangle_{\mathbf{g}} = l\varrho\, J u^n \qquad \text{on } \gamma_t\,. \tag{3.35}$$

Thus, the heat entering the solid from the phase change interface is equal to the heat generated in the process of solidification.

4. Radially inward solidification in a cold rigid container

Consider a spherical container of radius R_0, filled with a liquid initially at uniform temperature T_0. The inner wall of the container is maintained at a constant temperature T_c. Let T_m denote the melting point of the material, satisfying the condition $T_c < T_m \leq T_0$. At $t = 0$, the outermost layer of liquid begins to cool down and solidifies when the melting point is reached. The container wall acts as a rigid substrate to which the outermost accreted layer firmly attaches, resulting in no displacement of the outer boundary

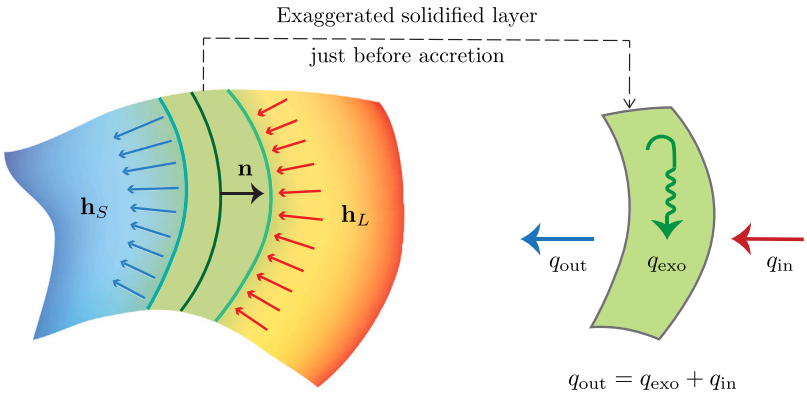

Fig. 3. The heat flux $\mathbf{h}_L$ is directed into the interface in the fluid medium due to its higher temperature compared to the melting point. However, in the solid, where the temperature is lower than the melting point, $\mathbf{h}_S$ is directed into the solid. The heat entering the solid comprises of the heat released during solidification and the heat transferred from the liquid medium.

of the accreting body. Layers of liquid solidify and attach to the inner surface of the accreting body—a spherical shell, causing the solidification front to progress inward (Fig. 4). The temperature fields within the accreting body and the liquid are both unknowns.[24]

We model both the liquid and solid phases as isotropic compressible hyperelastic materials. To simplify the analysis, an assumption can be made that $T_m = T_0$, allowing for solidification to initiate near the container wall at $t = 0$ (Stewartson and Waechter, 1976; Rabin and Steif, 1998).

4.1. Kinematics

The ambient space has the Euclidean metric, which in spherical coordinates, i.e., with respect to the frame $\left\{\frac{\partial}{\partial r}, \frac{\partial}{\partial \theta}, \frac{\partial}{\partial \phi}\right\}$ has the following representation

$$\mathbf{g} = \begin{bmatrix} 1 & 0 & 0 \\ 0 & r^2 & 0 \\ 0 & 0 & r^2 \sin^2\theta \end{bmatrix}, \tag{4.1}$$

in terms of the spherical coordinates (r, θ, ϕ), where $r \geq 0$, $0 \leq \theta \leq \pi$ and $0 \leq \phi < 2\pi$.

Let $S(t)$ denote the material radius corresponding to the inner surface of the solid at any time $t \leq t_f$, where t_f is the time taken for the completion of freezing.[25] Note that $S(t)$ is assumed to be a continuous bijective map on $[0, t_f]$ with the initial condition $S(0) = R_0$. The inverse map $\tau = S^{-1}$ assigns the time of attachment to each spherical layer in the material manifold. The accreting solid and the ablating fluid are identified with the following time-dependent material manifolds

$$\mathcal{B}_t = \{(R, \Theta, \Phi) : S(t) \leq R \leq R_0\,,\ 0 \leq \Theta \leq \pi\,,\ 0 \leq \Phi < 2\pi\}\,, \qquad \mathcal{L}_t = \{(R, \Theta, \Phi) : 0 \leq R \leq S(t)\,,\ 0 \leq \Theta \leq \pi\,,\ 0 \leq \Phi < 2\pi\}\,. \tag{4.2}$$

Let the temperature field be denoted as $T(R, t)$, and defined piece-wise as follows

$$T(R,t) = \begin{cases} T^{\text{s}}(R,t)\,, & S(t) \leq R \leq R_0\,, \\ T^{\text{f}}(R,t)\,, & 0 \leq R \leq S(t)\,. \end{cases} \tag{4.3}$$

Note that $T_t(R) = T(R, t)$ is continuous at the solidification interface $R = S(t)$, i.e., $T^{\text{s}}(S(t), t) = T^{\text{f}}(S(t), t) = T_m$. The material metric for the liquid phase in its initial state is the flat Euclidean metric restricted to $\mathcal{L}$ and has the following representation

$$\overset{\mathcal{L}}{\mathbf{G}}_0 = \begin{bmatrix} 1 & 0 & 0 \\ 0 & R^2 & 0 \\ 0 & 0 & R^2 \sin^2\Theta \end{bmatrix}, \tag{4.4}$$

where (R, Θ, Φ) are the material spherical coordinates. Thus, the temperature-dependent material metric for the liquid phase is written as

$$\overset{\mathcal{L}}{\mathbf{G}} = e^{2\omega^{\text{f}}(T^{\text{f}}(R,t))} \begin{bmatrix} 1 & 0 & 0 \\ 0 & R^2 & 0 \\ 0 & 0 & R^2 \sin^2\Theta \end{bmatrix}, \tag{4.5}$$

[24] This problem draws inspiration from the experiments conducted by Chan and Tan (2006) who investigated the inward solidification of an n−hexadecane in a spherical enclosure (capsule) with walls maintained at a constant temperature. They placed this capsule in a cool water tank that was consistently stirred and supplied with cold water from a refrigerated bath. They attached thermocouples to the capsule walls to track its temperature and ensure that it remains constant throughout the process.

[25] Note that the freezing time may be quite large or even infinite. In that case one would need to solve the problem in the time interval $[0, \infty)$ instead.

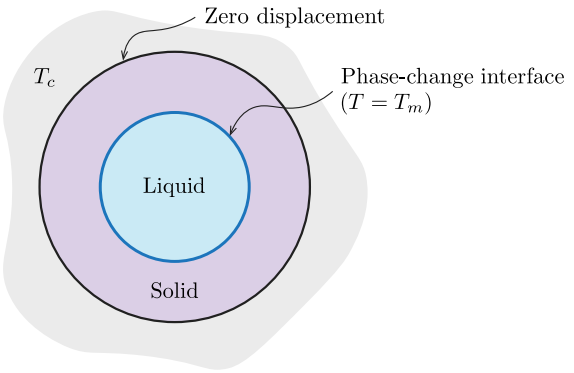

Fig. 4. Schematic representation of radially inward solidification in a spherical rigid container with cold walls maintained at the temperature $T_c < T_m$.

where the scalar function $\omega^{\mathrm{f}}(T^{\mathrm{f}})$ characterizes isotropic and homogeneous thermal expansion in the liquid phase. We consider radial deformations $\varphi_t(R,\Theta,\Phi) = (r(R,t),\theta,\phi)$, where $\theta = \Theta$, $\phi = \Phi$, and

$$r(R,t) = \begin{cases} r^{\mathrm{s}}(R,t)\,, & S(t) \le R \le R_0\,, \\ r^{\mathrm{f}}(R,t)\,, & 0 \le R \le S(t)\,, \end{cases} \tag{4.6}$$

and $r^{\mathrm{s}}(R_0,t) = R_0$, $r^{\mathrm{f}}(0,t) = 0$.[26] Note that $r(R,t)$ is continuous at $R = S(t)$ for all $t \ge 0$. Let $s(t) := r^{\mathrm{s}}(S(t),t) = r^{\mathrm{f}}(S(t),t)$ and $\bar{r}(R) := r^{\mathrm{s}}(R,\tau(R)) = r^{\mathrm{f}}(R,\tau(R))$. Thus, $\bar{r} = s\circ\tau$, or $s = \bar{r}\circ S$.[27] The moving phase-change interface in the reference and current configurations are represented as

$$\Omega_t = \{(S(t),\Theta,\Phi) : 0 \le \Theta \le \pi\,,\ 0 \le \Phi < 2\pi\}\,, \qquad \omega_t = \{(s(t),\theta,\phi) : 0 \le \theta \le \pi\,,\ 0 \le \phi < 2\pi\}\,. \tag{4.9}$$

The respective deformation gradients in the solid and liquid phases read

$$\mathbf{F}^{\mathrm{s}}(R,t) = \begin{bmatrix} r^{\mathrm{s}}{}_{,R}(R,t) & 0 & 0 \\ 0 & 1 & 0 \\ 0 & 0 & 1 \end{bmatrix}, \qquad \mathbf{F}^{\mathrm{f}}(R,t) = \begin{bmatrix} r^{\mathrm{f}}{}_{,R}(R,t) & 0 & 0 \\ 0 & 1 & 0 \\ 0 & 0 & 1 \end{bmatrix}. \tag{4.10}$$

Let $U(t) := \dot{S}(t) < 0$ be the material growth velocity. Let $u(t)$ denote the growth velocity in the current configuration, i.e., $-u(t)$ is the relative velocity of the accreting liquid particles with respect to the interface ω_t. Further define $\bar{u}(R) := u(\tau(R))$ and $\bar{U}(R) := U(\tau(R))$. Thus, the accretion tensor $\mathbf{Q}$ has the following representation with respect to the frames $\left\{\frac{\partial}{\partial R}, \frac{\partial}{\partial\Theta}, \frac{\partial}{\partial\Phi}\right\}$ and $\left\{\frac{\partial}{\partial r}, \frac{\partial}{\partial\theta}, \frac{\partial}{\partial\phi}\right\}$:[28]

$$\mathbf{Q}(R) = \begin{bmatrix} \frac{\bar{u}(R)}{\bar{U}(R)} & 0 & 0 \\ 0 & 1 & 0 \\ 0 & 0 & 1 \end{bmatrix}. \tag{4.13}$$

The accreting layer is not stress free due to the pressure exerted by the fluid. Let $\boldsymbol{\lambda}$ be the natural metric of the pre-stressed layers that are accreting to the solid. This metric $\boldsymbol{\lambda}$ is obtained by transforming the Euclidean metric $\mathbf{g}$ via a pre-deformation tensor $\boldsymbol{\Lambda}$ as $\lambda_{ij} = \Lambda^k{}_i(g_{kl}\circ\bar{\varphi})\,\Lambda^l{}_j$. In this case, the material metric for the accreted layer is calculated by pulling back the natural metric $\boldsymbol{\lambda}$

[26] Podio-Guidugli et al. (1985) investigated cavitation in hyperelastic fluids undergoing similar radial deformations. They called the deformations satisfying the condition $r^{\mathrm{f}}(0,t) = 0$ *regular*, and those with $r^{\mathrm{f}}(0,t) > 0$, *irregular* deformations corresponding to a cavity (hole) of radius $r^{\mathrm{f}}(0,t)$.

[27] Note that

$$\dot{s}(t) = r^{\mathrm{s}}{}_{,R}(S(t),t)\,\dot{S}(t) + r^{\mathrm{s}}{}_{,t}(S(t),t) = r^{\mathrm{f}}{}_{,R}(S(t),t)\,\dot{S}(t) + r^{\mathrm{f}}{}_{,t}(S(t),t)\,, \tag{4.7}$$

and thus

$$\left[r^{\mathrm{s}}{}_{,R}(S(t),t) - r^{\mathrm{f}}{}_{,R}(S(t),t)\right]\,\dot{S}(t) + r^{\mathrm{s}}{}_{,t}(S(t),t) - r^{\mathrm{f}}{}_{,t}(S(t),t) = 0\,. \tag{4.8}$$

Hence, the velocity field $r_{,t}(R,t)$ is continuous at $R = S(t)$ if and only if the partial derivative $r_{,R}(R,t)$ is also continuous at $R = S(t)$.

[28] In our example, $\mathbf{u}_{\tau(R)}(\varphi_{\tau(R)}(R,\Theta,\Phi)) = \bar{u}(R)\frac{\partial}{\partial r}$ and $\mathbf{U}_{\tau(R)}(R,\Theta,\Phi) = \bar{U}(R)\frac{\partial}{\partial R}$. Recall that the components of the accretion tensor are defined as

$$Q^i{}_I(X) = \bar{F}^i{}_I(X) + \left[u^i\,(\bar{\varphi}(X),\tau(X)) - \bar{F}^i{}_J(X)\,U^J\,(X,\tau(X))\right](\mathrm{d}\tau)_I(X)\,, \tag{4.11}$$

where $\bar{F}^i{}_I$ are the components of $\bar{\mathbf{F}}(X) = \mathbf{F}^{\mathrm{s}}(X,\tau(X))$. Further, $\frac{\mathrm{d}\tau(R)}{\mathrm{d}R} = \frac{1}{S(\tau(R))} = \frac{1}{\bar{U}(R)}$. Thus, the nonzero components of $\mathbf{Q}$ are

$$Q^r{}_R = \bar{F}^r{}_R + \left[\bar{u} - \bar{F}^r{}_R\bar{U}\right]\frac{\mathrm{d}\tau}{\mathrm{d}R} = \frac{\bar{u}}{\bar{U}}\,, \qquad Q^\theta{}_\Theta = \bar{F}^\theta{}_\Theta = 1\,, \qquad Q^\phi{}_\Phi = \bar{F}^\phi{}_\Phi = 1\,. \tag{4.12}$$

via the accretion tensor $\mathbf{Q}$ (Sozio and Yavari, 2019). Therefore, one has

$$(\overset{\mathcal{B}}{G}_0)_{IJ} = Q^i{}_I\, \lambda_{ij}\, Q^j{}_J = Q^i{}_I\, \Lambda^k{}_i\, (g_{kl}\circ\bar{\varphi})\, \Lambda^l{}_j\, Q^j{}_J\,. \tag{4.14}$$

In this example, it is assumed that

$$\boldsymbol{\Lambda}(R) = \eta(R)\frac{\partial}{\partial r}\otimes \mathrm{d}r + \frac{\partial}{\partial\theta}\otimes \mathrm{d}\theta + \frac{\partial}{\partial\phi}\otimes \mathrm{d}\phi\,, \tag{4.15}$$

where the function $\eta(R)$ is used to transform the Euclidean metric $\mathbf{g}\circ\bar{\varphi}$ by scaling its rr-component by a factor of $\eta^2(R)$,[29] such that the resulting metric λ reads

$$\lambda(R) = \begin{bmatrix} \eta^2(R) & 0 & 0 \\ 0 & \bar{r}^2(R) & 0 \\ 0 & 0 & \bar{r}^2(R)\sin^2\Theta \end{bmatrix}. \tag{4.16}$$

λ is the metric that measures natural distances in the radially stressed, deformed configuration of the accreting layers at the time of attachment. $\eta^2(R) > 1$ indicates radial dilation of accreting layers just before attachment, while $\eta^2(R) < 1$ indicates radial contraction. Thus, by substituting (4.13) and (4.16) into (4.14), the temperature-independent material metric at the time of accretion is written as

$$\overset{\mathcal{B}}{\mathbf{G}}_0 = \begin{bmatrix} \varsigma^2(R) & 0 & 0 \\ 0 & \bar{r}^2(R) & 0 \\ 0 & 0 & \bar{r}^2(R)\sin^2\Theta \end{bmatrix}, \tag{4.17}$$

where $\varsigma(R) = \frac{\bar{u}(R)\eta(R)}{\bar{U}(R)}$. Hence, the temperature-dependent material metric for the solid phase is written as

$$\overset{\mathcal{B}}{\mathbf{G}} = e^{2\omega^{\mathrm{s}}(T^{\mathrm{s}}(R,t))}\begin{bmatrix} \varsigma^2(R) & 0 & 0 \\ 0 & \bar{r}^2(R) & 0 \\ 0 & 0 & \bar{r}^2(R)\sin^2\Theta \end{bmatrix}, \tag{4.18}$$

where the scalar function $\omega^{\mathrm{s}}(T^{\mathrm{s}})$ characterizes isotropic and homogeneous thermal expansion in the solid phase. Substituting the determinants of (4.1), (4.18), (4.5) and (4.10) into (2.12), the Jacobian of the deformation is written as

$$J(R,t) = \begin{cases} \sqrt{\dfrac{\det\mathbf{g}}{\det\overset{\mathcal{L}}{\mathbf{G}}}}\,\det\mathbf{F}^{\mathrm{f}}\,, & 0\le R\le S(t)\,, \\ \sqrt{\dfrac{\det\mathbf{g}}{\det\overset{\mathcal{B}}{\mathbf{G}}}}\,\det\mathbf{F}^{\mathrm{s}}\,, & S(t)\le R\le R_0\,, \end{cases} = \begin{cases} \dfrac{\left[r^{\mathrm{f}}(R,t)\right]^2 r^{\mathrm{f}}{}_{,R}(R,t)}{e^{3\omega^{\mathrm{f}}(T^{\mathrm{f}}(R,t))}\,R^2}\,, & 0\le R\le S(t)\,, \\ \dfrac{\left[r^{\mathrm{s}}(R,t)\right]^2 r^{\mathrm{s}}{}_{,R}(R,t)}{e^{3\omega^{\mathrm{s}}(T^{\mathrm{s}}(R,t))}\bar{r}^2(R)\,\varsigma(R)}\,, & S(t)\le R\le R_0\,. \end{cases} \tag{4.19}$$

Further, $\alpha^{\mathrm{s}}(T^{\mathrm{s}}) = \dfrac{\mathrm{d}\omega^{\mathrm{s}}(T^{\mathrm{s}})}{\mathrm{d}T^{\mathrm{s}}}$ and $\alpha^{\mathrm{f}}(T^{\mathrm{f}}) = \dfrac{\mathrm{d}\omega^{\mathrm{f}}(T^{\mathrm{f}})}{\mathrm{d}T^{\mathrm{f}}}$ are the coefficients of thermal expansion in the solid and liquid phases, respectively.

Remark 4.1. Since $\dot{s}(t)$ is the radial velocity of ω_t and $r^{\mathrm{f}}{}_{,t}(S(t),t)$ is the radial velocity of liquid points just before attachment, the accretion velocity is $u(t) = \dot{s}(t) - r^{\mathrm{f}}{}_{,t}(S(t),t)$. Further, it follows from (4.7) that $r^{\mathrm{f}}{}_{,R}(S(t),t) = \frac{u(t)}{U(t)}$, i.e., $Q^r{}_R(R) = (F^{\mathrm{f}})^r{}_R(R,\tau(R))$.

4.2. Balance laws

4.2.1. Conservation of mass

The mass of the liquid and solid portions are calculated as[30]

$$\begin{aligned} m^{\mathrm{f}}(t) &= \int_0^{S(t)} e^{3\omega^{\mathrm{f}}\left(T^{\mathrm{f}}(R,t)\right)}\rho^{\mathrm{f}}(R,t)\,4\pi R^2\,\mathrm{d}R = \int_0^{S(t)}\rho_0^{\mathrm{f}}(R)\,4\pi R^2\,\mathrm{d}R\,, \\ m^{\mathrm{s}}(t) &= \int_{S(t)}^{R_0} e^{3\omega^{\mathrm{s}}(T^{\mathrm{s}}(R,t))}\rho^{\mathrm{s}}(R,t)\,4\pi\bar{r}^2(R)\,\varsigma(R)\,\mathrm{d}R = \int_{S(t)}^{R_0}\rho_0^{\mathrm{s}}(R)\,4\pi\bar{r}^2(R)\,\varsigma(R)\,\mathrm{d}R\,. \end{aligned} \tag{4.20}$$

Thus, the total mass of the system $m(t) = m^{\mathrm{f}}(t) + m^{\mathrm{s}}(t)$ is written as

$$m(t) = \int_0^{S(t)}\rho_0^{\mathrm{f}}(R)\,4\pi R^2\,\mathrm{d}R + \int_{S(t)}^{R_0}\rho_0^{\mathrm{s}}(R)\,4\pi\bar{r}^2(R)\,\varsigma(R)\,\mathrm{d}R\,. \tag{4.21}$$

Using the Leibniz rule, it can be shown that

$$\dot{m}(t) = 4\pi\left[\rho_0^{\mathrm{f}}(S(t))\,S^2(t) - \rho_0^{\mathrm{s}}(S(t))\,s^2(t)\,\varsigma(S(t))\right]\dot{S}(t)\,. \tag{4.22}$$

[29] This scaling is essential to account for the deformation present in the accreting layer just before attachment. The specific format assumed in (4.15) ensures that there are only radial deformations, i.e., the accreting layers are radially dilated or contracted just before attachment.

[30] Alternatively, one has $m^{\mathrm{f}}(t) = \int_0^{s(t)}\varrho^{\mathrm{f}}(r,t)\,4\pi r^2\,\mathrm{d}r$, and $m^{\mathrm{s}}(t) = \int_{s(t)}^{R_0}\varrho^{\mathrm{s}}(r,t)\,4\pi r^2\,\mathrm{d}r$.

As the mass of the entire body is conserved, $\dot{m}(t) = 0$. Since $\dot{S}(t)$ is nonzero, it follows from (4.22) that

$$\rho_0^{\mathrm{f}}(S(t))\, S^2(t) = \rho_0^{\mathrm{s}}(S(t))\, s^2(t)\, \varsigma(S(t))\,. \tag{4.23}$$

The material continuity in the respective phases read[31]

$$\rho^{\mathrm{s}}{}_{,t}(R,t) + \beta^{\mathrm{s}}\big(T^{\mathrm{s}}(R,t)\big)\, T^{\mathrm{s}}{}_{,t}(R,t)\rho^{\mathrm{s}}(R,t) = 0\,, \qquad \rho^{\mathrm{f}}{}_{,t}(R,t) + \beta^{\mathrm{f}}\big(T^{\mathrm{f}}(R,t)\big)\, T^{\mathrm{f}}{}_{,t}(R,t)\rho^{\mathrm{f}}(R,t) = 0\,. \tag{4.25}$$

The density is assumed to be a function of temperature, i.e., $\rho^{\mathrm{s}}(R,t) = \hat{\rho}^{\mathrm{s}}(T^{\mathrm{s}}(R,t))$ and $\rho^{\mathrm{f}}(R,t) = \hat{\rho}^{\mathrm{f}}(T^{\mathrm{f}}(R,t))$. It follows that $\rho_0^{\mathrm{s}}(R) = \hat{\rho}^{\mathrm{s}}(T_0^{\mathrm{s}}(R))$ and $\rho_0^{\mathrm{f}}(R) = \hat{\rho}^{\mathrm{f}}(T_0^{\mathrm{f}}(R))$, where $T_0^{\mathrm{s}}(R)$ and $T_0^{\mathrm{f}}(R)$ are the reference temperatures for the solid and liquid phases, respectively. Thus, the respective continuity equations in (4.25) are rewritten as

$$\frac{\mathrm{d}\hat{\rho}^{\mathrm{s}}}{\mathrm{d}T^{\mathrm{s}}} + \beta^{\mathrm{s}}\hat{\rho}^{\mathrm{s}} = 0\,, \qquad \frac{\mathrm{d}\hat{\rho}^{\mathrm{f}}}{\mathrm{d}T^{\mathrm{f}}} + \beta^{\mathrm{f}}\hat{\rho}^{\mathrm{f}} = 0\,. \tag{4.26}$$

This is integrated to obtain

$$\hat{\rho}^{\mathrm{s}}(T^{\mathrm{s}}) = \hat{\rho}^{\mathrm{s}}(T_0^{\mathrm{s}}) - \int_{T_0^{\mathrm{s}}}^{T^{\mathrm{s}}} \beta^{\mathrm{s}}(\tau)\,\hat{\rho}^{\mathrm{s}}(\tau)\,\mathrm{d}\tau\,, \qquad \hat{\rho}^{\mathrm{f}}(T^{\mathrm{f}}) = \hat{\rho}^{\mathrm{f}}(T_0^{\mathrm{f}}) - \int_{T_0^{\mathrm{f}}}^{T^{\mathrm{f}}} \beta^{\mathrm{f}}(\tau)\,\hat{\rho}^{\mathrm{f}}(\tau)\,\mathrm{d}\tau\,, \tag{4.27}$$

which are equivalent to

$$\rho^{\mathrm{s}}(R,t) = \rho_0^{\mathrm{s}}(R) - \int_{T_0^{\mathrm{s}}(R)}^{T^{\mathrm{s}}(R,t)} \beta^{\mathrm{s}}(\tau)\,\hat{\rho}^{\mathrm{s}}(\tau)\,\mathrm{d}\tau\,, \qquad \rho^{\mathrm{f}}(R,t) = \rho_0^{\mathrm{f}}(R) - \int_{T_0^{\mathrm{f}}(R)}^{T^{\mathrm{f}}(R,t)} \beta^{\mathrm{f}}(\tau)\,\hat{\rho}^{\mathrm{f}}(\tau)\,\mathrm{d}\tau\,. \tag{4.28}$$

Note that $T_0^{\mathrm{f}}(R)$ is the initial temperature of the liquid, while $T_0^{\mathrm{s}}(R)$ represents the accretion temperature, i.e., $T_0^{\mathrm{s}}(R) = T_m$.

Remark 4.2. To simplify the problem, it can be assumed that the liquid is initially at the solidification temperature, i.e., $T_0^{\mathrm{f}}(R) = T_m$. Thus, there is no heat transfer in the liquid medium, i.e., $T^{\mathrm{f}}(R,t) = T_m$. Hence, it follows from $(4.28)_2$ that $\rho^{\mathrm{f}}(R,t) = \rho^{\mathrm{f}}(R,0) = \rho_0^{\mathrm{f}}(R) = \rho_0^{\mathrm{f}}$, which is a constant for homogeneous fluids.[32] Similarly, $\rho^{\mathrm{s}}(R,t) = \rho_0^{\mathrm{s}} - \int_{T_m}^{T^{\mathrm{s}}(R,t)} \beta^{\mathrm{s}}(\tau)\,\hat{\rho}^{\mathrm{s}}(\tau)\,\mathrm{d}\tau$, where ρ_0^{s} is a constant for homogeneous solids. As $T^{\mathrm{s}}(S(t),t) = T_m$, it follows from $(4.25)_2$ that $\rho^{\mathrm{s}}(S(t),t) = \rho_0^{\mathrm{s}}$. Therefore, one has

$$\varsigma(S(t)) = \frac{\rho_0^{\mathrm{f}}\, S^2(t)}{\rho_0^{\mathrm{s}}\, s^2(t)}\,, \qquad \text{or equivalently,} \qquad \varsigma(R) = \frac{\rho_0^{\mathrm{f}}\, R^2}{\rho_0^{\mathrm{s}}\, \bar{r}^2(R)}\,. \tag{4.29}$$

Thus

$$\eta(S(t)) = \frac{\rho_0^{\mathrm{f}}\, S^2(t)\, U(t)}{\rho_0^{\mathrm{s}}\, s^2(t)\, u(t)}\,, \qquad \text{or equivalently,} \qquad \eta(R) = \frac{\rho_0^{\mathrm{f}}\, R^2 \bar{U}(R)}{\rho_0^{\mathrm{s}}\, \bar{r}^2(R)\bar{u}(R)}\,. \tag{4.30}$$

Further, the mass fraction solidified up to time t is simplified as $\frac{m^{\mathrm{s}}(t)}{m(t)} = 1 - \frac{S^3(t)}{R_0^3}$.

Remark 4.3. The material metric for the solid phase has the following representation

$$\overset{B}{\mathbf{G}} = e^{2\omega^{\mathrm{s}}(T^{\mathrm{s}}(R,t))} \begin{bmatrix} \frac{(\rho_0^{\mathrm{f}})^2\, R^4}{(\rho_0^{\mathrm{s}})^2\, \bar{r}^4(R)} & 0 & 0 \\ 0 & \bar{r}^2(R) & 0 \\ 0 & 0 & \bar{r}^2(R)\sin^2\Theta \end{bmatrix}. \tag{4.31}$$

The Jacobian is rewritten as

$$J(R,t) = \begin{cases} \dfrac{\big[r^{\mathrm{f}}(R,t)\big]^2\, r^{\mathrm{f}}{}_{,R}(R,t)}{e^{3\omega^{\mathrm{f}}(T^{\mathrm{f}}(R,t))}\, R^2}\,, & 0 \le R \le S(t)\,, \\ \dfrac{\rho_0^{\mathrm{s}}\,\big[r^{\mathrm{s}}(R,t)\big]^2\, r^{\mathrm{s}}{}_{,R}(R,t)}{\rho_0^{\mathrm{f}}\, e^{3\omega^{\mathrm{s}}(T^{\mathrm{s}}(R,t))}\, R^2}\,, & S(t) \le R \le R_0\,. \end{cases} \tag{4.32}$$

4.2.2. Heat equation

Let $\mathbf{q}(R,t)$ denote the spatial heat flux in material coordinates, i.e., $\mathbf{q}(R,t) = \mathbf{h}(r(R,t),t)$, with $\mathbf{H}(R,t)$ being the material heat flux. In the model $\mathbf{H} = -K\mathbf{G}^{\sharp}\mathrm{d}T$, the radial components of $\mathbf{H}(R,t)$ and $\mathbf{q}(R,t)$ within the solid are as follows

$$H^{R}(R,t) = -\frac{K(T(R,t))\, T_{,R}(R,t)}{e^{2\omega^{\mathrm{s}}(T(R,t))}\, \varsigma^2(R)}\,, \qquad q^{r}(R,t) = -\frac{1}{\varsigma(R)} e^{\omega^{\mathrm{s}}(T(R,t))} K(T(R,t))\, T_{,R}(R,t)\,. \tag{4.33}$$

[31] Note that

$$\mathrm{tr}_{\overset{B}{\mathbf{G}}}\Big(\overset{B}{\mathbf{G}}_{,t}\Big) = 6\dot{T}^{\mathrm{s}}\frac{\mathrm{d}\omega^{\mathrm{s}}}{\mathrm{d}T^{\mathrm{s}}} = 6\alpha^{\mathrm{s}}\dot{T}^{\mathrm{s}} = 2\beta^{\mathrm{s}}\dot{T}^{\mathrm{s}}\,, \qquad \mathrm{tr}_{\overset{c}{\mathbf{G}}}\Big(\overset{c}{\mathbf{G}}_{,t}\Big) = 6\dot{T}^{\mathrm{f}}\frac{\mathrm{d}\omega^{\mathrm{f}}}{\mathrm{d}T^{\mathrm{f}}} = 6\alpha^{\mathrm{f}}\dot{T}^{\mathrm{f}} = 2\beta^{\mathrm{f}}\dot{T}^{\mathrm{f}}\,, \tag{4.24}$$

where the relations $\beta^{\mathrm{s}} = 3\alpha^{\mathrm{s}}$ and $\beta^{\mathrm{f}} = 3\alpha^{\mathrm{f}}$ have been used. Therefore, (4.25) follows from (3.3) and (4.24).

[32] Alternatively, by substituting $T^{\mathrm{f}}{}_{,t} = 0$ into $(4.25)_2$, it is implied that $\rho^{\mathrm{f}}{}_{,t} = 0$.

Note that[33]

$$\mathrm{Div}_{\mathbf{G}}\,\mathbf{H} = -\frac{1}{e^{2\omega}\,\varsigma^2}\left[\left(\frac{\mathrm{d}K}{\mathrm{d}T} + \alpha^{\mathrm{s}}K\right)T_{,R}{}^2 + KT_{,RR} + \left(\frac{2\bar{r}'}{\bar{r}} - \frac{\varsigma'}{\varsigma}\right)KT_{,R}\right], \tag{4.36}$$

where the notation $(\cdot)' := \frac{\mathrm{d}}{\mathrm{d}R}(\cdot)$ has been used. Therefore, the heat equation (3.29) inside the solid is written as

$$KT_{,RR} + \left(\frac{\mathrm{d}K}{\mathrm{d}T} + \alpha^{\mathrm{s}}K\right)T_{,R}{}^2 + \left(\frac{2\bar{r}'}{\bar{r}} - \frac{\varsigma'}{\varsigma}\right)KT_{,R} = e^{2\omega^{\mathrm{s}}}\,\varsigma^2\rho\,c_E\,\dot{T}\,. \tag{4.37}$$

Let us assume that the heat conduction coefficient is independent of temperature, i.e., $K(T) = K^{\mathrm{s}}$, a constant. Thus, using (4.29), the heat equation (4.37) is simplified as follows

$$D^{\mathrm{s}}_{\mathrm{f}}\left\{T_{,RR}(R,t) + \alpha^{\mathrm{s}}(T(R,t))\left[T_{,R}(R,t)\right]^2 + \left[\frac{4\bar{r}'(R)}{\bar{r}(R)} - \frac{2}{R}\right]T_{,R}(R,t)\right\} = \frac{R^4\,\dot{T}(R,t)}{\bar{r}^4(R)\,e^{\omega^{\mathrm{s}}(T(R,t))}}\,, \tag{4.38}$$

where the constant $D^{\mathrm{s}}_{\mathrm{f}} = \dfrac{K^{\mathrm{s}}(\rho^{\mathrm{s}}_0)^3}{c_E(\rho^{\mathrm{f}}_0)^4}$ is analogous to thermal diffusivity. Further, the temperature field $T^{\mathrm{s}}(R,t)$ satisfies the following boundary conditions

$$-K^{\mathrm{s}}T^{\mathrm{s}}_{,R}(R_0,t) = h_c\left[T^{\mathrm{s}}(R_0,t) - T_c\right], \qquad T^{\mathrm{s}}(S(t),t) = T_m\,, \tag{4.39}$$

where h_c is the coefficient of heat transfer between the walls of the container and the solidified material. Thus, for the temperature field, we have a Neumann boundary condition near the fixed wall of the container and a Dirichlet boundary condition on the moving interface.

4.2.3. Stefan's condition

The rate of mass transferred from liquid to solid phase is $\dot{m}^{\mathrm{s}}(t) = -\dot{m}^{\mathrm{f}}(t)$. The rate of mass solidified is

$$\dot{m}^{\mathrm{s}}(t) = -4\pi\rho^{\mathrm{s}}_0\,s^2(t)\,\varsigma\,(S(t))\,\dot{S}(t) = -4\pi\rho^{\mathrm{s}}_0\,s^2(t)\,u(t)\,. \tag{4.40}$$

Alternatively, $\dot{m}^{\mathrm{s}}$ can be expressed as

$$\dot{m}^{\mathrm{s}}(t) = -\dot{m}^{\mathrm{f}}(t) = -4\pi\rho^{\mathrm{f}}_0\,S^2(t)\,U(t)\,. \tag{4.41}$$

The time rate of heat released during solidification is $l\,\dot{m}^{\mathrm{s}}(t)$. Further, the heat transferred into the solid medium is

$$-\int_{\Omega_t}\langle\!\langle\mathbf{H},\mathbf{N}\rangle\!\rangle_{\overset{\mathcal{B}}{\mathbf{G}}}\mathrm{d}A = -4\pi S^2(t)\left[H^R N^R G_{RR}\right]\Big|_{R=S(t)} = -4\pi S^2(t)\,K(T_m)\,T_{,R}(S(t),t)\,. \tag{4.42}$$

If the liquid is initially at the solidification temperature, there is no heat flux within it, and the heat entering the solid from the phase change interface is equal to the heat generated during solidification. Thus, Stefan's condition is written as

$$S^2(t)\,K(T_m)\,T_{,R}(S(t),t) = l\,\rho^{\mathrm{s}}_0\,s^2(t)\,u(t)\,, \tag{4.43}$$

or equivalently,

$$K(T_m)\,T_{,R}(S(t),t) = l\,\rho^{\mathrm{f}}_0\,\dot{S}(t)\,. \tag{4.44}$$

Assuming a constant heat conduction coefficient $K(T) = K^{\mathrm{s}}$, Stefan's condition is written as

$$T_{,R}(S(t),t) = L\,\dot{S}(t)\,, \tag{4.45}$$

where $L = \frac{\rho^{\mathrm{f}}_0 l}{K^{\mathrm{s}}}$.

4.2.4. Conservation of linear momentum in the solid portion

The Cauchy stress tensor in the solid portion is related to the free energy function $\check{W}(I_1,I_2,J,T)$ as follows[34]

$$\boldsymbol{\sigma} = \left[2J^{-1}I_2\,\frac{\partial\check{W}}{\partial I_2} + \frac{\partial\check{W}}{\partial J}\right]\mathbf{g}^{\sharp} + 2\left[J^{-1}\frac{\partial\check{W}}{\partial I_1}\,\mathbf{b}^{\sharp} - J\frac{\partial\check{W}}{\partial I_2}\,\mathbf{c}^{\sharp}\right]. \tag{4.47}$$

---

[33] Here, we have used the fact that

$$H^A{}_{|A} = -\left[K(T)\,G^{AB}T_{,B}\right]_{|A} = -\frac{\mathrm{d}K}{\mathrm{d}T}\,G^{AB}T_{,A}T_{,B} - KG^{AB}\left(T_{,AB} - \Gamma^C{}_{AB}T_{,C}\right). \tag{4.34}$$

In spherical coordinates, one has

$$\mathrm{Div}_{\mathbf{G}}\,\mathbf{H} = -G^{RR}\left[\frac{\mathrm{d}K}{\mathrm{d}T}T_{,R}{}^2 + KT_{,RR}\right] + KT_{,R}\left[G^{RR}\,\Gamma^R{}_{RR} + G^{\Theta\Theta}\,\Gamma^R{}_{\Theta\Theta} + G^{\Phi\Phi}\,\Gamma^R{}_{\Phi\Phi}\right]. \tag{4.35}$$

The Christoffel symbols $\Gamma^C{}_{AB}$ for the material metric $\overset{\mathcal{B}}{\mathbf{G}}$ are given in (C.3).

[34] Note that the first Piola–Kirchhoff stress tensor $\mathbf{P} = J\boldsymbol{\sigma}\mathbf{F}^{-\star}$ is written as

$$\mathbf{P} = \left[2I_2\,\frac{\partial\check{W}}{\partial I_2} + J\,\frac{\partial\check{W}}{\partial J}\right]\mathbf{F}\mathbf{B}^{\sharp} + 2\left[\frac{\partial\check{W}}{\partial I_1}\,\mathbf{b}^{\sharp}\mathbf{F}^{-\star} - J^2\frac{\partial\check{W}}{\partial I_2}\,\mathbf{F}^{-\mathsf{T}}\mathbf{B}^{\sharp}\right], \tag{4.46}$$

where $\mathbf{b}^{\sharp} = \mathbf{F}\mathbf{G}^{\sharp}\mathbf{F}^{\star}$ and $\mathbf{B}^{\sharp} = \mathbf{F}^{-1}\mathbf{g}^{\sharp}\mathbf{F}^{-\star}$.

Since $V^r(R,t) = r_{,t}(R,t)$, $V^\theta(R,t) = V^\phi(R,t) = 0$, one has $A^r(R,t) = r_{,tt}(R,t)$, and $A^\theta(R,t) = A^\phi(R,t) = 0$.[35] Using (3.16) and (C.1), the radial equilibrium equation (3.17) is simplified to read

$$\frac{\partial \sigma^{rr}}{\partial r} + \frac{2}{r}\sigma^{rr} - r\left[\sigma^{\theta\theta} + \sin^2\theta\,\sigma^{\phi\phi}\right] + \varrho\, b^r = \varrho\, r_{,tt}. \tag{4.48}$$

The inertial effects can be ignored if the solidification process is slow, and hence in the absence of body forces, it follows from (4.48) that

$$\frac{\partial \sigma^{rr}}{\partial R} = \left[\left(\sigma^{\theta\theta} + \sin^2\theta\,\sigma^{\phi\phi}\right) r - \frac{2}{r}\sigma^{rr}\right]\frac{\partial r}{\partial R}. \tag{4.49}$$

In this example,[36]

$$\mathbf{b}^\sharp = e^{-2\omega^s}\begin{bmatrix} \dfrac{r_{,R}^{\,2}}{\varsigma^2} & 0 & 0 \\ 0 & \dfrac{1}{\bar r^2} & 0 \\ 0 & 0 & \dfrac{1}{\bar r^2\sin^2\Theta} \end{bmatrix}, \qquad \mathbf{c}^\sharp = e^{2\omega^s}\begin{bmatrix} \dfrac{\varsigma^2}{r_{,R}^{\,2}} & 0 & 0 \\ 0 & \dfrac{\bar r^2}{r^4} & 0 \\ 0 & 0 & \dfrac{\bar r^2}{r^4\sin^2\Theta} \end{bmatrix}. \tag{4.50}$$

Further, the principal invariants of $\mathbf{b}$ read[37]

$$I_1 = e^{-2\omega^s}\left[\frac{r_{,R}^{\,2}}{\varsigma^2} + \frac{2r^2}{\bar r^2}\right], \qquad I_2 = \frac{1}{2}\left[I_1^2 - e^{-4\omega^s}\left(\frac{r_{,R}^{\,4}}{\varsigma^4} + \frac{2r^4}{\bar r^4}\right)\right] = \frac{r^2}{e^{4\omega^s}\bar r^2}\left[\frac{r^2}{\bar r^2} + \frac{2r_{,R}^{\,2}}{\varsigma^2}\right]. \tag{4.52}$$

The Cauchy stress has the following nonzero components

$$\begin{aligned} \sigma^{rr} &= 2J^{-1}I_2\frac{\partial \check W}{\partial I_2} + \frac{\partial \check W}{\partial J} + 2\left[\frac{r_{,R}^{\,2}}{Je^{2\omega^s}\varsigma^2}\frac{\partial \check W}{\partial I_1} - \frac{Je^{2\omega^s}\varsigma^2}{r_{,R}^{\,2}}\frac{\partial \check W}{\partial I_2}\right], \\ \sigma^{\theta\theta} &= \left[2J^{-1}I_2\frac{\partial \check W}{\partial I_2} + \frac{\partial \check W}{\partial J}\right]\frac{1}{r^2} + 2\left[\frac{1}{Je^{2\omega^s}\bar r^2}\frac{\partial \check W}{\partial I_1} - \frac{Je^{2\omega^s}\bar r^2}{r^4}\frac{\partial \check W}{\partial I_2}\right], \\ \sigma^{\phi\phi} &= \frac{\sigma^{\theta\theta}}{\sin^2\Theta}. \end{aligned} \tag{4.53}$$

Substituting (4.53) in (4.49), one obtains[38]

$$\frac{\partial \sigma^{rr}}{\partial R} = \frac{4r_{,R}}{r}\left[\frac{1}{J\,e^{2\omega^s}}\left(\frac{r^2}{\bar r^2} - \frac{r_{,R}^{\,2}}{\varsigma^2}\right)\frac{\partial \check W}{\partial I_1} + J\,e^{2\omega^s}\left(\frac{\bar r^2}{r^2} - \frac{\varsigma^2}{r_{,R}^{\,2}}\right)\frac{\partial \check W}{\partial I_2}\right]. \tag{4.54}$$

In the solid, one has $J = \dfrac{r^2 r_{,R}}{e^{3\omega^s}\bar r^2\varsigma_2}$. Thus, (4.54) is simplified as

$$\frac{\partial \sigma^{rr}}{\partial R} = 4\check W_1 e^{\omega^s}\left[\frac{\varsigma}{r} - \frac{\bar r^2 r_{,R}}{\varsigma r^3}\right] + \frac{4\check W_2}{e^{\omega^s}}\left[\frac{r_{,R}^{\,2}}{\varsigma r} - \frac{\varsigma r}{\bar r^2}\right], \tag{4.55}$$

where $\check W_i = \frac{\partial \check W}{\partial I_i}$ for $i = 1, 2$. Using (4.29), (4.55) is rewritten as follows

$$\sigma^{rr}_{,R} = 4\left[\check W_1 e^{\omega^s} - \frac{\check W_2\, r^2}{e^{\omega^s}\bar r^2}\right]\left[\frac{\rho_0^{\rm f} R^2}{\rho_0^{\rm s}\bar r^2 r} - \frac{\rho_0^{\rm s}\bar r^4 r_{,R}^{\,2}}{\rho_0^{\rm f} R^2 r^3}\right]. \tag{4.56}$$

Hence, (4.56) can be integrated to obtain

$$\sigma^{rr}(R,t) = \sigma^{rr}(S(t),t) + 4\int_{S(t)}^{R}\left[\check W_1(\xi,t)e^{\omega^s(T(\xi,t))} - \frac{\check W_2(\xi,t)r^2(\xi,t)}{e^{\omega^s(T(\xi,t))}\bar r^2(\xi)}\right]\left[\frac{\rho_0^{\rm f}\xi^2}{\rho_0^{\rm s}\bar r^2(\xi)r(\xi,t)} - \frac{\rho_0^{\rm s}\bar r^4(\xi)\,r_{,R}^{\,2}(\xi,t)}{\rho_0^{\rm f}\xi^2 r^3(\xi,t)}\right]{\rm d}\xi. \tag{4.57}$$

Remark 4.4. Note that $\sigma^{rr}(R,t)$ has to be continuous at $R = S(t)$ in order to satisfy the traction continuity across the phase change interface.

---

[35] The Christoffel symbols for the Euclidean metric $\mathbf{g}$ are given in (C.1).

[36] Recall that the components of $\mathbf{c}^\sharp$ and $\mathbf{c}^\flat$ are related as $c^{ab} = g^{am}c_{mn}g^{nb}$. Thus, the components $c^\sharp$ are $c^{ab} = g^{am}F^{-A}{}_m G_{AB}F^{-B}{}_n g^{nb}$.

[37] Here, we have used the fact that

$$I_1 = g_{ab}F^a{}_A F^b{}_B G^{AB}, \qquad I_2 = \frac{1}{2}\left(I_1^2 - g_{mb}g_{na}F^m{}_M F^n{}_N F^a{}_A F^b{}_B G^{AM}G^{BN}\right). \tag{4.51}$$

.

[38] The relation $r^2\left[g^{\theta\theta} + \sin^2\theta\, g^{\phi\phi}\right] = 2g^{rr}$ has been used here.

4.2.5. Conservation of linear momentum inside the liquid

The Cauchy stress inside the liquid is related to the free energy function $\check{W}(J,T)$ as $\boldsymbol{\sigma} = \frac{\partial \check{W}}{\partial J}\mathbf{g}^{\sharp}$, i.e.,

$$\boldsymbol{\sigma} = \frac{\partial \check{W}}{\partial J}\begin{bmatrix} 1 & 0 & 0 \\ 0 & \frac{1}{r^2} & 0 \\ 0 & 0 & \frac{1}{r^2\sin^2\theta} \end{bmatrix}. \tag{4.58}$$

Note that $r^2\left[\sigma^{\theta\theta} + \sin^2\theta\,\sigma^{\phi\phi}\right] = 2\sigma^{rr}$. In the absence of inertial effects and body forces, the radial equilibrium equation is written as

$$r\frac{\partial \sigma^{rr}}{\partial R} = \left[(\sigma^{\theta\theta} + \sin^2\theta\,\sigma^{\phi\phi})\,r^2 - 2\sigma^{rr}\right]\frac{\partial r}{\partial R} = 0\,. \tag{4.59}$$

Hence, it follows that $\frac{\partial \sigma^{rr}}{\partial R}$, i.e., $\sigma^{rr}(R,t)$ is independent of R. Moreover, one has

$$\frac{\partial}{\partial R}\left(\frac{\partial \check{W}}{\partial J}\right) = 0\,. \tag{4.60}$$

If the liquid is initially at the melting temperature, then $T^{\mathrm{f}}(R,t) = T_m$ and there is no heat transfer occurring inside the liquid during the entire process. Because there are no temperature changes, $\check{W}$ and, consequently, $\frac{\partial \check{W}}{\partial J}$ remain independent of temperature. Let us define the temperature-independent function $\check{p}(J)$ as $\check{p} = \frac{\partial \check{W}}{\partial J}$, and denote $p(R,t) = \check{p}(J(R,t))$. Since $\frac{\partial}{\partial R}\left(\frac{\partial \check{W}}{\partial J}\right) = \frac{\mathrm{d}\check{p}}{\mathrm{d}J}\frac{\partial J}{\partial R}$, it follows from (4.60) that $\frac{\partial J}{\partial R} = 0$ (Podio-Guidugli et al., 1985). Thus, J is independent of R, which is indicated as $J(R,t) = J_0(t)$, for some function $J_0(t) > 0$. Note that $\omega^{\mathrm{f}}(T^{\mathrm{f}}) = 0$ because $T^{\mathrm{f}} = T_m$ throughout the process. Since $(4.32)_1$ is simplified as $J = \frac{r^2 r_{,R}}{R^2}$, it is implied that inside the liquid one has

$$r^3(R,t) = s^3(t) + J_0(t)\left[R^3 - S^3(t)\right]\,. \tag{4.61}$$

Since $r(0,t) = 0$, it follows from (4.61) that $J_0(t) = \frac{s^3(t)}{S^3(t)}$, and hence $r(R,t) = \frac{R\,s(t)}{S(t)}$.[39] Thus,

$$\sigma^{rr}(R,t) = \sigma^{rr}(S(t),t) = \check{p}\left(\frac{s^3(t)}{S^3(t)}\right)\,. \tag{4.62}$$

In our numerical examples, we consider the following temperature-independent free energy function

$$\check{W}(J) = \pi_0^{\mathrm{f}} J + \kappa_0^{\mathrm{f}}(J-1)^2\,, \tag{4.63}$$

where κ_0^{f} denotes the bulk modulus of the liquid at temperature T_0, while π_0^{f} represents the initial pressure in the liquid (Ghosh and Lopez-Pamies, 2022). Hence, $\check{p}(J) = \pi_0^{\mathrm{f}} + \kappa_0^{\mathrm{f}}(J-1)$, and $\boldsymbol{\sigma} = \left[\pi_0^{\mathrm{f}} + \kappa_0^{\mathrm{f}}(J-1)\right]\mathbf{g}^{\sharp}$. If the liquid is initially stress-free, i.e., $\boldsymbol{\sigma}(R,0) = \mathbf{0}$, then, it can be deduced from $J_0(0) = 1$ that $\pi_0^{\mathrm{f}} = 0$. Therefore, one has

$$p(R,t) = \sigma^{rr}(R,t) = \kappa_0^{\mathrm{f}}\left[\frac{s^3(t)}{S^3(t)} - 1\right]\,. \tag{4.64}$$

This means that the Cauchy stress remains uniform in a compressible hyperelastic fluid in the absence of inertial effects, body forces, and heat flow.

4.2.6. The moving boundary problem

The balance laws from the previous subsections are combined into the following system of general governing equations to model the accretion problem

$$\begin{cases} \mathrm{div}_{\mathbf{g}}\,\boldsymbol{\sigma} = \mathbf{0} & \text{in } \mathcal{Z}\setminus(\Omega_0\cup\Omega_t)\,, \\ [\![\boldsymbol{\sigma}\overset{\mathcal{L}}{\mathbf{n}}{}^{\flat}]\!] = \mathbf{0} & \text{across } \omega_t\,, \\ \varphi_t = \mathrm{id}_{\mathcal{Z}} & \text{on } \Omega_0 \\ \rho\,c_E\,\dot{T} = \mathrm{Div}_{\mathbf{G}}\left(K\mathbf{G}^{\sharp}\,\mathrm{d}T\right) & \text{in } \mathcal{Z}\setminus(\Omega_0\cup\Omega_t)\,, \\ T = T_m & \text{on } \Omega_t\,, \\ \langle\!\langle \mathbf{H}, \overset{S}{\mathbf{N}}\rangle\!\rangle_{\mathbf{G}} = h_c\left[T - T_c\right] & \text{on } \Omega_0\,, \\ [\![\langle\!\langle \mathbf{H}, \overset{\mathcal{L}}{\mathbf{N}}\rangle\!\rangle_{\mathbf{G}}]\!] = l\rho\,U & \text{across } \Omega_t\,, \end{cases} \tag{4.65}$$

where $[\![\cdot]\!]$ denotes the jump across the moving interface, as one goes from the liquid phase to the solid phase. $\overset{\mathcal{L}}{\mathbf{N}}$ and $\overset{\mathcal{L}}{\mathbf{n}}$ are the outward unit normals to the liquid inclusion in the reference and deformed configurations, $\mathcal{L}_t$ and $\varphi_t(\mathcal{L}_t)$, respectively. $\overset{S}{\mathbf{N}}$ is the unit

[39] Furthermore, it is implied that $r^{\mathrm{f}}{}_{,R}(R,t) = \frac{s(t)}{S(t)}$ and $r^{\mathrm{f}}{}_{,t}(R,t) = \frac{R[S(t)\dot{s}(t) - s(t)\dot{S}(t)]}{S^2(t)}$ inside the liquid. Thus, $r^{\mathrm{f}}{}_{,R}(S(t),t) = \frac{s(t)}{S(t)}$ and $r^{\mathrm{f}}{}_{,t}(S(t),t) = \dot{s}(t) - \frac{s(t)\dot{S}(t)}{S(t)}$, which agrees with the fact that $\dot{s}(t) = r^{\mathrm{f}}{}_{,R}(S(t),t)\,\dot{S}(t) + r^{\mathrm{f}}{}_{,t}(S(t),t)$.

normal to $\mathcal{B}_t$. Note that the conservation of linear momentum $(4.65)_1$ and the heat equation $(4.65)_4$ must be solved separately in the solid and liquid regions. Since the liquid is initially at the melting point, the heat equation admits a constant trivial solution inside the inclusion. Recall that the spatial metric $\mathbf{g}$ is the flat Euclidean metric. The material metric in the liquid $\overset{\mathcal{L}}{\mathbf{G}}$, is also the flat Euclidean metric, while the material metric $\overset{\mathcal{B}}{\mathbf{G}}$ for the accreted solid was obtained in (4.31), using the conservation of mass for the entire $\mathcal{Z}$. The Cauchy stress $\boldsymbol{\sigma}$ is computed using (3.14) inside the solid and using (3.15) inside the liquid. In the absence of body forces, inertial effects, and thermal effects, the liquid deformation was given in (4.61), and for the simple energy function (4.63), the Cauchy stress is given in (4.64). Thus, it remains to solve $(4.65)_1$ and $(4.65)_4$ inside the solid to obtain the deformation and temperature fields, along with the location of Ω_t. This is done in the following subsection for a neo-Hookean solid.

4.3. Stefan's problem for a neo-Hookean solid

Consider the following free energy function for a thermoelastic neo-Hookean solid (Sozio et al., 2020)

$$\check{W}(I_1,J,T)=\left[\frac{\mu_0^{\mathrm{s}}}{2}(J^{-\frac{2}{3}}I_1-3)+\frac{\kappa_0^{\mathrm{s}}}{2}(J-1)^2\right]\frac{T}{T_0}-\kappa_0^{\mathrm{s}}\beta_0^{\mathrm{s}}(J-1)(T-T_0)\,, \tag{4.66}$$

where $I_1=e^{-2\omega^{\mathrm{s}}}\left[\frac{(\rho_0^{\mathrm{s}})^2\bar{r}^4 r_{,R}{}^2}{(\rho_0^{\mathrm{f}})^2R^4}+\frac{2r^2}{\bar{r}^2}\right]$ and $J=\frac{\rho_0^{\mathrm{s}}r^2\,r_{,R}}{\rho_0^{\mathrm{f}}e^{3\omega^{\mathrm{s}}}R^2}$. For more details, refer to Appendix B. The nonzero components of Cauchy stress read

$$\sigma^{rr}=\check{W}_J+\frac{2\check{W}_1\,r_{,R}{}^2}{Je^{2\omega^{\mathrm{s}}}\varsigma^2}\,,\qquad \sigma^{\theta\theta}=\frac{\check{W}_J}{r^2}+\frac{2\check{W}_1}{Je^{2\omega^{\mathrm{s}}}\bar{r}^2}\,,\qquad \sigma^{\phi\phi}=\frac{\sigma^{\theta\theta}}{\sin^2\Theta}\,, \tag{4.67}$$

where $\check{W}_J:=\frac{\partial\check{W}}{\partial J}$. These coefficients are calculated as follows

$$\check{W}_1=\frac{\mu_0^{\mathrm{s}}T}{2T_0}J^{-\frac{2}{3}}\,,\qquad \check{W}_J=\left[\kappa_0^{\mathrm{s}}(J-1)-\frac{\mu_0^{\mathrm{s}}}{3}J^{-\frac{5}{3}}I_1\right]\frac{T}{T_0}-\kappa_0^{\mathrm{s}}\beta_0^{\mathrm{s}}(T-T_0)\,. \tag{4.68}$$

Further, we assume that ω^{s} depends on the temperature as per the following relation (see (B.4))

$$e^{3\omega^{\mathrm{s}}(T)}=1+\beta_0^{\mathrm{s}}T_0^{\mathrm{s}}\left(1-\frac{T_0^{\mathrm{s}}}{T}\right). \tag{4.69}$$

Since σ^{rr} is continuous across $R=S(t)$, it follows from (4.57) and (4.64) that

$$\sigma^{rr}(R,t)=\kappa_0^{\mathrm{f}}\left[\frac{s^3(t)}{S^3(t)}-1\right]+4\int_{S(t)}^{R}\check{W}_1(\xi,t)e^{\omega^{\mathrm{s}}(T(\xi,t))}\left[\frac{\rho_0^{\mathrm{f}}\xi^2}{\rho_0^{\mathrm{s}}\bar{r}^2(\xi)r(\xi,t)}-\frac{\rho_0^{\mathrm{s}}\bar{r}^4(\xi)\,r_{,R}{}^2(\xi,t)}{\rho_0^{\mathrm{f}}\xi^2r^3(\xi,t)}\right]\mathrm{d}\xi\,. \tag{4.70}$$

Thus, using $(4.67)_1$ and (4.29), (4.70) is rewritten as

$$\begin{aligned}\check{W}_J(R,t)+\frac{2\rho_0^{\mathrm{s}}\bar{r}^4(R)\,r_{,R}(R,t)}{\rho_0^{\mathrm{f}}R^2\,r^2(R,t)}\check{W}_1(R,t)\,e^{\omega^{\mathrm{s}}(T(R,t))}&=\kappa_0^{\mathrm{f}}\left[\frac{s^3(t)}{S^3(t)}-1\right]\\&+4\int_{S(t)}^{R}\check{W}_1(\xi,t)e^{\omega^{\mathrm{s}}(T(\xi,t))}\left[\frac{\rho_0^{\mathrm{f}}\xi^2}{\rho_0^{\mathrm{s}}\bar{r}^2(\xi)r(\xi,t)}-\frac{\rho_0^{\mathrm{s}}\bar{r}^4(\xi)\,r_{,R}{}^2(\xi,t)}{\rho_0^{\mathrm{f}}\xi^2r^3(\xi,t)}\right]\mathrm{d}\xi\,,\end{aligned} \tag{4.71}$$

where

$$\begin{aligned}\check{W}_1&=\frac{\mu_0^{\mathrm{s}}T\,e^{2\omega^{\mathrm{s}}}}{2T_0}\left[\frac{\rho_0^{\mathrm{f}}R^2}{\rho_0^{\mathrm{s}}r^2\,r_{,R}}\right]^{\frac{2}{3}}\,,\\ \check{W}_J&=\frac{\kappa_0^{\mathrm{s}}T}{T_0}\left[\frac{\rho_0^{\mathrm{s}}r^2\,r_{,R}}{\rho_0^{\mathrm{f}}e^{3\omega^{\mathrm{s}}}R^2}-1\right]-\kappa_0^{\mathrm{s}}\beta_0^{\mathrm{s}}(T-T_0)-\frac{\mu_0^{\mathrm{s}}T\,e^{3\omega^{\mathrm{s}}}}{3T_0}\left[\frac{\rho_0^{\mathrm{f}}R^2}{\rho_0^{\mathrm{s}}r^2\,r_{,R}}\right]^{\frac{5}{3}}\left[\frac{(\rho_0^{\mathrm{s}})^2\bar{r}^4r_{,R}{}^2}{(\rho_0^{\mathrm{f}})^2R^4}+\frac{2r^2}{\bar{r}^2}\right]\,.\end{aligned} \tag{4.72}$$

Therefore, for the neo-Hookean solid, the moving boundary problem (4.65) on the domain $R_0 \geq R \geq S(t)$ is written as[40]

$$\begin{cases} \check{W}_J(R,t) + \dfrac{2\rho_0^{\mathrm{s}}\,\check{W}_1(R,t)\,e^{\omega^{\mathrm{s}}(T(R,t))}\,\bar{r}^4(R)\,r_{,R}(R,t)}{\rho_0^{\mathrm{f}}\,R^2\,r^2(R,t)} = \kappa_0^{\mathrm{f}}\left[\dfrac{s^3(t)}{S^3(t)} - 1\right] \\ \qquad\qquad +4\displaystyle\int_{S(t)}^{R} \check{W}_1(\xi,t) e^{\omega^{\mathrm{s}}(T(\xi,t))}\left[\dfrac{\rho_0^{\mathrm{f}}\,\xi^2}{\rho_0^{\mathrm{s}}\,\bar{r}^2(\xi) r(\xi,t)} - \dfrac{\rho_0^{\mathrm{s}}\,\bar{r}^4(\xi)\,r_{,R}{}^2(\xi,t)}{\rho_0^{\mathrm{f}}\,\xi^2 r^3(\xi,t)}\right]\mathrm{d}\xi\,, \\ \dfrac{K^{\mathrm{s}}(\rho_0^{\mathrm{s}})^3}{c_E(\rho_0^{\mathrm{f}})^4}\left[T_{,RR}(R,t) + \alpha^{\mathrm{s}}(T(R,t))\left[T_{,R}(R,t)\right]^2 + \left[\dfrac{4\bar{r}'(R)}{\bar{r}(R)} - \dfrac{2}{R}\right] T_{,R}(R,t)\right] = \dfrac{R^4\,\dot{T}(R,t)}{\bar{r}^4(R) e^{\omega^{\mathrm{s}}(T(R,t))}}\,, \\ T_{,R}(S(t),t) = \dfrac{\rho_0^{\mathrm{f}}\,l}{K^{\mathrm{s}}}\,\dot{S}(t)\,, \\ T(S(t),t) = T_m\,, \\ r(S(t),t) = \bar{r}(S(t)) = s(t)\,, \\ K^{\mathrm{s}} T_{,R}(R_0,t) = h_c\left[T_c - T(R_0,t)\right]\,, \\ r(R_0,t) = R_0\,, \\ S(0) = R_0\,, \end{cases} \tag{4.73}$$

where the temperature field $T(R,t)$, the radial placement map $r(R,t)$, and the location of the moving boundary $S(t)$ are unknown.

Remark 4.5. On the moving boundary, (4.71) is rewritten as

$$\check{W}_J(S(t),t) + \frac{2\rho_0^{\mathrm{s}}\,s^2(t)\,r_{,R}(S(t),t)}{\rho_0^{\mathrm{f}}\,S^2(t)}\,\check{W}_1(S(t),t) = \kappa_0^{\mathrm{f}}\left[\frac{s^3(t)}{S^3(t)} - 1\right]\,, \tag{4.74}$$

where

$$\begin{aligned} \check{W}_1(S(t),t) &= \frac{\mu_0^{\mathrm{s}}}{2}\left[\frac{\rho_0^{\mathrm{f}}\,S^2(t)}{\rho_0^{\mathrm{s}}\,s^2(t)\,r_{,R}(S(t),t)}\right]^{\frac{2}{3}}\,, \\ \check{W}_J(S(t),t) &= \kappa_0^{\mathrm{s}}\left[\frac{\rho_0^{\mathrm{s}} s^2(t)\,r_{,R}(S(t),t)}{\rho_0^{\mathrm{f}}\,S^2(t)} - 1\right] - \frac{\mu_0^{\mathrm{s}}}{3}\left[\frac{\rho_0^{\mathrm{f}}\,S^2(t)}{\rho_0^{\mathrm{s}}\,s^2(t)\,r_{,R}(S(t),t)}\right]^{\frac{5}{3}}\left[\frac{(\rho_0^{\mathrm{s}})^2\,s^4(t)\,r_{,R}{}^2(S(t),t)}{(\rho_0^{\mathrm{f}})^2 S^4(t)} + 2\right]\,. \end{aligned} \tag{4.75}$$

Therefore, traction continuity (4.74) across the moving interface $R = S(t)$ is written as $\mathcal{F}\left(\frac{s(t)}{S(t)}, r_{,R}(S(t),t)\right) = 0$, where

$$\mathcal{F}(x,y) := \kappa_0^{\mathrm{s}}\left[\frac{\rho_0^{\mathrm{s}} x^2\,y}{\rho_0^{\mathrm{f}}} - 1\right] + \frac{2\mu_0^{\mathrm{s}}}{3}\left(\frac{\rho_0^{\mathrm{s}}\,x^2\,y}{\rho_0^{\mathrm{f}}}\right)^{\frac{1}{3}}\left[1 - \frac{(\rho_0^{\mathrm{f}})^2}{(\rho_0^{\mathrm{s}})^2\,x^4\,y^2}\right] + \kappa_0^{\mathrm{f}}\left[1 - x^3\right]\,. \tag{4.76}$$

Since $r^{\mathrm{f}}{}_{,R}(S(t),t) = \frac{s(t)}{S(t)}$, traction continuity implies an implicit relation between $r^{\mathrm{s}}{}_{,R}(S(t),t)$ and $r^{\mathrm{f}}{}_{,R}(S(t),t)$.

Non-dimensionalization. Let $0 \leq \mathtt{R} \leq 1$ and $\mathtt{t} \geq 0$ be the dimensionless radial coordinate and time variable, respectively. The dimensionless radial placement map, temperature field and the location of phase-change interface are denoted by $\mathtt{r}(\mathtt{R},\mathtt{t})$, $\mathtt{T}(\mathtt{R},\mathtt{t})$ and $\mathtt{S}(\mathtt{t})$, respectively. These dimensionless quantities are defined in Table 1. It follows from $(4.73)_1$ and (4.72) that for $1 > R \geq \mathtt{S}(\mathtt{t})$:[41]

$$\begin{aligned} &\mathtt{q}[1 - \mathtt{a}\mathtt{T}(\mathtt{R},\mathtt{t})]\left[\frac{\mathtt{f}\mathtt{r}^2(\mathtt{R},\mathtt{t})\mathtt{r}_{,\mathtt{R}}(\mathtt{R},\mathtt{t})[1 - \mathtt{a}\mathtt{T}(\mathtt{R},\mathtt{t})]}{\mathtt{R}^2[1 - (\mathtt{a}+\mathtt{b})\mathtt{T}(\mathtt{R},\mathtt{t})]} - 1\right] + \mathtt{p}\mathtt{b}\mathtt{T}(\mathtt{R},\mathtt{t}) + 1 - \frac{\mathtt{s}^3(\mathtt{t})}{\mathtt{S}^3(\mathtt{t})} \\ &+ \mathtt{p}[1 - (\mathtt{a}+\mathtt{b})\mathtt{T}(\mathtt{R},\mathtt{t})]\left(\frac{\mathtt{f}\mathtt{r}^2(\mathtt{R},\mathtt{t})\mathtt{r}_{,\mathtt{R}}(\mathtt{R},\mathtt{t})}{\mathtt{R}^2}\right)^{\frac{1}{3}}\left[\frac{\bar{\mathtt{r}}^4(\mathtt{R})}{\mathtt{r}^4(\mathtt{R},\mathtt{t})} - \frac{1}{3}\left(\frac{2\,\mathtt{R}^4}{\mathtt{f}^2\,\bar{\mathtt{r}}^2(\mathtt{R})\,\mathtt{r}^2(\mathtt{R},\mathtt{t})\,\mathtt{r}_{,\mathtt{R}}^2(\mathtt{R},\mathtt{t})} + 1\right)\right] \\ &- 2\mathtt{p}\int_{\mathtt{S}(\mathtt{t})}^{\mathtt{R}}[1 - (\mathtt{a}+\mathtt{b})\mathtt{T}(\zeta,\mathtt{t})]\left(\frac{\mathtt{f}\mathtt{r}^2(\zeta,\mathtt{t})\mathtt{r}_{,\mathtt{R}}(\zeta,\mathtt{t})}{\zeta^2}\right)^{-\frac{2}{3}}\left[\frac{\zeta^2}{\mathtt{f}\bar{\mathtt{r}}^2(\zeta)\mathtt{r}(\zeta,\mathtt{t})} - \frac{\mathtt{f}\,\bar{\mathtt{r}}^4(\zeta)\,\mathtt{r}_{,\mathtt{R}}^2(\zeta,\mathtt{t})}{\zeta^2\mathtt{r}^3(\zeta,\mathtt{t})}\right]\mathrm{d}\zeta = 0\,, \end{aligned} \tag{4.77}$$

[40] Recall that $(4.73)_1$ was obtained in (4.71), while $(4.73)_2$ restates the heat equation (4.38), and $(4.73)_3$ is Stefan's condition (4.45). The thermal boundary conditions are written in $(4.73)_4$ and $(4.73)_6$, while $(4.73)_5$ and $(4.73)_7$ are the kinematic boundary conditions. Finally, $(4.73)_8$ denotes the initial condition for the position of the moving interface.

[41] Since $\mathtt{a} = 1 - \frac{T_c}{T_m}$ and $\mathtt{b} = \beta_0^{\mathrm{s}}[T_m - T_c]$, it follows from (4.69) that $e^{\omega^{\mathrm{s}}(T)} = \left[\frac{1-(\mathtt{a}+\mathtt{b})\mathtt{T}}{1-\mathtt{a}\mathtt{T}}\right]^{\frac{1}{3}}$ and $[T_m - T_c]\,\alpha^{\mathrm{s}}(T) = \frac{\mathtt{b}}{3[1-(\mathtt{a}+\mathtt{b})\mathtt{T}][1-\mathtt{a}\mathtt{T}]}$.

Table 1
Definitions of the scaled variables and the dimensionless parameters incorporated in (4.77)–(4.80).

Category	Definitions
Independent variables	$\mathtt{R} = \frac{R}{R_0}$
	$\mathtt{t} = \frac{K^s(\rho_0^s)^3 t}{c_E(\rho_0^f)^4 R_0^2}$
Dependent unknown variables	$\mathtt{r}(\mathtt{R},\mathtt{t}) = \frac{1}{R_0} r\left(R_0\mathtt{R}, \frac{c_E(\rho_0^f)^4 R_0^2 \mathtt{t}}{K^s(\rho_0^s)^3}\right)$
	$\mathtt{T}(\mathtt{R},\mathtt{t}) = \frac{1}{T_c - T_m}\left[T\left(R_0\mathtt{R}, \frac{c_E(\rho_0^f)^4 R_0^2 \mathtt{t}}{K^s(\rho_0^s)^3}\right) - T_m\right]$
	$\mathtt{S}(\mathtt{t}) = \frac{1}{R_0} S\left(\frac{c_E(\rho_0^f)^4 R_0^2 \mathtt{t}}{K^s(\rho_0^s)^3}\right)$
Dimensionless constant parameters	$\mathtt{p} = \frac{\mu_0^s}{\kappa_0^f}$
	$\mathtt{q} = \frac{\kappa_0^s}{\kappa_0^f}$
	$\mathtt{f} = \frac{\rho_0^s}{\rho_0^f}$
	$\mathtt{a} = 1 - \frac{T_c}{T_m}$
	$\mathtt{b} = \beta_0^s[T_m - T_c]$
	$\mathtt{h} = \frac{h_c R_0}{K^s}$
	$\mathtt{L} = \frac{(\rho_0^s)^3 l}{(\rho_0^f)^3 c_E[T_m - T_c]}$

where $\bar{\mathtt{r}}(\mathtt{R}) = \mathtt{r}(\mathtt{R}, \mathtt{S}^{-1}(\mathtt{R}))$, $\mathtt{s}(\mathtt{t}) = \mathtt{r}(\mathtt{S}(\mathtt{t}),\mathtt{t})$ and $\mathtt{a}$, $\mathtt{b}$, $\mathtt{f}$, $\mathtt{p}$, $\mathtt{q}$ are dimensionless constant parameters defined in Table 1.[42] Similarly, for $1 > R > \mathtt{S}(\mathtt{t})$, the heat equation $(4.73)_2$ is rewritten as

$$\mathtt{T}_{,\mathtt{R}\mathtt{R}}(\mathtt{R},\mathtt{t}) - \frac{\mathtt{b}\mathtt{T}_{,\mathtt{R}}^2(\mathtt{R},\mathtt{t})}{3[1-(\mathtt{a}+\mathtt{b})\mathtt{T}(\mathtt{R},\mathtt{t})][1-\mathtt{a}\mathtt{T}(\mathtt{R},\mathtt{t})]} + \left[\frac{4\bar{\mathtt{r}}'(\mathtt{R})}{\bar{\mathtt{r}}(\mathtt{R})} - \frac{2}{\mathtt{R}}\right]\mathtt{T}_{,\mathtt{R}}(\mathtt{R},\mathtt{t}) = \frac{\mathtt{R}^4[1-\mathtt{a}\mathtt{T}(\mathtt{R},\mathtt{t})]^{\frac{1}{3}}\mathtt{T}_{,\mathtt{t}}(\mathtt{R},\mathtt{t})}{\bar{\mathtt{r}}^4(\mathtt{R})[1-(\mathtt{a}+\mathtt{b})\mathtt{T}(\mathtt{R},\mathtt{t})]^{\frac{1}{3}}}, \tag{4.79}$$

and, $(4.73)_{3-8}$ are rewritten as

$$\begin{cases} \mathtt{T}_{,\mathtt{R}}(\mathtt{S}(\mathtt{t}),\mathtt{t}) &= -\mathtt{L}\dfrac{\mathrm{d}\mathtt{S}(\mathtt{t})}{\mathrm{d}\mathtt{t}}, \\ \mathtt{T}(\mathtt{S}(\mathtt{t}),\mathtt{t}) &= 0, \\ \mathtt{r}(\mathtt{S}(\mathtt{t}),\mathtt{t}) &= \bar{\mathtt{r}}(\mathtt{S}(\mathtt{t})) = \mathtt{s}(\mathtt{t}), \\ \mathtt{T}_{,\mathtt{R}}(1,\mathtt{t}) &= \mathtt{h}[1-\mathtt{T}(1,\mathtt{t})], \\ \mathtt{r}(1,\mathtt{t}) &= 1, \\ \mathtt{S}(0) &= 1, \end{cases} \tag{4.80}$$

where $\mathtt{h}$, $\mathtt{L}$ are dimensionless constant parameters defined in Table 1. Thus, (4.77)–(4.80) constitute the non-dimensionalized boundary-value problem on the evolving domain $\{(\mathtt{R},\mathtt{t}) : 0 \le \mathtt{S}(\mathtt{t}) \le \mathtt{R} \le 1 = \mathtt{S}(0)\}$ (Fig. 5).[43] Further, the physical components of the Cauchy stress in the solid are non-dimensionalized as $\mathring{\sigma}^{ab} = \dfrac{\sigma^{ab}\sqrt{g_{aa}g_{bb}}}{\kappa_0^{\mathrm{f}}}$ (no summation).[44] Similarly, the pressure in the liquid, which is independent of R, is non-dimensionalized as $\mathring{p}(\mathtt{t}) = \frac{p(t)}{\kappa_0^{\mathrm{f}}}$.[45]

Remark 4.6. Note that (4.79) is rewritten as

$$\left[\frac{\bar{\mathtt{r}}^4(\mathtt{R})}{\mathtt{R}^2}\left[\frac{1-(\mathtt{a}+\mathtt{b})\mathtt{T}(\mathtt{R},\mathtt{t})}{1-\mathtt{a}\mathtt{T}(\mathtt{R},\mathtt{t})}\right]^{\frac{1}{3}}\mathtt{T}_{,\mathtt{R}}(\mathtt{R},\mathtt{t})\right]_{,\mathtt{R}} = \mathtt{R}^2\mathtt{T}_{,\mathtt{t}}(\mathtt{R},\mathtt{t}), \tag{4.81}$$

which is integrated using $(4.80)_{1-6}$ to obtain

$$\mathtt{h}[1-\mathtt{T}(1,\mathtt{t})]\left[\frac{1-(\mathtt{a}+\mathtt{b})\mathtt{T}(1,\mathtt{t})}{1-\mathtt{a}\mathtt{T}(1,\mathtt{t})}\right]^{\frac{1}{3}} + \frac{\mathtt{L}\mathtt{s}^4(\mathtt{t})\dot{\mathtt{S}}(\mathtt{t})}{\mathtt{S}^2(\mathtt{t})} = \int_{\mathtt{S}(\mathtt{t})}^1 \xi^2\,\mathtt{T}_{,\mathtt{t}}(\xi,\mathtt{t})\,\mathrm{d}\xi. \tag{4.82}$$

[42] The non-dimensionalized traction continuity condition across the moving interface reads

$$\mathtt{q}\left[\frac{\mathtt{f}\mathtt{s}^2(\mathtt{t})\mathtt{r}_{,\mathtt{R}}(\mathtt{S}(\mathtt{t}),\mathtt{t})}{\mathtt{S}^2(\mathtt{t})} - 1\right] + \frac{2\mathtt{p}}{3}\left(\frac{\mathtt{f}\mathtt{s}^2(\mathtt{t})\mathtt{r}_{,\mathtt{R}}(\mathtt{S}(\mathtt{t}),\mathtt{t})}{\mathtt{S}^2(\mathtt{t})}\right)^{\frac{1}{3}}\left[1 - \frac{\mathtt{S}^4(\mathtt{t})}{\mathtt{f}^2\mathtt{s}^4(\mathtt{t})\mathtt{r}_{,\mathtt{R}}^2(\mathtt{S}(\mathtt{t}),\mathtt{t})}\right] = \frac{\mathtt{s}^3(\mathtt{t})}{\mathtt{S}^3(\mathtt{t})} - 1. \tag{4.78}$$

[43] Recall that $\mathtt{m}(\mathtt{t}) := 1 - \mathtt{S}^3(\mathtt{t})$ represents the mass fraction solidified.

[44] Note that $\mathring{\sigma}^{\theta\theta} = \mathring{\sigma}^{\phi\phi}$.

[45] It is implied from (4.64) that $\mathring{p}(\mathtt{t}) = 1 - \frac{\mathtt{s}^3(\mathtt{t})}{\mathtt{S}^3(\mathtt{t})}$.

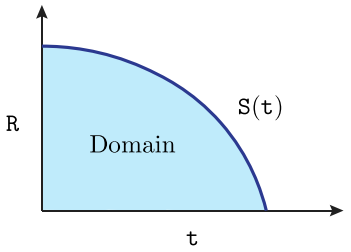

Fig. 5. A sketch of the domain $\{(\mathtt{R},\mathtt{t}) : 0 \le \mathtt{S}(\mathtt{t}) \le \mathtt{R} \le 1 = \mathtt{S}(0)\}$ for the non-dimensionalized moving boundary problem, where $\mathtt{S}(\mathtt{t})$ is an unknown. Additionally, the temperature field $\mathtt{T}(\mathtt{R},\mathtt{t})$ and the deformation field $\mathtt{r}(\mathtt{R},\mathtt{t})$ are unknown over this evolving domain.

Since[46]

$$\int_0^{\mathtt{t}} \left[\int_{\mathtt{S}(\tau)}^1 \xi^2\, \mathtt{T}_{,\tau}(\xi,\tau)\mathrm{d}\xi \right] \mathrm{d}\tau = \int_{\mathtt{S}(\mathtt{t})}^1 \xi^2\, \mathtt{T}(\xi,\mathtt{t})\mathrm{d}\xi\,, \tag{4.83}$$

it follows from (4.82) that[47]

$$\int_0^{\mathtt{t}} \mathtt{h}[1-\mathtt{T}(1,\tau)] \left[\frac{1-(\mathtt{a}+\mathtt{b})\mathtt{T}(1,\tau)}{1-\mathtt{a}\mathtt{T}(1,\tau)} \right]^{\frac{1}{3}} \mathrm{d}\tau = \int_{\mathtt{S}(\mathtt{t})}^1 \left[\xi^2\, \mathtt{T}(\xi,\mathtt{t}) + \frac{\mathtt{L}\,\bar{\mathtt{r}}^4(\xi)}{\xi^2} \right] \mathrm{d}\xi\,. \tag{4.84}$$

Thus, Stefan's condition $(4.80)_1$ can be replaced with the integral constraint (4.84).

Remark 4.7. Let $\mathtt{z} \ge 0$ be the time when the layer with radial coordinate $\mathtt{R}$ solidifies and attaches to the shell, i.e., $\mathtt{R} = \mathtt{S}(\mathtt{z})$. Let ρ and Y denote the radial placement and temperature fields, respectively, expressed as functions of $\mathtt{z}$ and $\mathtt{t}$, i.e.,

$$\rho(\mathtt{z},\mathtt{t}) = \mathtt{r}(\mathtt{S}(\mathtt{z}),\mathtt{t})\,, \qquad Y(\mathtt{z},\mathtt{t}) = \mathtt{T}(\mathtt{S}(\mathtt{z}),\mathtt{t})\,. \tag{4.85}$$

Thus, the heat equation (4.79) is rewritten in terms of ρ and Y as[48]

$$Y_{,\mathtt{z}\mathtt{z}}(\mathtt{z},\mathtt{t}) - \frac{\mathtt{b}Y_{,\mathtt{z}}^2(\mathtt{z},\mathtt{t})}{3[1-\mathtt{a}Y(\mathtt{z},\mathtt{t})][1-(\mathtt{a}+\mathtt{b})Y(\mathtt{z},\mathtt{t})]} + \left[\frac{4\dot{\mathtt{s}}(\mathtt{z})}{\mathtt{s}(\mathtt{z})} - \frac{2\dot{\mathtt{S}}(\mathtt{z})}{\mathtt{S}(\mathtt{z})} - \frac{\ddot{\mathtt{S}}(\mathtt{z})}{\dot{\mathtt{S}}(\mathtt{z})} \right] Y_{,\mathtt{z}}(\mathtt{z},\mathtt{t}) = \frac{\mathtt{S}^4(\mathtt{z})\dot{\mathtt{S}}^2(\mathtt{z})[1-\mathtt{a}Y(\mathtt{z},\mathtt{t})]^{\frac{1}{3}} Y_{,\mathtt{t}}(\mathtt{z},\mathtt{t})}{\mathtt{s}^4(\mathtt{z})[1-(\mathtt{a}+\mathtt{b})Y(\mathtt{z},\mathtt{t})]^{\frac{1}{3}}}\,, \tag{4.87}$$

where $\mathtt{s}(\mathtt{t}) = \bar{\mathtt{r}}(\mathtt{S}(\mathtt{t})) = \rho(\mathtt{t},\mathtt{t})$, and thus $\dot{\mathtt{s}}(\mathtt{t}) = \rho_{,\mathtt{z}}(\mathtt{t},\mathtt{t}) + \rho_{,\mathtt{t}}(\mathtt{t},\mathtt{t})$. Note that (4.87) can be rearranged as follows

$$\frac{\partial}{\partial \mathtt{z}} \left[\frac{\mathtt{s}^4(\mathtt{z})[1-(\mathtt{a}+\mathtt{b})Y(\mathtt{z},\mathtt{t})]^{\frac{1}{3}} Y_{,\mathtt{z}}(\mathtt{z},\mathtt{t})}{\mathtt{S}^2(\mathtt{z})\dot{\mathtt{S}}(\mathtt{z})[1-\mathtt{a}Y(\mathtt{z},\mathtt{t})]^{\frac{1}{3}}} \right] = \mathtt{S}^2(\mathtt{z})\dot{\mathtt{S}}(\mathtt{z}) Y_{,\mathtt{t}}(\mathtt{z},\mathtt{t})\,. \tag{4.88}$$

Similarly, (4.77) is rewritten as

$$\begin{aligned} &\mathtt{q}[1-\mathtt{a}Y(\mathtt{z},\mathtt{t})] \left[\frac{\mathtt{f}\rho^2(\mathtt{z},\mathtt{t})\rho_{,\mathtt{z}}(\mathtt{z},\mathtt{t})[1-\mathtt{a}Y(\mathtt{z},\mathtt{t})]}{\mathtt{S}^2(\mathtt{z})\dot{\mathtt{S}}(\mathtt{z})[1-(\mathtt{a}+\mathtt{b})Y(\mathtt{z},\mathtt{t})]} - 1 \right] + 1 - \frac{\mathtt{s}^3(\mathtt{z})}{\mathtt{S}^3(\mathtt{z})} \\ &+ \mathtt{p}[1-(\mathtt{a}+\mathtt{b})Y(\zeta,\mathtt{t})] \left(\frac{\mathtt{f}\rho^2(\mathtt{z},\mathtt{t})\rho_{,\mathtt{z}}(\mathtt{z},\mathtt{t})}{\mathtt{S}^2(\mathtt{z})\dot{\mathtt{S}}(\mathtt{z})} \right)^{\frac{1}{3}} \left[\frac{\mathtt{s}^4(\mathtt{z})}{\rho^4(\mathtt{z},\mathtt{t})} - \frac{1}{3} \left(\frac{2\,\mathtt{S}^4(\mathtt{z})\dot{\mathtt{S}}^2(\mathtt{z})}{\mathtt{f}^2\mathtt{s}^2(\mathtt{z})\rho^2(\mathtt{z},\mathtt{t})\rho_{,\mathtt{z}}^2(\mathtt{z},\mathtt{t})} + 1 \right) \right] \\ &+ 2\mathtt{p} \int_{\mathtt{z}}^{\mathtt{t}} [1-(\mathtt{a}+\mathtt{b})Y(\zeta,\mathtt{t})] \left(\frac{\mathtt{f}\rho^2(\zeta,\mathtt{t})\rho_{,\mathtt{z}}(\zeta,\mathtt{t})}{\mathtt{S}^2(\zeta)\dot{\mathtt{S}}(\zeta)} \right)^{-\frac{2}{3}} \left[\frac{\mathtt{S}^2(\zeta)}{\mathtt{f}\mathtt{s}^2(\zeta)\rho(\zeta,\mathtt{t})} - \frac{\mathtt{f}\,\mathtt{s}^4(\zeta)\rho_{,\mathtt{z}}^2(\zeta,\mathtt{t})}{\mathtt{S}^2(\zeta)\dot{\mathtt{S}}^2(\zeta)\rho^3(\zeta,\mathtt{t})} \right] \mathrm{d}\zeta = 0\,, \end{aligned} \tag{4.89}$$

[46] This is implied from the fact that $\frac{\partial}{\partial \mathtt{t}} \int_{\mathtt{S}(\mathtt{t})}^1 \xi^2\, \mathtt{T}(\xi,\mathtt{t})\,\mathrm{d}\xi = \int_{\mathtt{S}(\mathtt{t})}^1 \xi^2\, \mathtt{T}_{,\mathtt{t}}(\xi,\mathtt{t})\,\mathrm{d}\xi$.

[47] Note that the change of variable $\int_0^{\mathtt{t}} \frac{\mathtt{s}^4(\tau)\dot{\mathtt{S}}(\tau)}{\mathtt{S}^2(\tau)}\mathrm{d}\tau = \int_1^{\mathtt{S}(\mathtt{t})} \frac{\bar{\mathtt{r}}^4(\xi)\,\mathrm{d}\xi}{\xi^2}$ has been used here.

[48] The following relations have been used here

$$\mathtt{r}_{,\mathtt{R}}(\mathtt{R},\mathtt{t}) = \frac{\rho_{,\mathtt{z}}(\mathtt{z},\mathtt{t})}{\dot{\mathtt{S}}(\mathtt{z})}\,, \qquad \mathtt{T}_{,\mathtt{R}}(\mathtt{R},\mathtt{t}) = \frac{Y_{,\mathtt{z}}(\mathtt{z},\mathtt{t})}{\dot{\mathtt{S}}(\mathtt{z})}\,, \qquad \mathtt{T}_{,\mathtt{R}\mathtt{R}}(\mathtt{R},\mathtt{t}) = \frac{Y_{,\mathtt{z}\mathtt{z}}(\mathtt{z},\mathtt{t})}{\dot{\mathtt{S}}^2(\mathtt{z})} - \frac{Y_{,\mathtt{z}}(\mathtt{z},\mathtt{t})\,\ddot{\mathtt{S}}(\mathtt{z})}{\dot{\mathtt{S}}^3(\mathtt{z})}\,, \tag{4.86}$$

where $\mathtt{R} = \mathtt{S}(\mathtt{z})$. These are obtained by differentiating the definition (4.85) with respect to $\mathtt{z}$.

and, (4.80) is rewritten as

$$\begin{cases} Y_{,z}(t,t) &= -L\,\dot{S}^2(t)\,, \\ Y(t,t) &= 0\,, \\ \rho(t,t) &= s(t)\,, \\ Y_{,z}(0,t) &= h\,\dot{S}(0)\,[1-Y(0,t)]\,, \\ \rho(0,t) &= 1\,, \\ S(0) &= 1\,. \end{cases} \tag{4.90}$$

Hence, the transformed system of equations (4.88)–(4.90) form a boundary-value problem over the fixed triangular domain $\{(z,t) : 0 \le z \le t \le t_{end}\}$, where t_{end} is the time taken for complete solidification, i.e., $S(t_{end}) = 0$.

Remark 4.8. For $t > 0$, consider the ratio $u = \frac{z}{t} \in [0,1]$. Let α and γ denote the radial placement and temperature fields, respectively, expressed as functions of u and t, i.e.,

$$\gamma(u,t) = Y(ut,t)\,, \qquad \alpha(u,t) = \rho(ut,t)\,. \tag{4.91}$$

This change of variable transforms the triangular domain $\{(z,t) : 0 < z \le t \le t_{end}\}$ into the rectangular domain $\{(u,t) : 0 \le u \le 1, 0 < t \le t_{end}\}$. Further, the derivatives of ρ and Y are related to those of α and γ as

$$\rho_{,z}(z,t) = \frac{\alpha_{,u}(u,t)}{t}\,, \qquad Y_{,z}(z,t) = \frac{\gamma_{,u}(u,t)}{t}\,, \qquad Y_{,zz}(z,t) = \frac{\gamma_{,uu}(u,t)}{t^2}\,, \qquad Y_{,t}(z,t) = \gamma_{,t}(u,t) - \frac{u}{t}\gamma_{,u}(u,t)\,, \tag{4.92}$$

where $u = \frac{z}{t}$. Note that the thermal and displacement boundary conditions in (4.90) are expressed in terms α and γ as follows

$$\begin{cases} \gamma_{,u}(1,t) &= -Lt\,\dot{S}^2(t)\,, \\ \gamma(1,t) &= 0\,, \\ \alpha(1,t) &= s(t)\,, \\ \gamma_{,u}(0,t) &= h\,\dot{S}(0)\,t\,[1-\gamma(0,t)]\,, \\ \alpha(0,t) &= 1\,, \\ S(0) &= 1\,. \end{cases} \tag{4.93}$$

Thus, it follows from $(4.93)_3$ that $\dot{s}(t) = \alpha_{,t}(1,t)$. Therefore, (4.87) is rewritten in terms of α and γ as

$$\begin{aligned} &\gamma_{,uu}(u,t) - \frac{b\,\gamma_{,u}^2(u,t)}{3[1-a\,\gamma(u,t)][1-(a+b)\,\gamma(u,t)]} + \left[\frac{4\alpha_{,t}(1,ut)}{\alpha(1,ut)} - \frac{2\dot{S}(ut)}{S(ut)} - \frac{\ddot{S}(ut)}{\dot{S}(ut)}\right] t\gamma_{,u}(u,t) \\ &\quad + \frac{S^4(ut)\,\dot{S}^2(ut)[1-a\,\gamma(u,t)]^{\frac{1}{3}}\,\left[u\gamma_{,u}(u,t) - t\gamma_{,t}(u,t)\right]}{\alpha^4(1,ut)[1-(a+b)\,\gamma(u,t)]^{\frac{1}{3}}} = 0\,. \end{aligned} \tag{4.94}$$

Similarly, (4.89) is rewritten as

$$\begin{aligned} &q[1-a\gamma(u,t)]\left[\frac{f\alpha^2(u,t)\,\alpha_{,u}(u,t)[1-a\gamma(u,t)]}{t\,S^2(ut)\,\dot{S}(ut)[1-(a+b)\gamma(u,t)]} - 1\right] + 1 - \frac{\alpha^3(1,ut)}{S^3(ut)} \\ &+ p[1-(a+b)\gamma(u,t)]\left(\frac{f\alpha^2(u,t)\,\alpha_{,u}(u,t)}{t\,S^2(ut)\,\dot{S}(ut)}\right)^{\frac{1}{3}}\left[\frac{\alpha^4(1,ut)}{\alpha^4(u,t)} - \frac{1}{3}\left(\frac{2\,t^2\,S^4(ut)\,\dot{S}^2(ut)}{f^2\alpha^2(1,ut)\alpha^2(u,t)\,\alpha_{,u}^2(u,t)} + 1\right)\right] \\ &+ 2p\int_u^1 [1-(a+b)\gamma(v,t)]\left(\frac{f\alpha^2(v,t)\,\alpha_{,u}(v,t)}{t\,S^2(vt)\,\dot{S}(vt)}\right)^{-\frac{2}{3}}\left[\frac{S^2(vt)}{f\alpha^2(1,vt)\,\alpha(v,t)} - \frac{f\alpha^4(1,vt)\,\alpha_{,u}^2(v,t)}{t^2S^2(vt)\,\dot{S}^2(vt)\,\alpha^3(v,t)}\right] t\,dv = 0\,. \end{aligned} \tag{4.95}$$

Hence, (4.94), (4.93) and (4.95) form a system of nonlinear PDEs coupled with an ODE,[49] with the unknown fields $\alpha(u,t)$, $\gamma(u,t)$, and $S(t)$ over the rectangular domain $\{(u,t) : 0 \le u \le 1, 0 < t \le t_{end}\}$.

Remark 4.9. Note that the standard heat equation is recovered by setting $\bar{r}(R) = R$ and $\alpha^s(T) = 0$ in (4.38), which is written as

$$D_f^s\left[T_{,RR}(R,t) + \frac{2}{R}T_{,R}(R,t)\right] = \dot{T}(R,t)\,. \tag{4.96}$$

[49] Note that the integral equation (4.95) can be differentiated with respect to u to get rid of the integral term. Thus, (4.94) and (4.95) are second-order nonlinear PDEs in terms of the unknown fields $\alpha(u,t)$ and $\gamma(u,t)$. Similarly, $(4.93)_1$ is an ODE in terms of the unknown function $S(t)$.

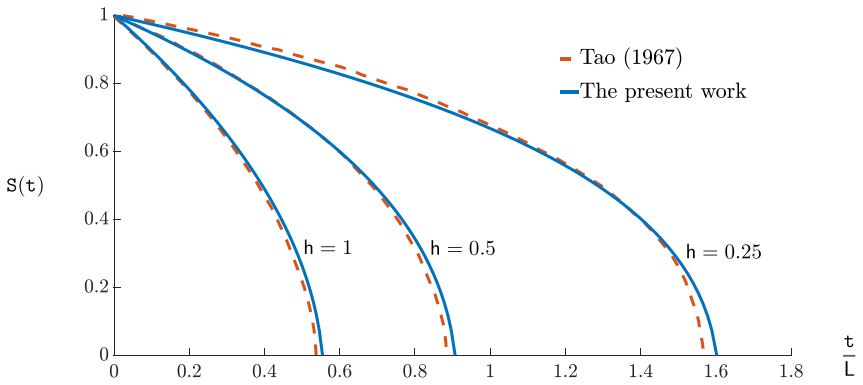

Fig. 6. The numerical solution for the evolution of the moving boundary obtained in the present work for the rigid conductor problem (4.97) with $\mathsf{L} = 10$, is compared with that obtained by Tao (1967).

Therefore, in the absence of any elastic deformation or thermal expansion, the non-dimensionalized moving boundary problem reads

$$\begin{cases} \mathsf{T}_{,\mathsf{RR}}(\mathsf{R},\mathsf{t}) + \dfrac{2}{\mathsf{R}}\mathsf{T}_{,\mathsf{R}}(\mathsf{R},\mathsf{t}) & = \mathsf{T}_{,\mathsf{t}}(\mathsf{R},\mathsf{t})\,, \\ \mathsf{T}_{,\mathsf{R}}(\mathsf{S}(\mathsf{t}),\mathsf{t}) & = -\mathsf{L}\dfrac{\mathrm{d}\mathsf{S}(\mathsf{t})}{\mathrm{d}\mathsf{t}}\,, \\ \mathsf{T}(\mathsf{S}(\mathsf{t}),\mathsf{t}) & = 0\,, \\ \mathsf{T}_{,\mathsf{R}}(1,\mathsf{t}) & = \mathsf{h}\,[1-\mathsf{T}(1,\mathsf{t})]\,, \\ \mathsf{S}(0) & = 1\,, \end{cases} \tag{4.97}$$

where $1 \geq \mathsf{R} \geq \mathsf{S}(\mathsf{t})$ and $\mathsf{t} \geq 0$. Here, h is the Biot number, and L^{-1} is the Stefan number. The phase change problem (4.97) has been analyzed by London and Seban (1943), Tao (1967), Shih and Chou (1971), Hill and Kucera (1983), and possibly others. Furthermore, (4.84) is simplified as

$$\mathsf{h}\,\mathsf{t} + \frac{\mathsf{L}}{3}\left[\mathsf{S}^3(\mathsf{t}) - 1\right] - \int_0^{\mathsf{t}} \mathsf{h}\,\mathsf{T}(1,\tau)\mathrm{d}\tau = \int_{\mathsf{S}(\mathsf{t})}^1 \xi^2\,\mathsf{T}(\xi,\mathsf{t})\,\mathrm{d}\xi\,. \tag{4.98}$$

Alternatively, since $(4.97)_1$ is rewritten as $[\mathsf{RT}(\mathsf{R},\mathsf{t})]_{,\mathsf{RR}} = [\mathsf{RT}(\mathsf{R},\mathsf{t})]_{,\mathsf{t}}$, it can be shown using $(4.97)_{2-5}$ that Stefan's condition $(4.97)_2$ is equivalent to[50]

$$\mathsf{h}\,\mathsf{t} + \frac{\mathsf{L}}{2}\left[\mathsf{S}^2(\mathsf{t}) - 1\right] + (1-\mathsf{h})\int_0^{\mathsf{t}} \mathsf{T}(1,\tau)\mathrm{d}\tau = \int_{\mathsf{S}(\mathsf{t})}^1 \xi\,\mathsf{T}(\xi,\mathsf{t})\,\mathrm{d}\xi\,. \tag{4.101}$$

Thus, for a rigid conductor, Stefan's condition $(4.97)_2$ can be replaced with the integral constraint (4.98), or equivalently with (4.101).

4.4. Residual stresses

The solidification process is stopped at time t_e, when the solid–liquid interface is at $R_e = S(t_e)$ in the reference configuration, or equivalently at $s(t_e) = \bar{r}(R_e)$ in the current configuration. Imagine that the accreted solid is drained of the remaining liquid and is

[50] Using $(4.97)_{2-4}$, it is implied that

$$\int_{\mathsf{S}(\mathsf{t})}^1 [\mathsf{RT}(\mathsf{R},\mathsf{t})]_{,\mathsf{RR}}\,\mathrm{d}\mathsf{R} = \mathsf{h} + [1-\mathsf{h}]\mathsf{T}(1,\mathsf{t}) + \mathsf{L}\mathsf{S}(\mathsf{t})\dot{\mathsf{S}}(\mathsf{t})\,. \tag{4.99}$$

Therefore, since $[\mathsf{RT}(\mathsf{R},\mathsf{t})]_{,\mathsf{RR}} = [\mathsf{RT}(\mathsf{R},\mathsf{t})]_{,\mathsf{t}}$, (4.101) follows from $(4.97)_5$ and the fact that

$$\int_{\mathsf{S}(\mathsf{t})}^1 \mathsf{RT}(\mathsf{R},\mathsf{t})\mathrm{d}\mathsf{R} = \int_0^{\mathsf{t}} \left[\int_{\mathsf{S}(\tau)}^1 \mathsf{RT}_{,\tau}(\mathsf{R},\tau)\mathrm{d}\mathsf{R}\right]\mathrm{d}\tau\,. \tag{4.100}$$

.

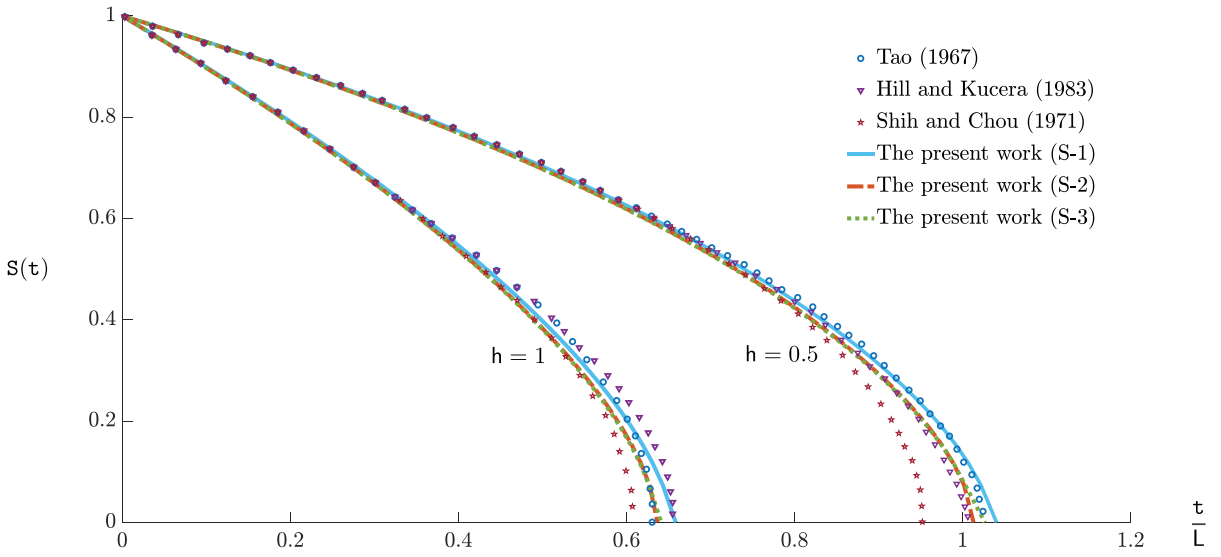

Fig. 7. The moving boundary evolution for the rigid conductor problem with $\mathsf{L} = 2$ obtained in the present work is compared with numerical data from the literature (Tao, 1967; Shih and Chou, 1971; Hill and Kucera, 1983). Here, S-1 refers to the solution of system (4.97), while S-2 and S-3 correspond to the systems where $(4.97)_2$ is replaced by (4.98) and (4.101), respectively.

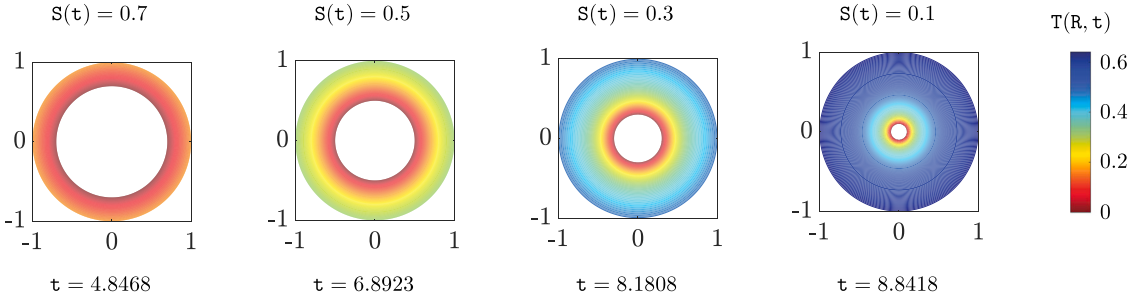

Fig. 8. The non-dimensionalized temperature field $\mathsf{T}(\mathsf{R},\mathsf{t})$ for the rigid conductor problem (4.97) with $\mathsf{h} = 0.5$, $\mathsf{L} = 10$ is depicted at various instances of time as the solidification interface moves inward.

allowed to reach a steady-state uniform temperature of $T_a < T_m$ in an ambient environment, while its inner and outer boundaries are traction-free. The resulting residually-stressed configuration is denoted by $\tilde{\mathcal{C}} \subset \mathcal{S}$. The material metric for the solid is written as

$$\overset{\mathcal{B}}{\mathbf{G}} = e^{2\omega^{\mathrm{s}}(T_a)} \begin{bmatrix} \frac{(\rho_0^{\mathrm{f}})^2 R^4}{(\rho_0^{\mathrm{s}})^2 \bar{r}^4(R)} & 0 & 0 \\ 0 & \bar{r}^2(R) & 0 \\ 0 & 0 & \bar{r}^2(R)\sin^2\Theta \end{bmatrix}. \tag{4.102}$$

Recall that

$$e^{3\omega^{\mathrm{s}}(T_a)} = 1 + \beta_0^{\mathrm{s}} T_m \Big(1 - \frac{T_m}{T_a}\Big). \tag{4.103}$$

Note that since $\bar{r}(R)$ is now a known function defined on the interval $[R_e, R_0]$, determined from the solution of the IBVP during accretion, the material metric $\overset{\mathcal{B}}{\mathbf{G}}$ is considered to be given.

Let $\tilde{\varphi} : \mathcal{B}_{t_e} \to \tilde{\mathcal{C}}$ denote the deformation map corresponding to the residually-stressed configuration. In spherical coordinates $\tilde{\varphi}(R,\Theta,\Phi) = (\tilde{r}(R),\Theta,\Phi)$, where the placement map $\tilde{r}(R)$ represents the residual radial distortion. The deformation gradient reads

$$\mathbf{F}(R) = \begin{bmatrix} \tilde{r}'(R) & 0 & 0 \\ 0 & 1 & 0 \\ 0 & 0 & 1 \end{bmatrix}. \tag{4.104}$$

The Jacobian of the deformation is written as

$$J(R) = \frac{\rho_0^{\mathrm{s}}\,\tilde{r}^2(R)\,\tilde{r}'(R)}{\rho_0^{\mathrm{f}}\,e^{3\omega^{\mathrm{s}}(T_a)}R^2}\,. \tag{4.105}$$

The strain tensors for this configuration are given as

$$\mathbf{b}^{\sharp} = e^{-2\omega^{\mathrm{s}}(T_a)}\begin{bmatrix}\left(\dfrac{\rho_0^{\mathrm{s}}\tilde{r}^2\tilde{r}'}{\rho_0^{\mathrm{f}}R^2}\right)^2 & 0 & 0\\ 0 & \dfrac{1}{\tilde{r}^2} & 0\\ 0 & 0 & \dfrac{1}{\tilde{r}^2\sin^2\Theta}\end{bmatrix}, \qquad \mathbf{c}^{\sharp} = e^{2\omega^{\mathrm{s}}(T_a)}\begin{bmatrix}\left(\dfrac{\rho_0^{\mathrm{f}}R^2}{\rho_0^{\mathrm{s}}\tilde{r}^2\tilde{r}'}\right)^2 & 0 & 0\\ 0 & \dfrac{\tilde{r}^2}{\tilde{r}'^4} & 0\\ 0 & 0 & \dfrac{\tilde{r}^2}{\tilde{r}'^4\sin^2\Theta}\end{bmatrix}. \tag{4.106}$$

Further, the principal invariants of $\mathbf{b}$ read

$$I_1 = e^{-2\omega^{\mathrm{s}}(T_a)}\left[\left(\frac{\rho_0^{\mathrm{s}}\,\tilde{r}^2\,\tilde{r}'}{\rho_0^{\mathrm{f}}R^2}\right)^2 + 2\left(\frac{\tilde{r}}{\tilde{r}}\right)^2\right], \qquad I_2 = e^{-4\omega^{\mathrm{s}}(T_a)}\left[\left(\frac{\tilde{r}}{\tilde{r}}\right)^4 + 2\left(\frac{\rho_0^{\mathrm{s}}\,\tilde{r}\,\tilde{r}\,\tilde{r}'}{\rho_0^{\mathrm{f}}\,R^2}\right)^2\right]. \tag{4.107}$$

Example 4.10 (*A neo-Hookean solid*)**.** The thermoelastic neo-Hookean solid considered in (4.66) is now at a constant temperature, and thus, is characterized by the temperature-independent free energy function

$$\tilde{W}(I_1, J) = \frac{T_a}{2T_m}\left[\mu_0^{\mathrm{s}}[J^{-\frac{2}{3}}I_1 - 3] + \kappa_0^{\mathrm{s}}[J-1]^2\right] + \kappa_0^{\mathrm{s}}\,\beta_0^{\mathrm{s}}(T_m - T_a)\,[J-1]\,. \tag{4.108}$$

The nonzero components of residual Cauchy stress $\tilde{\boldsymbol{\sigma}}(R)$ are written as

$$\tilde{\sigma}^{rr} = \tilde{W}_J + \frac{2(\rho_0^{\mathrm{s}})^2\tilde{W}_1\,\tilde{r}^4(\tilde{r}')^2}{(\rho_0^{\mathrm{f}})^2 J e^{2\omega^{\mathrm{s}}(T_a)}R^4}\,, \qquad \tilde{\sigma}^{\theta\theta} = \frac{\tilde{W}_J}{\tilde{r}^2} + \frac{2\tilde{W}_1}{J e^{2\omega^{\mathrm{s}}(T_a)}\,\tilde{r}^2}\,, \qquad \tilde{\sigma}^{\phi\phi} = \frac{\tilde{\sigma}^{\theta\theta}}{\sin^2\Theta}\,, \tag{4.109}$$

where the coefficients $\tilde{W}_1$ and $\tilde{W}_J$ are given as

$$\tilde{W}_1 = \frac{\mu_0^{\mathrm{s}}T_a}{2T_m}J^{-\frac{2}{3}}\,, \qquad \tilde{W}_J = \frac{T_a}{T_m}\left[\kappa_0^{\mathrm{s}}(J-1) - \frac{\mu_0^{\mathrm{s}}}{3}J^{-\frac{5}{3}}I_1\right] + \kappa_0^{\mathrm{s}}\,\beta_0^{\mathrm{s}}\,(T_m - T_a)\,. \tag{4.110}$$

The balance of linear momentum in the absence of body forces and inertial effects is simplified to yield the following radial equilibrium equation

$$\frac{\mathrm{d}\tilde{\sigma}^{rr}}{\mathrm{d}R} = \left[\left(\tilde{\sigma}^{\theta\theta} + \sin^2\theta\,\tilde{\sigma}^{\phi\phi}\right)\tilde{r}^2 - 2\tilde{\sigma}^{rr}\right]\frac{\tilde{r}'}{\tilde{r}}\,. \tag{4.111}$$

Furthermore, the outer and inner boundaries are traction-free, i.e.,

$$\tilde{\sigma}^{rr}(R_0) = \tilde{\sigma}^{rr}(R_e) = 0\,. \tag{4.112}$$

It follows from (4.109), (4.107) and $(4.110)_1$ that (4.111) is a nonlinear ODE in terms of $\tilde{r}(R)$, with the boundary conditions (4.112). Thus, the problem of finding the residual stresses and distortions boils down to solving the boundary-value problem (4.111)–(4.112) for the unknown function $\tilde{r}(R)$. This problem is then non-dimensionalized according to Table 1. The dimensionless radial displacement $\frac{\tilde{r}-R}{R_0}$ and the dimensionless physical components of the Cauchy stress $\overset{\circ}{\tilde{\sigma}}{}^{ab} = \frac{1}{\kappa_0^{\mathrm{f}}}\overset{\circ}{\tilde{\sigma}}{}^{ab}\sqrt{g_{aa}g_{bb}}$ (no summation) in the residually-stressed configuration at a given dimensionless steady state temperature $\mathtt{T}_{\mathtt{a}} = \frac{T_a - T_m}{T_c - T_m}$ are illustrated in Fig. 14.[51]

4.5. Numerical results and discussion

Several numerical methods for the solution of moving boundary value problems have been proposed over the years (Rubinšteĭn, 1971; Crank, 1984). In this work, we follow the approach of Douglas and Gallie (1955), where for a specified space grid, the corresponding instances of time are calculated as the moving boundary assumes these discrete positions in progression. It should be noted that the bijectivity of $S(t)$ is exploited here, allowing us to treat the time of accretion as the unknown. For each unknown time step, the moving interface is first assigned a position. Treating the domain as fixed, we calculate the deformation and temperature fields, along with the instant of time for this interface location, by solving the conservation of linear momentum, transient heat equation, and Stefan's condition. This is implemented using a finite difference approximation (an implicit scheme) in MATLAB. The optimum time step that minimizes the residue from Stefan's condition to ensure a sufficiently small magnitude is calculated using `fminunc`, while the corresponding numerical solution for the radial equilibrium and the heat equation is simultaneously obtained using `fsolve`. Extensive parametric studies are conducted by varying the numerical values of the dimensionless constants in Table 1. The observations from the numerical results are qualitatively described in the following.

[51] Note that $\overset{\circ}{\tilde{\sigma}}{}^{rr} = \frac{\tilde{\sigma}^{rr}}{\kappa_0^{\mathrm{f}}}$ and $\overset{\circ}{\tilde{\sigma}}{}^{\phi\phi} = \overset{\circ}{\tilde{\sigma}}{}^{\theta\theta} = \frac{\tilde{r}^2\tilde{\sigma}^{\theta\theta}}{\kappa_0^{\mathrm{f}}}$.

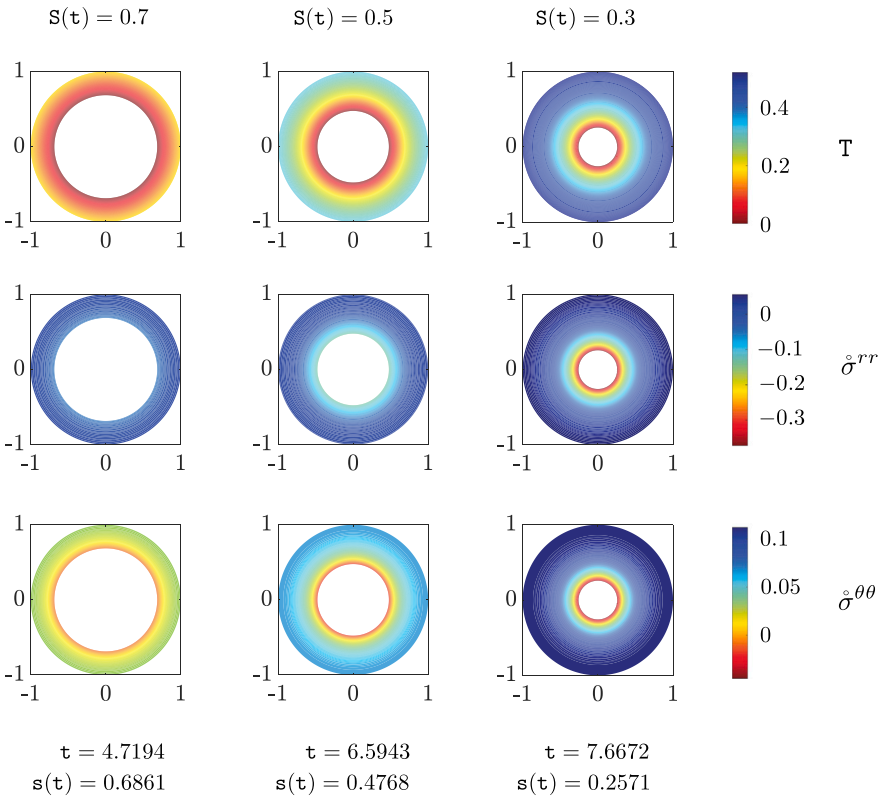

Fig. 9. The non-dimensionalized temperature field $\mathtt{T}$, as well as the dimensionless physical components $\mathring{\sigma}^{rr}$ and $\mathring{\sigma}^{\theta\theta}$ of the Cauchy stress within the deformed solid are illustrated via color maps. These depictions are based on the solution of the general problem (4.77)–(4.80), with $\mathtt{f} = 0.95$, $\mathtt{a} = 0.8$, $\mathtt{b} = 0.1$, $\mathtt{p} = 1.1$, $\mathtt{q} = 1.2$, $\mathtt{h} = 0.5$, and $\mathtt{L} = 10$, at various instances of time as the phase-change interface moves inward.

- The radial speed of the interface, in both the reference and the current configurations, is observed to increase as the interface moves inward with time (Fig. 10). As expected, the fraction of the initial liquid mass solidified increases over time. However, the rate of mass fraction solidified decreases with time (Fig. 10). These trends are similar to what has been observed in the rigid conductor case (see Figs. 6 and 7). The temperature field inside a rigid conductor is shown at different instances of time in Fig. 8. It should be noted that most numerical studies in the literature for the rigid conductor case only depict the motion of the interface (Tao, 1967; Shih and Chou, 1971; Hill and Kucera, 1983). The experimental studies report the rate of solidification with the rate of change of mass fraction of the total initial liquid solidified with respect to time (Chan and Tan, 2006). This is possibly because the liquid inclusion tends to lose its spherical shape and concentricity with the previously accreted layers as the inclusion size decreases. The trend we observe for the variation of mass fraction solidified qualitatively agrees with that of Chan and Tan (2006), although a direct comparison with the experimental data is not feasible due to the unavailability of a complete set of material properties of the materials used. The temperature field and the physical components of the Cauchy stress in the deformed solid for the coupled problem (4.77)–(4.80) are shown in Fig. 9.
- The symbol $\mathtt{f}$ denotes the ratio of the density of the undeformed solid to that of the liquid near the melting point. Solidification of a given mass of a liquid with $\mathtt{f} > 1$ results in a reduction of the occupied volume. As the accretion surface moves inward, layers of liquid are replaced with denser solid layers, leading to a decrease in volume. Furthermore, since the container has fixed walls and, therefore, a fixed volume, the liquid inclusion naturally develops positive hydrostatic stress as soon as solidification begins, indicating possibility of cavitation. Although this is confirmed numerically, the observed data is excluded from figures as positive liquid pressure is not physically possible. Moreover, it follows from $\mathring{p}(\mathtt{t}) = 1 - \frac{\mathtt{s}^3(\mathtt{t})}{\mathtt{S}^3(\mathtt{t})}$ that a negative liquid pressure is equivalent to a negative radial displacement of the accreting layers (see Figs. 11(b) and 11(a)).[52] As the solidification interface approaches the center, the magnitude of the displacement of the accreting layers increases rapidly, requiring it to decelerate and decrease swiftly to ultimately vanish at the center.[53] Thus, the mesh near the center must be much finer; otherwise, numerical techniques that better accommodate such sudden fluctuations need to be used.

[52] Since $\mathtt{s}(\mathtt{t}) = \mathtt{r}(\mathtt{S}(\mathtt{t}), \mathtt{t})$ is the position of the solidification interface in the deformed configuration, and $\mathtt{R} = \mathtt{S}(\mathtt{t})$ was its position in the initial liquid pool, $\mathtt{s}(\mathtt{t}) - \mathtt{S}(\mathtt{t})$, or equivalently, $\mathring{\mathtt{r}}(\mathtt{R}) - \mathtt{R}$, denotes the radial displacement of an accreting layer.

[53] The time instant $\mathtt{t}_c$ marking the completion of solidification must satisfy $\mathtt{S}(\mathtt{t}_c) = 0$. Further, if this is achieved without cavitation, then $\mathtt{s}(\mathtt{t}_c) = 0$. Thus, $\mathtt{s}(\mathtt{t}_c) - \mathtt{S}(\mathtt{t}_c) = 0$.

- The figures shown in this section are based on the assumption $\mathtt{f} < 1$. With this assumption, an accreting layer with a given mass tends to occupy a larger volume upon solidification, compressing the liquid inclusion and resulting in negative hydrostatic stress. The magnitude of this negative hydrostatic stress increases with time as the solidification interface moves inward (Fig. 13). The extra volume occupied by the solidifying layers piles up to create a significant gap, causing the pressure in the liquid to become highly compressive as the interface approaches the center.
- Surface stresses play a significant role for liquid inclusions smaller than a certain limit determined by the elastocapillarity length—the ratio of surface tension to the bulk modulus (Bico et al., 2018). In this paper we do not consider surface stress, and hence, do not report the numerical results for very small liquid inclusions. Although the process is halted a while before complete solidification, the rate of increase in the magnitude of liquid pressure is significantly high by the time this margin is reached.
- Note that $\mathtt{T} = 0$ at the melting point, and since $T_c < T_m$, $\mathtt{T} = \frac{T_m - T}{T_m - T_c}$ increases as the real temperature T decreases (see Figs. 8 and 9). The moving interface is always at the melting point, and the temperature decreases as one moves towards the fixed wall (Fig. 11(c)). The temperature at a point decreases over time after it is accreted (Fig. 11(d)). Radial displacements are always negative, and the magnitude at any accreted point decreases over time (Fig. 11(b)). At any instant, the magnitude of radial displacement is maximum at the moving boundary and decreases to zero at the fixed boundary (Fig. 11(a)).
- Both $\mathring{\sigma}^{rr}$ and $\mathring{\sigma}^{\theta\theta}$ are negative near the moving boundary. $\mathring{\sigma}^{\theta\theta}$ increases as one moves away from the inclusion (i.e., decreases in magnitude), vanishes somewhere in between, and eventually becomes positive near the wall (Fig. 11(g)). $\mathring{\sigma}^{rr}$ decreases in magnitude as one moves away from the inclusion but remains negative if the inclusion size is too large (Fig. 11(e)). However, when the interface has moved far enough from the wall, $\mathring{\sigma}^{rr}$ can be positive near the wall, decreasing to a negative value near the inclusion. At any accreted point, $\mathring{\sigma}^{rr}$ is initially negative and decreases in magnitude over time (Fig. 11(f)). For points closer to the fixed wall, $\mathring{\sigma}^{rr}$ eventually becomes positive as the inclusion size decreases. $\mathring{\sigma}^{\theta\theta}$ is initially negative for all accreted points, and quickly transitions to a positive value, except for the points accreted just before the process is halted (Fig. 11(h)).
- The dimensionless parameter $\mathtt{b}$ describes the thermal expansion properties of the solid relative to the temperature difference between its melting point and the cold wall temperature. A larger $\mathtt{b}$ implies a higher contraction of the solid for a given temperature drop. It is observed that the rate of increase in liquid pressure magnitude is much faster for lower values of $\mathtt{b}$ (Fig. 13(d)). If $\mathtt{b}$ is too large, the liquid inclusion pressure decreases from zero until it reaches a minimum, and then increases until it becomes zero again (Fig. 13(b)). Positive pressure solutions beyond this point are physically irrelevant due to the possibility of cavitation and are therefore discarded. The reason behind this tendency of liquid cavitation, even with $\mathtt{f} < 1$, is the extremely high thermal contraction in the colder layers closer to the container walls. $\mathtt{a} < 1$ represents the ratio of the temperature difference between the cold container wall and the melting point of the liquid to the absolute melting temperature. Figs. 13(a) and 13(c) describe the influence of $\mathtt{a}$ on the evolution of the liquid pressure within the inclusion for the two distinct categories of $\mathtt{b}$ discussed above.
- The elastic material properties are captured by $\mathtt{p}$ and $\mathtt{q}$, which represent the shear and bulk moduli of the solid near the melting point as compared to the liquid bulk modulus near the solidification temperature. The magnitude of pressure in the liquid inclusion rises faster with larger $\mathtt{p}$ and $\mathtt{q}$ values (see Figs. 13(e) and 13(f)). The specific latent heat of solidification appears only in the dimensionless constant $\mathtt{L}$, which is loosely interpreted as a measure of the latent heat released relative to the heat capacity of the solid. The heat transfer with the container walls is incorporated in the coefficient $\mathtt{h}$, loosely quantifying how much of the heat conducted towards the outer boundary of the accreted solid is transferred out into the cold wall.
- The numerical variations in $\mathtt{a}$, $\mathtt{b}$, $\mathtt{p}$, and $\mathtt{q}$ used for the parametric studies do not significantly impact the solidification rate, indicating a lower sensitivity to these parameters (see Figs. 12(a), 12(b), 12(c) and 12(d)). A value of $\mathtt{f}$ closer to 1, with the liquid denser than the solid near melting, results in slower solidification (Fig. 12(g)); and the sensitivity to variations in $\mathtt{f}$ is moderate. The solidification rate is highly sensitive to $\mathtt{h}$ and $\mathtt{L}$. A larger $\mathtt{h}$ implies that the heat is able to flow more efficiently out of the solid into the container walls, facilitating in faster solidification (Fig. 12(e)). A smaller $\mathtt{L}$ implies less specific latent heat compared to the specific heat capacity, allowing the accreted solid to better absorb the heat released during solidification. This indirectly promotes outward heat conduction and results in a higher solidification rate (Fig. 12(f)). The higher rates of pressure drop in the liquid for larger $\mathtt{h}$ and smaller $\mathtt{L}$ values (see Figs. 13(g) and 13(h)) are attributed to the faster solidification rates.
- The configuration obtained by detaching the accreted solid from the rigid walls of the cold container after a given time, removing any remaining unsolidified liquid, and subsequently cooling the solid to a uniform steady-state temperature is not stress-free (see Figs. 14(d) and 14(e)). In this configuration, both the inner and outer boundaries are displaced inward relative to their positions in the initial liquid (Fig. 14(a)). The inward displacement of the outer boundary is likely caused by thermal contraction. The inner layers experience highly negative $\mathring{\sigma}^{rr}$ during accretion, owing to the presence of a pressurized liquid inclusion. When the liquid is removed and the inner boundary becomes traction-free, the inner layers naturally tend to move apart to relieve the negative stress. Moreover, the closer the layer is to the inner boundary, the more pronounced this tendency becomes. In the residually-stressed configuration, $\mathring{\overset{\circ}{\sigma}}^{rr}$ is zero at the inner boundary, increases as one moves outward, reaches a maximum, and then decreases to vanish at the outer boundary (Fig. 14(d)). The maximum value of $\mathring{\overset{\circ}{\sigma}}^{rr}$ is larger if the accretion process ends later (Fig. 14(b)). $\mathring{\overset{\circ}{\sigma}}^{\theta\theta}$ is negative at the inner boundary, increases as one moves outwards, eventually becoming positive at the outer boundary (Fig. 14(e)). The variation in $\mathring{\overset{\circ}{\sigma}}^{\theta\theta}$ is larger if the solidification process is stopped later (Fig. 14(c)). Consequently, the outer boundary is prone to developing cracks, while the inner boundary is prone to buckling instabilities.

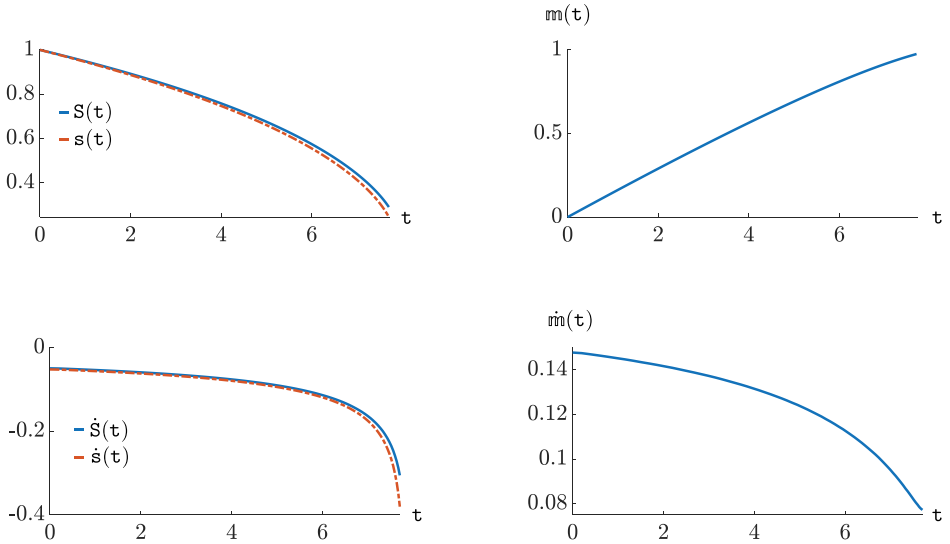

Fig. 10. The motion of the solidification interface is illustrated. $\mathtt{S}(\mathtt{t})$ and $\mathtt{s}(\mathtt{t})$ denote its radial position in the reference and current configurations, respectively, while $\dot{\mathtt{S}}(\mathtt{t})$ and $\dot{\mathtt{s}}(\mathtt{t})$ represent the respective velocities. $\mathtt{m}(\mathtt{t})$ denotes the fraction of the initial liquid mass solidified, and $\dot{\mathtt{m}}(\mathtt{t})$ represents the solidification rate. These figures depict the solution of the coupled problem (4.77)–(4.80) for $\mathtt{f} = 0.95$, $\mathtt{a} = 0.8$, $\mathtt{b} = 0.1$, $\mathtt{p} = 1.1$, $\mathtt{q} = 1.2$, $\mathtt{h} = 0.5$, and $\mathtt{L} = 10$.

4.6. Summary

In this paper, the process of liquid-to-solid phase change was modeled as a thermoelastic accretion problem. Several simplifying assumptions were made, such as neglecting inertial effects in both phases, assuming the melting temperature to be independent of pressure (hydrostatic stress in the liquid), ignoring surface stresses, and assuming that the thermal conductivity and heat capacity of the solid are temperature-independent. Since the primary focus was to study the solidification of a liquid inclusion, the liquid was assumed to be a compressible hyperelastic material. The problem of determining the reference configuration as the solid portion of a deformable body grows by accretion has the following challenging aspects: first, determining the set of material points that are part of the solid, i.e., the moving boundary location; second, determining the material metric at each point. The material metric depends on the state of deformation of the solidifying material during attachment and on the temperature evolution to account for the effects of thermal expansion. The boundary location, or the set of material points included in the solid at a given instant of time, is determined by the mass rate of solidification, which depends on the jump of the heat flux across the moving interface. Thus, this is a coupled nonlinear problem where the location of the boundary is an unknown, in addition to the deformation and temperature fields.

As a concrete example, the radially inward solidification of a liquid initially at the melting temperature was studied. The resulting moving boundary problem was numerically solved by treating the time of attachment map as an unknown, instead of the boundary location. In other words, for a given space grid, the time instances when the moving boundary crosses these grid points were calculated. This formulation enables one to study the deformation and stresses at any point inside the solid at any desired time, thus potentially highlighting critical zones prone to failures and instabilities. However, the solidification process is halted with a margin prior to completion due to multiple reasons. The numerical results become less accurate as one approaches the center, and they are also physically irrelevant as surface stresses, which become dominant for smaller inclusion sizes, are not considered in the formulation. A detailed parametric study was performed by varying all the dimensionless constants. In all the numerical examples, the solid was assumed to be less dense than the liquid near the melting point, commonly observed in water and some polymers, though rare in metals. This assumption is essential to avoid cavitation inside the liquid in the context of a solidifying inclusion. However, even with this assumption of denser liquids, our numerical results show that cavitation might be possible in the case of extreme thermal contraction in the solid. The accreted body—once it is detached from the rigid container, drained of the remaining unsolidified liquid, and cooled to an ambient temperature—is residually-stressed, in general. The residually-stressed configuration and its residual stresses were computed numerically.

The present study opens up several new avenues for future investigations. The zero-displacement boundary condition imposes a volumetric constraint, potentially causing cavitation for materials denser in the solid phase near the melting point. This results from volume changes due to jump in density across phases. Replacing it with, for instance, an applied pressure on the outer boundary may enable one to study solidification across a broader range of materials. Developing a variational theory to study instabilities in both solids and liquids during a solidification process is another extension. It is crucial to include surface stresses in the theory for a more realistic understanding of the physics and mechanics of solidification in simple, computationally feasible problems. Ultimately, a more general computational framework needs to be developed to fully utilize the benefits of this formulation for more complex geometries in real-world applications.

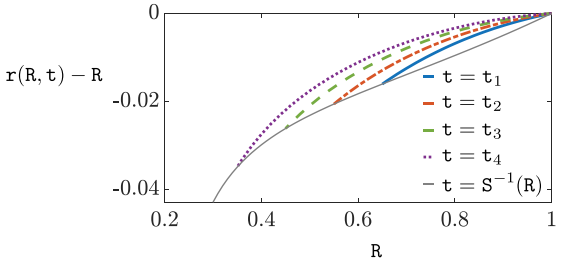

(a) *The variation of the displacement field with the material coordinate inside the solid.*

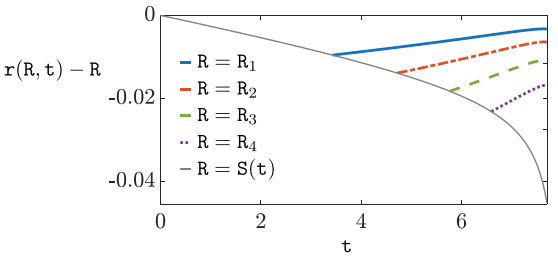

(b) *The time evolution of the radial displacement field within the solid.*

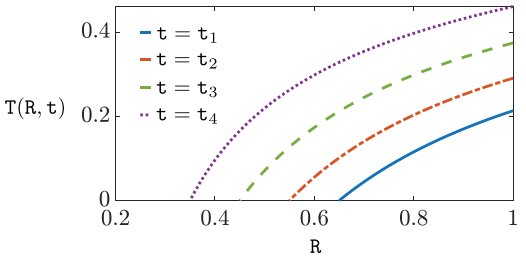

(c) *The variation of* $\mathtt{T}(\mathtt{R},\mathtt{t})$ *with* $\mathtt{R}$ *inside the solid.*

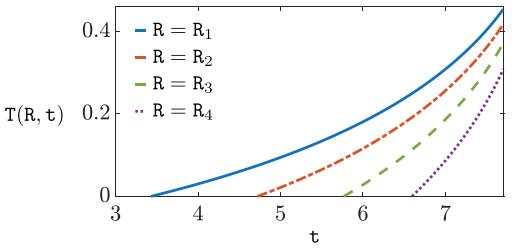

(d) *The time evolution of the temperature field within the solid.*

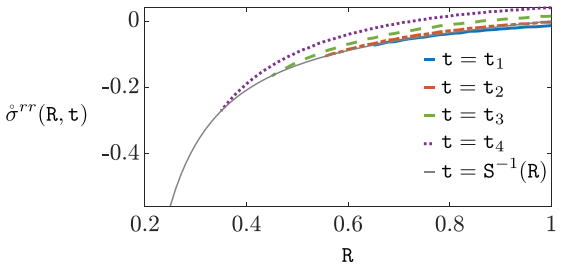

(e) *The dependence of* $\mathring{\sigma}^{rr}$ *on* $\mathtt{R}$ *within the solid.*

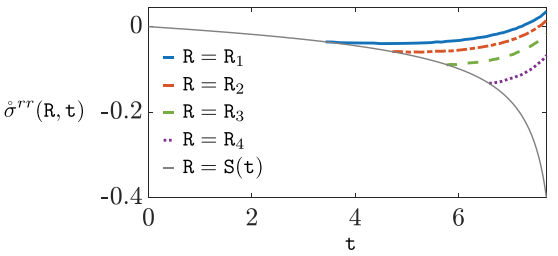

(f) *The time evolution of* $\mathring{\sigma}^{rr}$ *within the solid.*

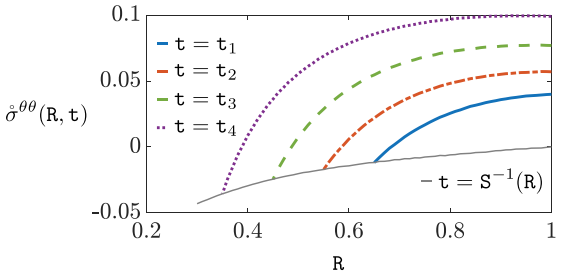

(g) *The dependence of* $\mathring{\sigma}^{\theta\theta}$ *on* $\mathtt{R}$ *within the solid.*

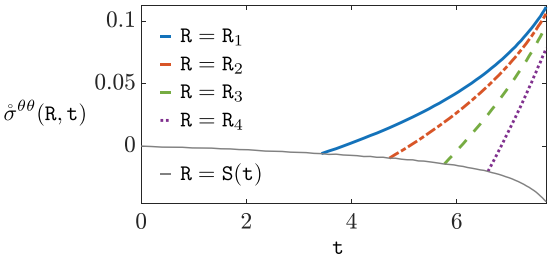

(h) *The time evolution of* $\mathring{\sigma}^{\theta\theta}$ *within the solid.*

Fig. 11. The variation of the radial displacement field $\mathtt{r}(\mathtt{R},\mathtt{t})-\mathtt{R}$, temperature field $\mathtt{T}(\mathtt{R},\mathtt{t})$, and dimensionless physical components $\mathring{\sigma}^{rr}(\mathtt{R},\mathtt{t})$ and $\mathring{\sigma}^{\theta\theta}(\mathtt{R},\mathtt{t})$ of the Cauchy stress inside the accreting solid, with material radial coordinate $\mathtt{R}$ and time $\mathtt{t}$, is depicted. These illustrations are based on the solution of the general problem (4.77)–(4.80), with $\mathtt{f}=0.95$, $\mathtt{a}=0.8$, $\mathtt{b}=0.1$, $\mathtt{p}=1.1$, $\mathtt{q}=1.2$, $\mathtt{h}=0.5$, and $\mathtt{L}=10$. The spatial variation is shown for the instances $\mathtt{t}_1<\mathtt{t}_2<\mathtt{t}_3<\mathtt{t}_4$, corresponding to $\mathtt{S}(\mathtt{t}_1)=0.65$, $\mathtt{S}(\mathtt{t}_2)=0.55$, $\mathtt{S}(\mathtt{t}_3)=0.45$, $\mathtt{S}(\mathtt{t}_4)=0.35$, respectively. Similarly, the temporal evolution is depicted at the radii $\mathtt{R}_1=0.8$, $\mathtt{R}_2=0.7$, $\mathtt{R}_3=0.6$, and $\mathtt{R}_4=0.5$.

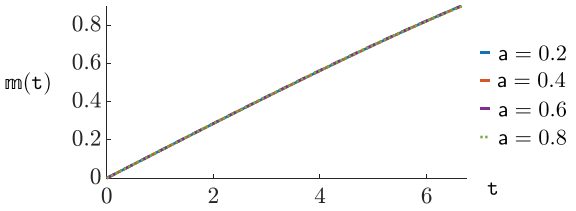

(a) a *is varied, while* f = 0.9, b = 0.25, p = 1.1, q = 1.2, h = 0.5, *and* L = 10.

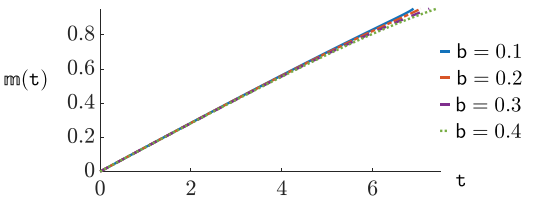

(b) b *is varied, while* f = 0.9, a = 0.5, p = 1.1, q = 1.2, h = 0.5, *and* L = 10.

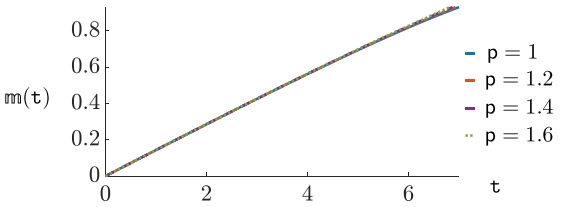

(c) p *is varied, while* f = 0.9, a = 0.8, b = 0.25, q = 1.2, h = 0.5, *and* L = 10.

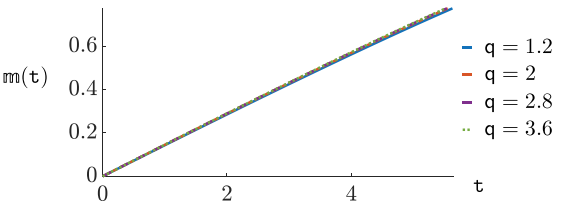

(d) q *is varied, while* f = 0.9, a = 0.8, b = 0.25, p = 1.1, h = 0.5, *and* L = 10.

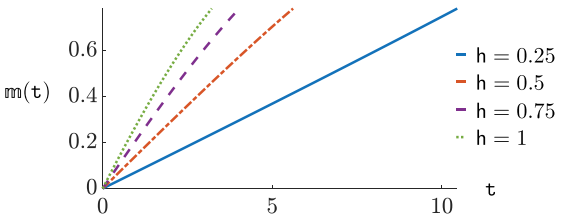

(e) h *is varied, while* f = 0.9, a = 0.8, b = 0.25, p = 1.1, q = 1.2, *and* L = 10.

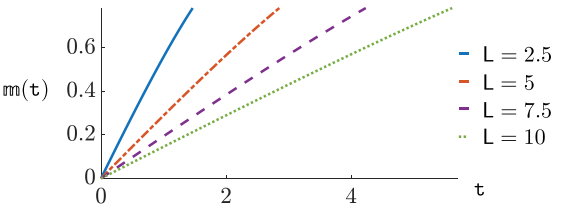

(f) L *is varied, while* f = 0.9, a = 0.8, b = 0.4, p = 1.1, q = 1.2 *and* h = 0.5.

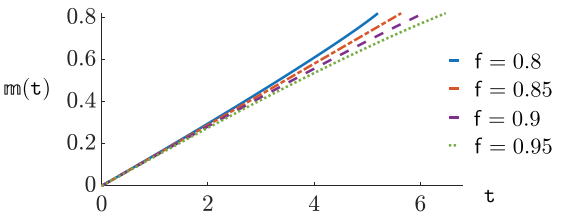

(g) f *is varied, while* a = 0.8, b = 0.25, p = 1.1, q = 1.2, h = 0.5, *and* L = 10.

Fig. 12. The dimensionless parameters f, a, b, p, q, h, and L are varied to investigate their effects on the accretion process. The assessment is based on m(t), which represents the fraction of the initial liquid mass solidified till time t.

5. Conclusions

The study of accretion in elastic bodies, also known as surface growth, has a long history in the mechanics community, with early works like Brown and Goodman (1963) restricted to linear elasticity and small strains. Similarly, the study of solidification dates back to Stefan (1891), and the concepts used in this paper are now well-established in the heat transfer literature.

In recent years, with growing interest in manufacturing techniques such as 3D printing and biological applications like actin polymerization around a rigid bead (Tomassetti et al., 2016; Zurlo and Truskinovsky, 2017), accretion mechanics has gained significant attention from mechanicians. The primary focus has been to study residual stresses, eigenstrains, and their dependence on the history of deformation in a nonlinear setting with finite deformations. Several theories of accretion mechanics have been proposed in the past few years, including the consideration of an accreting sphere as a 4D manifold (with generalization to arbitrary geometries unfeasible) (Tomassetti et al., 2016), the incremental theory of Truskinovsky and Zurlo (2019), and the Eulerian formulation of Naghibzadeh et al. (2021, 2022). Sozio and Yavari (2017, 2019) modeled an accreting solid as a Riemannian manifold,

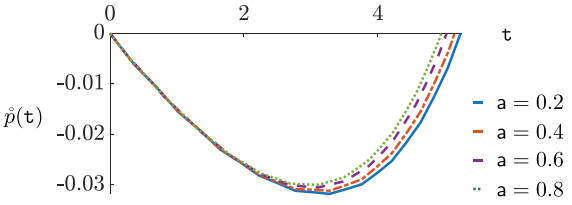

(a) a *is varied, while* f = 0.9, b = 1.5, p = 1.1, q = 1.2, h = 0.5, *and* L = 10.

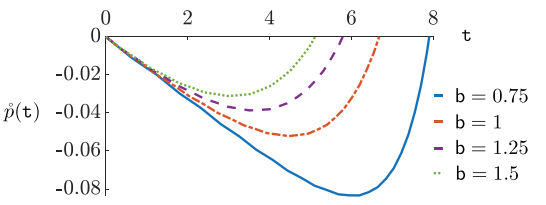

(b) b *is varied, while* f = 0.9, a = 0.5, p = 1.1, q = 1.2, h = 0.5, *and* L = 10.

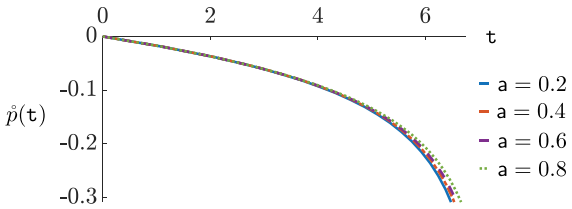

(c) a *is varied, while* f = 0.9, b = 0.25, p = 1.1, q = 1.2, h = 0.5, *and* L = 10.

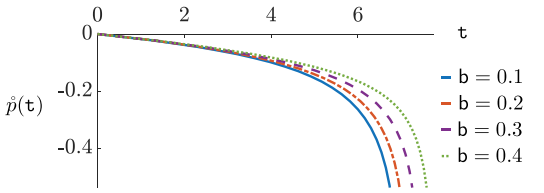

(d) b *is varied, while* f = 0.9, a = 0.5, p = 1.1, q = 1.2, h = 0.5, *and* L = 10.

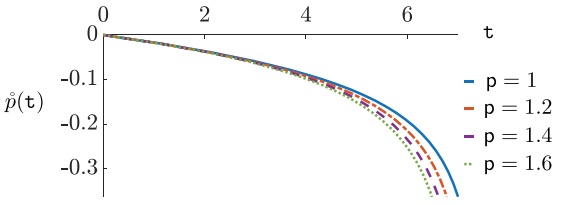

(e) p *is varied, while* f = 0.9, a = 0.8, b = 0.25, q = 1.2, h = 0.5, *and* L = 10.

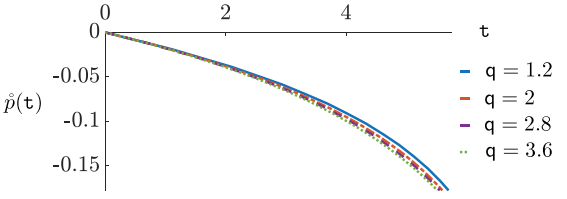

(f) q *is varied, while* f = 0.9, a = 0.8, b = 0.25, p = 1.1, h = 0.5, *and* L = 10.

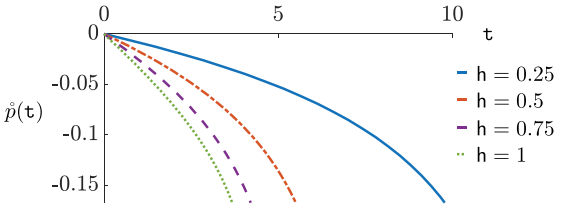

(g) h *is varied, while* f = 0.9, a = 0.8, b = 0.25, p = 1.1, q = 1.2, *and* L = 10.

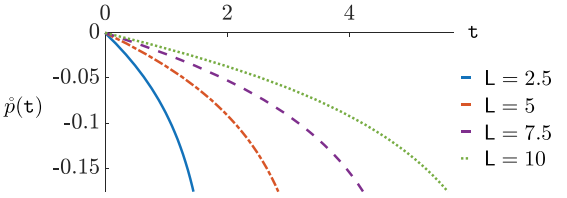

(h) L *is varied, while* f = 0.9, a = 0.8, b = 0.25, p = 1.1, q = 1.2 *and* h = 0.5.

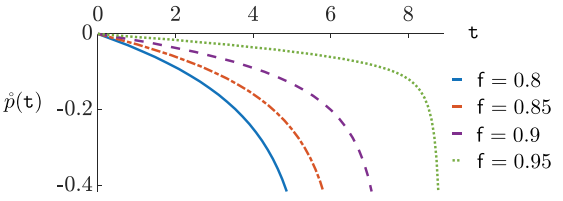

(i) f *is varied, while* a = 0.8, b = 0.25, p = 1.1, q = 1.2, h = 0.5, *and* L = 10.

Fig. 13. The dimensionless parameters f, a, b, p, q, h, and L are varied to investigate their effects on the evolution of pressure inside the liquid.

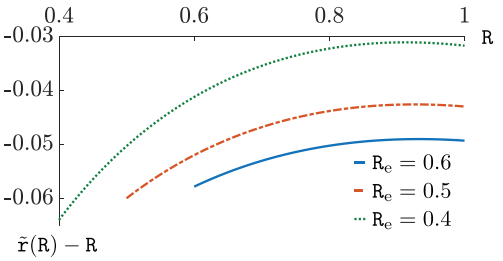

(a) *The displacement of a point in the residually-stressed configuration, relative to its position in the initial unsolidified liquid, is depicted as a function of the dimensionless material coordinate.*

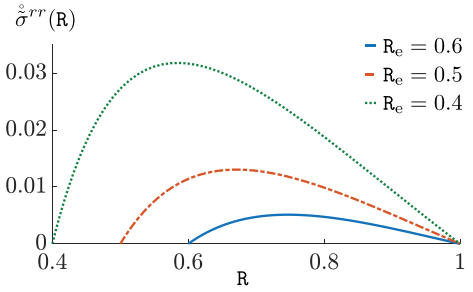

(b) *The dimensionless physical component $\mathring{\tilde{\sigma}}^{rr}$ of the Cauchy stress in the residually-stressed configuration is depicted as a function of the dimensionless material coordinate* R.

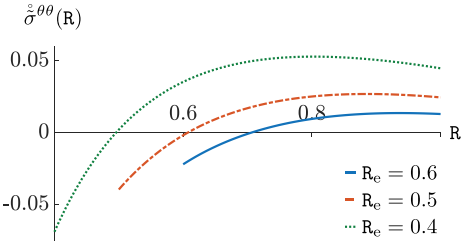

(c) *The dimensionless physical component $\mathring{\tilde{\sigma}}^{\theta\theta}$ of the Cauchy stress in the residually-stressed configuration is depicted as a function of the dimensionless material coordinate* R.

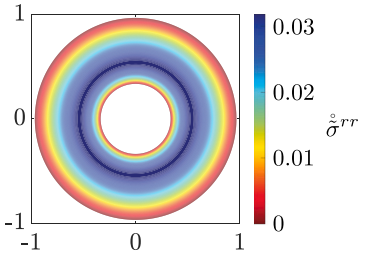

(d) *The residual stress $\mathring{\tilde{\sigma}}^{rr}$ in the body solidified till $R_e = 0.4$ is illustrated as a color plot in the deformed configuration.*

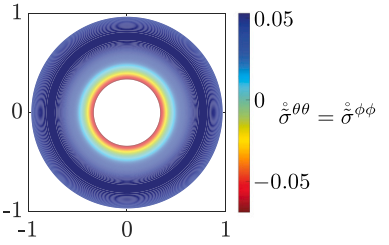

(e) *The residual stress $\mathring{\tilde{\sigma}}^{\theta\theta} = \mathring{\tilde{\sigma}}^{\phi\phi}$ in the body solidified till* $R_e = 0.4$ *is illustrated as a color plot in the deformed configuration.*

Fig. 14. The radial displacement $\tilde{r} - R$ and the physical components $\mathring{\tilde{\sigma}}^{rr}$, $\mathring{\tilde{\sigma}}^{\theta\theta} = \mathring{\tilde{\sigma}}^{\phi\phi}$ of the residual Cauchy stress in a body obtained by accretion till R_e are shown here, after detaching it from the rigid cold walls, emptying the remaining liquid and cooling the accreted portion to a uniform steady-state temperature T_a. These solutions are based on the boundary-value problem (4.111)–(4.112), assuming $f = 0.95$, $a = 0.8$, $b = 0.1$, $p = 1.1$, $q = 1.2$, $h = 0.5$, $L = 10$ and $T_a = 0.5$, post non-dimensionalization. The stopping times corresponding to material locations $R_e = 0.6, 0.5$ and 0.4 of the solidification interface at the end of accretion are $t_e = 5.7663, 6.5943$ and 7.2242, respectively.

avoiding the use of multiplicative decomposition of deformation gradient which is common in modeling anelasticity in biological growth and plasticity.

The present work reflects the culmination of progress by Sozio and Yavari (2017, 2019) and Sozio et al. (2020) in developing the geometric theory of thermoelastic accretion and is capable of calculating residual stress and eigenstrains induced during solidification. The next step was to determine the accretion rate governed by laws of mass and heat transfer, unlike previous works where it was assumed to be given a priori. The distinguishing feature of this geometric theory lies in capturing the effects of thermal expansion and the eigenstrains due to density and elastic property changes during a phase change. Moreover, in contrast to the existing studies with constant growth velocities, this work computes the non-steady movement of the solidification interface, which is controlled through heat extraction by a colder agent. Through a simple example, it is concluded that the radial motion of the interface speeds up as it moves inward, while the rate of mass solidified decreases over time. Solidification in an enclosed cavity induces stress in the liquid, leading to potential cavitation when the solid is denser than the liquid, while less dense solids create compressive stress in the liquid. The solidification rate is most sensitive to how well heat is transferred out of the body and the material's latent heat, and less to the material's elasticity and thermal expansion properties. The residual stresses and distortions

computed in a geometric setting with finite deformations provide insights into zones of significantly high stress, which may lead to cracks, part distortion, and delamination during and after manufacturing. In the example considered, after solidification, residual stresses make the outer surface prone to cracking and the inner layers susceptible to buckling.

The theory formulated in this paper is not the most general. A more general coupled theory would include stress–temperature moduli in the example problems, which were ignored in this work. In the future, a phase-field theory of thermoelastic accretion–ablation should be developed, where the material metric depends on both the phase parameter and temperature. This would better model the mushy transition between phases in certain problems and improve computational aspects in complex geometries. Additionally, at smaller scales with sharp moving interfaces where surface stresses play a significant role, the theory needs to be coupled with the theory of surface elasticity (Gurtin and Ian Murdoch, 1975) for a proper modeling and understanding of the underlying physics.

CRediT authorship contribution statement

Satya Prakash Pradhan: Writing – review & editing, Writing – original draft, Investigation, Formal analysis, Conceptualization. **Arash Yavari:** Writing – review & editing, Writing – original draft, Investigation, Funding acquisition, Formal analysis, Conceptualization.

Data availability

No data was used for the research described in the article.

Acknowledgments

We benefited from discussions with Aditya Kumar and Souhayl Sadik. This work was supported by National Science Foundation, USA – Grant No. CMMI 1939901.

Declaration of competing interest

The authors declare that they have no known competing financial interests or personal relationships that could have appeared to influence the work reported in this paper.

Appendix A. The first and second laws of thermodynamics and the heat equation

In this appendix, we derive the material and spatial heat equations from the laws of thermodynamics.

A.1. Material heat equation

Let $\mathcal{E}(X,t)$, $\Psi(X,t)$ and $\mathcal{N}(X,t)$ be, respectively, the specific internal energy, the specific free energy and the specific entropy in the material configuration. In a class of thermoelasticity theories, deformation gradient is multiplicatively decomposed into elastic and thermal parts: $\mathbf{F}=\overset{e}{\mathbf{F}}\overset{t}{\mathbf{F}}$ (Stojanović et al., 1964; Stojanović, 1969; Lubarda, 2004; Sadik and Yavari, 2017b). Let us denote the induced Euclidean metric on $\mathcal{B}$ by $\mathring{\mathbf{G}}=\mathbf{g}|_{\mathcal{B}}$. Internal energy and free energy explicitly depend on the elastic distortion $\overset{e}{\mathbf{F}}$:

$$\mathcal{E}=\mathcal{E}(X,\mathcal{N},\overset{e}{\mathbf{F}},\mathring{\mathbf{G}},\mathbf{g}),\qquad \Psi=\Psi(X,T,\overset{e}{\mathbf{F}},\mathring{\mathbf{G}},\mathbf{g}). \tag{A.1}$$

Objectivity implies that

$$\mathcal{E}=\hat{\mathcal{E}}(X,\mathcal{N},\overset{e}{\mathbf{C}}{}^{\flat},\mathring{\mathbf{G}}),\qquad \Psi=\hat{\Psi}(X,T,\overset{e}{\mathbf{C}}{}^{\flat},\mathring{\mathbf{G}}), \tag{A.2}$$

where $\overset{e}{\mathbf{C}}{}^{\flat}=\overset{t}{\mathbf{F}}{}^{*}\mathbf{g}=\overset{t}{\mathbf{F}}{}^{\star}\mathbf{g}\overset{t}{\mathbf{F}}$.[54]

Conservation of energy for an arbitrary sub-body $\mathcal{U}\subset\mathcal{B}_t$ is written as[55]

$$\frac{\mathrm{d}}{\mathrm{d}t}\int_{\mathcal{U}}\rho\left(\mathcal{E}+\frac{1}{2}\langle\!\langle\mathbf{V},\mathbf{V}\rangle\!\rangle_{\mathbf{g}}\right)\mathrm{d}V=\int_{\partial\mathcal{U}}\left(\langle\!\langle\mathbf{T},\mathbf{V}\rangle\!\rangle_{\mathbf{g}}-\langle\!\langle\mathbf{H},\mathbf{N}\rangle\!\rangle_{\mathbf{G}}\right)\mathrm{d}A+\int_{\mathcal{U}}\left(\rho\langle\!\langle\mathbf{B},\mathbf{V}\rangle\!\rangle_{\mathbf{g}}+R\right)\mathrm{d}V, \tag{A.3}$$

where $\mathbf{T}(X,t)$ is the traction vector, $\mathbf{B}(X,t)$ is the body force (per unit mass), $R(X,t)$ is a heat source/sink, i.e., $\int_{\mathcal{U}}R\mathrm{d}V$ is the rate at which the heat is generated or absorbed in $\mathcal{U}$, and $\mathbf{G}=\overset{t}{\mathbf{F}}{}^{*}\mathring{\mathbf{G}}$ is the material metric, which explicitly depends on the temperature

[54] One can show that for isotropic solids $\Psi=\hat{\Psi}(X,T,\overset{e}{\mathbf{C}}{}^{\flat},\mathring{\mathbf{G}})=\hat{\Psi}(X,T,\mathbf{C}^{\flat},\mathbf{G})$ (Yavari and Sozio, 2023). In the case of anisotropic solids, a similar identity holds, provided that structural tensors are included as arguments of the free energy.

[55] A term $\rho\frac{\partial\mathcal{E}}{\partial\mathbf{G}}:\frac{\partial\mathbf{G}}{\partial t}$ was included in the energy balance in Sadik and Yavari (2017a). It turns out that this term should not appear on the right-hand side of the energy balance, as it would lead to an incorrect heat equation. A detailed discussion of energy balance in the presence of eigenstrains will be given in Sadik and Yavari (2024).

field, c.f., (2.11) (Sadik and Yavari, 2017a; Yavari, 2010). Using (3.3), (3.17) and the fact that $\mathbf{P}\mathbf{N}^\flat = \mathbf{T}$ on $\partial\mathcal{U}$, (A.3) can be localized to read[56]

$$\rho\,\dot{\mathcal{E}} = \mathbf{S} : \mathbf{D} - \mathrm{Div}_{\mathbf{G}}\,\mathbf{H} + R\,, \tag{A.4}$$

where $\mathbf{S} = \mathbf{P}\mathbf{F}^\star$ is the second Piola–Kirchhoff stress and $\mathbf{D} = \frac{1}{2}\dot{\mathbf{C}}^\flat$. The localized Clausius–Duhem inequality reads

$$\rho\,\dot{\mathcal{N}} + \mathrm{Div}_{\mathbf{G}}\Big(\frac{\mathbf{H}}{T}\Big) - \frac{R}{T} \geq 0\,, \tag{A.5}$$

which can be rewritten in terms of the rate of energy dissipation as

$$\dot{\eta} = \rho T\dot{\mathcal{N}} + \mathrm{Div}_{\mathbf{G}}\,\mathbf{H} - \frac{1}{T}\langle \mathrm{d}T, \mathbf{H}\rangle - R \geq 0\,. \tag{A.6}$$

Note that $\mathbf{C}^\flat = \varphi^*\mathbf{g} = (\overset{e}{\mathbf{F}}\overset{t}{\mathbf{F}})^\star\mathbf{g}\,\overset{e}{\mathbf{F}}\overset{t}{\mathbf{F}} = \overset{t}{\mathbf{F}}{}^\star\overset{e}{\mathbf{F}}{}^\star\mathbf{g}\,\overset{e}{\mathbf{F}}\overset{t}{\mathbf{F}} = \overset{t}{\mathbf{F}}{}^\star\overset{e}{\mathbf{C}}{}^\flat\overset{t}{\mathbf{F}} = \overset{t}{\mathbf{F}}{}^*\overset{e}{\mathbf{C}}{}^\flat$. We assume an isotropic material, which is materially covariant[57] (Marsden and Hughes, 1983).[58] Thus

$$\hat{\Psi}(X, T, \overset{e}{\mathbf{C}}{}^\flat, \overset{e}{\mathbf{G}}) = \hat{\Psi}(X, T, \overset{t}{\mathbf{F}}{}^*\overset{e}{\mathbf{C}}{}^\flat, \overset{t}{\mathbf{F}}{}^*\overset{e}{\mathbf{G}}) = \hat{\Psi}(X, T, \mathbf{C}^\flat, \mathbf{G})\,, \tag{A.7}$$

where $\mathbf{G} = \overset{t}{\mathbf{F}}{}^*\overset{e}{\mathbf{G}}\overset{t}{\mathbf{F}}$ is the material metric. Therefore

$$\dot{\Psi} = \frac{\partial\hat{\Psi}}{\partial T}\dot{T} + \frac{\partial\hat{\Psi}}{\partial\mathbf{C}^\flat} : \dot{\mathbf{C}}^\flat + \frac{\partial\hat{\Psi}}{\partial\mathbf{G}} : \dot{\mathbf{G}} = \frac{d\hat{\Psi}}{dT}\dot{T} + \frac{\partial\hat{\Psi}}{\partial\mathbf{C}^\flat} : \dot{\mathbf{C}}^\flat\,, \tag{A.8}$$

where

$$\frac{d\hat{\Psi}}{dT} = \frac{\partial\hat{\Psi}}{\partial T} + \frac{\partial\hat{\Psi}}{\partial\mathbf{G}} : \frac{\partial\mathbf{G}}{\partial T}\,. \tag{A.9}$$

Recall that free energy, internal energy, entropy and temperature are related as

$$\mathcal{E} = \Psi + T\mathcal{N}\,. \tag{A.10}$$

Notice that $\mathcal{E} = \hat{\mathcal{E}}(X, \mathcal{N}, \mathbf{C}^\flat, \mathbf{G})$, $\Psi = \hat{\Psi}(X, T, \mathbf{C}^\flat, \mathbf{G})$, and $\mathcal{N} = \hat{\mathcal{N}}(X, \mathbf{C}^\flat, \mathbf{G})$. Taking partial derivatives of both sides with respect to T, one obtains

$$0 = \frac{\partial\Psi}{\partial T} + \mathcal{N}\,, \tag{A.11}$$

and hence

$$\mathcal{N} = -\frac{\partial\Psi}{\partial T}\,. \tag{A.12}$$

From (A.10), $\rho T\dot{\mathcal{N}} = \rho\dot{\mathcal{E}} - \rho\dot{T}\mathcal{N} - \rho\dot{\Psi}$. Substituting this relation and (A.4) into (A.6), the rate of energy dissipation is simplified to read

$$\dot{\eta} = \mathbf{S} : \mathbf{D} - \rho\dot{T}\mathcal{N} - \rho\dot{\Psi} - \frac{1}{T}\langle \mathrm{d}T, \mathbf{H}\rangle \geq 0\,. \tag{A.13}$$

Using (A.8) the energy dissipation rate is further simplified as

$$\dot{\eta} = \frac{1}{2}\left[\mathbf{S} - \rho\frac{\partial\hat{\Psi}}{\partial\mathbf{C}^\flat}\right] : \dot{\mathbf{C}}^\flat - \rho\dot{T}\left[\mathcal{N} + \frac{d\hat{\Psi}}{dT}\right] - \frac{1}{T}\langle \mathrm{d}T, \mathbf{H}\rangle = \left[\mathbf{S} - 2\rho\frac{\partial\hat{\Psi}}{\partial\mathbf{C}^\flat}\right] : \mathbf{D} - \rho\frac{\partial\hat{\Psi}}{\partial\mathbf{G}} : \frac{\partial\mathbf{G}}{\partial T}\,\dot{T} - \frac{1}{T}\langle \mathrm{d}T, \mathbf{H}\rangle \geq 0\,, \tag{A.14}$$

where (A.12) was used in the second equality. Thus

$$\mathbf{S} = 2\rho\frac{\partial\hat{\Psi}}{\partial\mathbf{C}^\flat}\,, \qquad \dot{\eta} = -\rho\frac{\partial\hat{\Psi}}{\partial\mathbf{G}} : \frac{\partial\mathbf{G}}{\partial T}\,\dot{T} - \frac{1}{T}\langle \mathrm{d}T, \mathbf{H}\rangle \geq 0\,. \tag{A.15}$$

From (A.10), $\rho\,\dot{\mathcal{E}} = \rho\dot{\Psi} + \rho\dot{T}\mathcal{N} + T\rho\,\dot{\mathcal{N}} = \mathbf{S} : \mathbf{D} + \rho T\dot{\mathcal{N}}$. Substituting this back into the energy balance equation (A.4), one obtains

$$\rho T\dot{\mathcal{N}} + \rho\,\dot{T}\,\frac{\partial\hat{\Psi}}{\partial\mathbf{G}} : \frac{\partial\mathbf{G}}{\partial T} = \rho R - \mathrm{Div}_{\mathbf{G}}\,\mathbf{H}\,. \tag{A.16}$$

Using (A.12), one writes

$$\dot{\mathcal{N}} = -\dot{T}\,\frac{d}{dT}\frac{\partial\hat{\Psi}}{\partial T} - \frac{\partial^2\hat{\Psi}}{\partial\mathbf{C}^\flat\partial T} : \dot{\mathbf{C}}^\flat\,. \tag{A.17}$$

Thus, (A.16) is written as

$$\rho\left[-T\,\frac{d}{dT}\frac{\partial\hat{\Psi}}{\partial T} + \frac{\partial\hat{\Psi}}{\partial\mathbf{G}} : \frac{\partial\mathbf{G}}{\partial T}\right]\dot{T} - \rho T\,\frac{\partial^2\hat{\Psi}}{\partial\mathbf{C}^\flat\partial T} : \dot{\mathbf{C}}^\flat = \rho R - \mathrm{Div}_{\mathbf{G}}\,\mathbf{H}\,. \tag{A.18}$$

[56] In components, $\mathbf{S} : \mathbf{D} = S^{AB}\,D_{AB}$.

[57] Let us consider an arbitrary material (referential) diffeomorphism $\Xi : \mathcal{B} \to \mathcal{B}$ such that $\Xi(X) = X$. A free energy function $\hat{\Psi}(X, T, \overset{e}{\mathbf{C}}{}^\flat, \overset{e}{\mathbf{G}})$ is materially covariant if it is invariant under Ξ, i.e., $\hat{\Psi}(X, T, \Xi_*\overset{e}{\mathbf{C}}{}^\flat, \Xi_*\overset{e}{\mathbf{G}}) = \hat{\Psi}(X, T, \overset{e}{\mathbf{C}}{}^\flat, \overset{e}{\mathbf{G}})$.

[58] Extension of this analysis to anisotropic solids involves including structural tensors as arguments of the free energy (Yavari and Sozio, 2023). In this paper, we restrict our analysis to isotropic materials.

Note that

$$-T\frac{d}{dT}\frac{\partial\hat{\Psi}}{\partial T}+\frac{\partial\hat{\Psi}}{\partial\mathbf{G}}:\frac{\partial\mathbf{G}}{\partial T}=-T\frac{d^2\hat{\Psi}}{dT^2}+T\frac{d}{dT}\left[\frac{\partial\hat{\Psi}}{\partial\mathbf{G}}:\frac{\partial\mathbf{G}}{\partial T}\right]+\frac{\partial\hat{\Psi}}{\partial\mathbf{G}}:\frac{\partial\mathbf{G}}{\partial T}=-T\frac{d^2\hat{\Psi}}{dT^2}+\frac{d}{dT}\left[T\frac{\partial\hat{\Psi}}{\partial\mathbf{G}}:\frac{\partial\mathbf{G}}{\partial T}\right]. \tag{A.19}$$

Hence, (A.18) is simplified to read

$$\rho\left\{-T\frac{d^2\hat{\Psi}}{dT^2}+\frac{d}{dT}\left[T\frac{\partial\hat{\Psi}}{\partial\mathbf{G}}:\frac{\partial\mathbf{G}}{\partial T}\right]\right\}\dot{T}+\mathrm{Div}_{\mathbf{G}}\,\mathbf{H}=\rho R+\rho T\frac{\partial^2\hat{\Psi}}{\partial\mathbf{C}^\flat\partial T}:\dot{\mathbf{C}}^\flat. \tag{A.20}$$

Therefore, the heat equation is written as

$$\rho\,C_E\,\dot{T}+\mathrm{Div}_{\mathbf{G}}\,\mathbf{H}=R+T\,\mathbf{M}:\mathbf{D}, \tag{A.21}$$

where the specific heat capacity per unit mass at constant strain C_E and the referential thermal stress coefficient tensor $\mathbf{M}$ are given as

$$C_E=-T\frac{d^2\hat{\Psi}}{dT^2}+\frac{d}{dT}\left[T\frac{\partial\hat{\Psi}}{\partial\mathbf{G}}:\frac{\partial\mathbf{G}}{\partial T}\right],\qquad \mathbf{M}=2\rho\frac{\partial^2\hat{\Psi}}{\partial\mathbf{C}^\flat\partial T}. \tag{A.22}$$

Here, the $\binom{2}{0}$-tensor $\mathbf{M}$ is also referred to as the stress–temperature moduli (Marsden and Hughes, 1983; Truesdell and Noll, 2004; Holzapfel, 2002; Gurtin et al., 2010).

A.2. Spatial heat equation

We next derive the spatial heat equation using the material heat equation (A.21). Let $\psi(x,t)$ represent the specific free energy in the current configuration, with the corresponding constitutive response function denoted as $\psi(x,t)=\hat{\psi}(x,\mathcal{T},\mathbf{g},\mathbf{c}^\flat)$. Since $\varphi_t(X)=x$, it follows that $\psi_t\circ\varphi_t=\Psi_t$. Moreover, the spatial and material response functions are related as

$$\hat{\psi}(x,\mathcal{T},\mathbf{g},\mathbf{c}^\flat)=\hat{\Psi}\left(\varphi_t^{-1}(x),\varphi_t{}^*\mathcal{T},\varphi_t{}^*\mathbf{g},\varphi_t{}^*\mathbf{c}^\flat\right). \tag{A.23}$$

Note that

$$\frac{d\hat{\psi}}{d\mathcal{T}}=\frac{\partial\hat{\psi}}{\partial\mathcal{T}}+\frac{\partial\hat{\psi}}{\partial\mathbf{c}^\flat}:\frac{\partial\mathbf{c}^\flat}{\partial\mathcal{T}}. \tag{A.24}$$

The specific heat capacity at constant strain c_E and the spatial thermal stress coefficient $\mathbf{m}$ in the current configuration are defined as

$$c_E=-T\frac{d^2\hat{\psi}}{d\mathcal{T}^2}+\frac{d}{d\mathcal{T}}\left[\mathcal{T}\frac{\partial\hat{\psi}}{\partial\mathbf{c}^\flat}:\frac{\partial\mathbf{c}^\flat}{\partial\mathcal{T}}\right],\qquad \mathbf{m}=2\rho\frac{\partial^2\hat{\psi}}{\partial\mathbf{g}\,\partial\mathcal{T}}. \tag{A.25}$$

Notice that $c_E=C_E$.[59] Further, since

$$\frac{\partial^2\hat{\psi}}{\partial g_{ab}\partial\mathcal{T}}=\frac{\partial C_{AB}}{\partial g_{ab}}\frac{\partial^2\hat{\Psi}}{\partial C_{AB}\partial T}=F^a{}_AF^b{}_B\frac{\partial^2\hat{\Psi}}{\partial C_{AB}\partial T}, \tag{A.26}$$

the spatial and material thermal stress coefficients are related as

$$J\,m^{ab}=2J\rho\frac{\partial^2\hat{\psi}}{\partial g_{ab}\partial\mathcal{T}}=2\rho\,F^a{}_AF^b{}_B\frac{\partial^2\hat{\Psi}}{\partial C_{AB}\partial T}=F^a{}_AF^b{}_BM^{AB}. \tag{A.27}$$

Thus, $\mathbf{m}$ and $\mathbf{M}$ are related as $\mathbf{M}=J\varphi_t{}^*\mathbf{m}$. Observe that[60]

$$\mathbf{M}:\mathbf{D}=J\,\mathbf{m}:\mathbf{d}, \tag{A.30}$$

where $\mathbf{d}=\frac{1}{2}\pounds_{\mathbf{v}}\mathbf{g}$ is the Lie derivative of the spatial metric along the spatial velocity. Let $\mathcal{U}\subset\mathcal{B}_t$ ($\mathcal{U}\cap\partial\mathcal{B}_t=\emptyset$) and $\mathcal{P}_t=\varphi_t(\mathcal{U})$. Notice that $\partial\mathcal{P}_t=\varphi_t(\partial\mathcal{U})$. Using the divergence theorem in the deformed and the material manifolds, one has

$$\int_{\mathcal{P}_t}\mathrm{div}_{\mathbf{g}}\,\mathbf{h}\,\mathrm{d}v=\int_{\partial\mathcal{P}_t}\langle\!\langle\mathbf{h},\mathbf{n}\rangle\!\rangle_{\mathbf{g}}\mathrm{d}a,\quad\text{and}\qquad\int_{\partial\mathcal{U}}\langle\!\langle\mathbf{H},\mathbf{N}\rangle\!\rangle_{\mathbf{G}}\mathrm{d}A=\int_{\mathcal{U}}\mathrm{Div}_{\mathbf{G}}\,\mathbf{H}\,\mathrm{d}V. \tag{A.31}$$

Further, by the change of variables formula

$$\int_{\partial\mathcal{P}_t}\langle\!\langle\mathbf{h},\mathbf{n}\rangle\!\rangle_{\mathbf{g}}\mathrm{d}a=\int_{\partial\mathcal{U}}\langle\!\langle\mathbf{H},\mathbf{N}\rangle\!\rangle_{\mathbf{G}}\mathrm{d}A. \tag{A.32}$$

---

[59] This is implied using $\frac{\partial\hat{\psi}}{\partial\mathcal{T}}=\frac{\partial\hat{\Psi}}{\partial T}$, $\frac{d\hat{\psi}}{d\mathcal{T}}=\frac{d\hat{\Psi}}{dT}$ and $\frac{\partial\hat{\psi}}{\partial\mathbf{c}^\flat}:\frac{\partial\mathbf{c}^\flat}{\partial\mathcal{T}}=\frac{\partial\hat{\Psi}}{\partial\mathbf{G}}:\frac{\partial\mathbf{G}}{\partial T}$.

[60] The components of $\dot{\mathbf{C}}^\flat$ read

$$\dot{C}_{AB}=F^a{}_AF^b{}_B\frac{\partial g_{ab}}{\partial x^c}V^c+g_{ab}\left[\frac{\partial V^b}{\partial X^B}F^a{}_A+\frac{\partial V^a}{\partial X^A}F^b{}_B\right]=g_{ab}\left[V^b{}_{|B}F^a{}_A+V^a{}_{|A}F^b{}_B\right], \tag{A.28}$$

and the components of $\pounds_{\mathbf{v}}\mathbf{g}$ are written as $(\pounds_{\mathbf{v}}\mathbf{g})_{ab}=g_{ac}v^c{}_{|b}+g_{cb}v^c{}_{|a}$. Since $V^a{}_{|B}=v^a{}_{|b}F^b{}_B$, the components of $\mathbf{D}=\frac{1}{2}\dot{\mathbf{C}}^\flat$ and $\mathbf{d}=\frac{1}{2}\pounds_{\mathbf{v}}\mathbf{g}$ can be related as

$$D_{AB}=d_{ab}\,F^a{}_AF^b{}_B, \tag{A.29}$$

i.e., $\mathbf{D}=\varphi_t^*\mathbf{d}$. Thus, (A.26) and (A.29) imply that $M^{AB}D_{AB}=J\,m^{ab}\,d_{ab}$.

Hence, it is implied from (3.1), (A.30), (A.31), (A.21) and (A.32) that[61]

$$\int_{\mathcal{P}_t} \left[\rho\, c_E \dot{\mathcal{T}} + \mathrm{div}_{\mathbf{g}}\, \mathbf{h} - \mathcal{T}\mathbf{m} : \mathbf{d} - r\right] \mathrm{d}v = \int_{\mathcal{U}} \left[\rho\, C_E \dot{T} + \mathrm{Div}_{\mathbf{G}}\, \mathbf{H} - T\mathbf{M} : \mathbf{D} - R\right] \mathrm{d}V = 0\,, \tag{A.34}$$

which holds for an arbitrary sub-body $\mathcal{P}_t$. Therefore, the localized spatial heat equation reads

$$\rho\, c_E \dot{\mathcal{T}} + \mathrm{div}_{\mathbf{g}}\, \mathbf{h} = \mathcal{T}\mathbf{m} : \mathbf{d} + r\,. \tag{A.35}$$

Notice that $\dot{(\,)} = \frac{\partial}{\partial t}\big|_X (\,)$ represents the material time derivative.

Appendix B. A constitutive model for thermoelastic solids

We consider the following constitutive model for thermoelastic solids

$$\check{\Psi}_{\mathrm{s}}(I_1, J, T) = \left[\frac{\mu_0^{\mathrm{s}}}{2}(J^{-\frac{2}{3}} I_1 - 3) + \frac{\kappa_0^{\mathrm{s}}}{2}(J-1)^2\right] \frac{T}{T_0^{\mathrm{s}}} - \kappa_0^{\mathrm{s}}\, \beta_0^{\mathrm{s}}\, (J-1)(T - T_0^{\mathrm{s}}) - \rho \int_{T_0^{\mathrm{s}}}^{T} \frac{T-\tau}{\tau} c_E(\tau)\, \mathrm{d}\tau\,. \tag{B.1}$$

Here, μ_0^{s}, κ_0^{s}, and β_0^{s} represent the shear modulus, bulk modulus, and volumetric thermal expansion coefficient of the solid at the reference temperature T_0^{s} (Ogden, 1992; Holzapfel and Simo, 1996; Sadik and Yavari, 2017a).[62] The shear and the bulk moduli are assumed to evolve linearly with temperature, i.e.,

$$\mu^{\mathrm{s}}(T) = \frac{\mu_0^{\mathrm{s}} T}{T_0^{\mathrm{s}}}\,, \qquad \kappa^{\mathrm{s}}(T) = \frac{\kappa_0^{\mathrm{s}} T}{T_0^{\mathrm{s}}}\,. \tag{B.2}$$

Consider a homogeneous body initially at a uniform temperature T_0, which, when changed to another uniform temperature T_1, undergoes a stress-free volumetric deformation in the process. The state of stress for a purely volumetric deformation is quantified by $\sigma = \frac{1}{3}\,\mathrm{tr}\,\boldsymbol{\sigma} = \frac{\partial \check{\Psi}_{\mathrm{s}}}{\partial J}$. Therefore, one has $\frac{\partial \check{\Psi}_{\mathrm{s}}}{\partial J} = \kappa_0^{\mathrm{s}}$, and hence it follows that

$$J = 1 + \beta_0^{\mathrm{s}} T_0^{\mathrm{s}} \left[1 - \frac{T_0^{\mathrm{s}}}{T}\right]\,. \tag{B.3}$$

Further, since the Jacobian in such a process is $J = e^{\beta^{\mathrm{s}}(T)}$, it is implied that

$$e^{3\omega^{\mathrm{s}}(T)} = 1 + \beta_0^{\mathrm{s}} T_0^{\mathrm{s}} \left[1 - \frac{T_0^{\mathrm{s}}}{T}\right]\,. \tag{B.4}$$

Thus, the coefficient of thermal expansion at temperature T is written as

$$\beta^{\mathrm{s}}(T) = \frac{\beta_0^{\mathrm{s}} \left[\frac{T_0^{\mathrm{s}}}{T}\right]^2}{1 + \beta_0^{\mathrm{s}} T_0^{\mathrm{s}} \left[1 - \frac{T_0^{\mathrm{s}}}{T}\right]}\,, \tag{B.5}$$

where the relation $\beta^{\mathrm{s}} = 3\frac{\mathrm{d}\omega^{\mathrm{s}}}{\mathrm{d}T}$ has been used. We shall use this model in our numerical examples. For more details, see Sadik and Yavari (2017a).

Appendix C. Christoffel symbols of the spatial and material metrics

The nonzero Christoffel symbols for the spatial metric $\mathbf{g}$ (4.1) read

$$\gamma^r_{\theta\theta} = -r\,, \qquad \gamma^r_{\phi\phi} = -r\sin^2\theta\,, \qquad \gamma^\theta_{r\theta} = \gamma^\phi_{r\phi} = \frac{1}{r}\,, \qquad \gamma^\theta_{\phi\phi} = -\sin\theta\cos\theta\,, \qquad \gamma^\phi_{\phi\theta} = \cot\theta\,. \tag{C.1}$$

The nonzero Christoffel symbols for the material metric $\overset{\mathcal{L}}{\mathbf{G}}$ given in (4.5) are listed as

$$\begin{aligned} &\mathring{\Gamma}^R_{RR} = \alpha^{\mathrm{f}} T_{,R}\,, \qquad \mathring{\Gamma}^R_{\Theta\Theta} = -\left[\alpha^{\mathrm{f}} T_{,R} + \frac{1}{R}\right] R^2\,, \qquad \mathring{\Gamma}^R_{\Phi\Phi} = -\left[\alpha^{\mathrm{f}} T_{,R} + \frac{1}{R}\right] R^2 \sin^2\Theta\,, \\ &\mathring{\Gamma}^\Theta_{R\Theta} = \mathring{\Gamma}^\Phi_{R\Phi} = \alpha^{\mathrm{f}} T_{,R} + \frac{1}{R}\,, \qquad \mathring{\Gamma}^\Theta_{\Phi\Phi} = -\sin\Theta\cos\Theta\,, \qquad \mathring{\Gamma}^\Phi_{\Phi\Theta} = \cot\Theta\,, \end{aligned} \tag{C.2}$$

[61] Here,

$$\int_{\mathcal{P}_t} h^b{}_{|b}\, \mathrm{d}v = \int_{\partial\mathcal{P}_t} h^b n_b\, \mathrm{d}a = \int_{\partial\mathcal{U}} H^B N_B\, \mathrm{d}A = \int_{\mathcal{U}} H^B{}_{|B}\, \mathrm{d}V\,, \tag{A.33}$$

and $\int_{\mathcal{U}} R\mathrm{d}V = \int_{\mathcal{P}_t} r\mathrm{d}v$.

[62] Recall that, in the thermally accreted part of the body, $T_0(X)$ represents the temperature during accretion, while in the initial body, it denotes the initial temperature.

where $\alpha^{\mathrm{f}}(T)=\frac{\mathrm{d}\omega^{\mathrm{f}}(T)}{\mathrm{d}T}$. Here we have used the notation $(\cdot)'\,:=\,\frac{\mathrm{d}}{\mathrm{d}R}(\cdot)$. Similarly, the nonzero Christoffel symbols for the material metric $\overset{\mathcal{B}}{\mathbf{G}}$ given in (4.18) are

$$\begin{aligned}
&\Gamma^{R}_{RR}=\alpha^{\mathrm{s}}\,T_{,R}+\frac{\varsigma'}{\varsigma}\,,\qquad \Gamma^{R}_{\Theta\Theta}=-\left[\alpha^{\mathrm{s}}\,T_{,R}+\frac{\bar{r}'}{\bar{r}}\right]\frac{\bar{r}^2}{\varsigma^2}\,,\qquad \Gamma^{R}_{\Phi\Phi}=-\left[\alpha^{\mathrm{s}}\,T_{,R}+\frac{\bar{r}'}{\bar{r}}\right]\frac{\bar{r}^2}{\varsigma^2}\sin^2\Theta\,,\\
&\Gamma^{\Theta}_{R\Theta}=\Gamma^{\Phi}_{R\Phi}=\alpha^{\mathrm{s}}\,T_{,R}+\frac{\bar{r}'}{\bar{r}}\,,\qquad \Gamma^{\Theta}_{\Phi\Phi}=-\sin\Theta\cos\Theta\,,\qquad \Gamma^{\Phi}_{\Phi\Theta}=\cot\Theta\,,
\end{aligned}\tag{C.3}$$

where $\alpha^{\mathrm{s}}(T)=\frac{\mathrm{d}\omega^{\mathrm{s}}(T)}{\mathrm{d}T}$ and $\varsigma(R)=\frac{\bar{u}(R)\eta^2(R)}{\bar{U}(R)}$.

Appendix D. Constitutive equations for hyperelastic fluids

The constitutive equation of an elastic fluid explicitly depends only on the mass density (Truesdell and Noll, 2004; Gurtin et al., 2010). The specific free energy function $\psi(X,T,\mathbf{F},\mathbf{G},\mathbf{g})$ for hyperelastic fluids can be expressed as a function of $J=\sqrt{\frac{\det\mathbf{g}}{\det\mathbf{G}}}\det\mathbf{F}$[63] (Wang and Truesdell, 1973, p. 198), such that $\psi(X,T,\mathbf{F},\mathbf{G},\mathbf{g})=\hat{\psi}(X,T,J)$. Using this function, the Cauchy, the first and the second Piola–Kirchhoff stress tensors can be expressed as

$$\boldsymbol{\sigma}=-\hat{p}\,\mathbf{g}^{\sharp}\,,\qquad \mathbf{P}=-J\hat{p}\,\mathbf{g}^{\sharp}\mathbf{F}^{-\star}\,,\qquad \mathbf{S}=J\hat{p}\,\mathbf{F}^{-1}\mathbf{g}^{\sharp}\mathbf{F}^{-\star}\,,\tag{D.3}$$

where $\hat{p}=-\frac{\partial\hat{\psi}}{\partial J}$. Since hydrostatic stresses are compressive in fluids, one must have $\frac{\partial\hat{\psi}}{\partial J}<0$. Note that

$$(\mathrm{div}_{\mathbf{g}}\,\boldsymbol{\sigma})^{a}=-\left(\hat{p}\,g^{ab}\right)_{|b}=-g^{ab}\frac{\partial\hat{p}}{\partial x^{b}}=\left[\frac{\partial^2\hat{\psi}}{\partial J^2}\frac{\partial J}{\partial x^{b}}+\frac{\partial^2\hat{\psi}}{\partial J\partial T}\frac{\partial T}{\partial x^{b}}+\frac{\partial^2\hat{\psi}}{\partial X^{A}\partial J}(F^{-1})^{A}{}_{b}\right]g^{ab}\,.\tag{D.4}$$

For homogeneous fluids, $\hat{\psi}$ is independent of X, and hence, the term $\frac{\partial^2\hat{\psi}}{\partial X^{A}\partial J}$ vanishes. In the absence of any heat flow, one can simply work with the smooth and strictly convex free energy function $\breve{W}(J)$, with the property that $\lim_{J\to0^{+}}\breve{W}=+\infty$. The Cauchy, the first, and the second Piola–Kirchhoff stress tensors are calculated using this free energy function $\breve{W}$ as per the formulae described in (3.15). Since $(\mathrm{div}_{\mathbf{g}}\,\boldsymbol{\sigma})^{a}=\breve{W}''(J)\frac{\partial J}{\partial x^{b}}\,g^{ab}$, the balance of linear momentum reads

$$\breve{W}''(J)\frac{\partial J}{\partial x^{b}}\,g^{bc}+f^{c}=a^{c}\,,\tag{D.5}$$

where $\breve{W}''=\frac{\mathrm{d}^2\breve{W}}{\mathrm{d}J^2}$. Moreover, in the absence of inertial and body forces, one can assume that $\breve{W}''(J)>0$. Thus, one concludes that $\frac{\partial J}{\partial x^{b}}=0$. Hence, in the absence of body and inertial forces, $J=J(t)$ in homogeneous fluids at constant temperature (Podio-Guidugli et al., 1985). For example, Ghosh and Lopez-Pamies (2022) considered the following free energy function for hyperelastic liquid inclusions

$$\breve{W}(X,J)=J\eta(X)+\frac{\kappa}{2}[J-1]^2\,.\tag{D.6}$$

It is implied that $\boldsymbol{\sigma}=\left[\eta+\kappa(J-1)\right]\mathbf{g}^{\sharp}$.[64] Here, $\eta(X)$ represents the pressure in the undeformed liquid (which is not necessarily zero) while the bulk modulus κ quantifies compressibility.

In the fluid mechanics literature, a compressible hyperelastic fluid is analogous to an unconstrained elastic fluid, which is characterized by the constitutive relation $\boldsymbol{\sigma}=-\mathcal{P}(\varrho)\,\mathbf{g}^{\sharp}$. It is known by several other names, such as, Euler fluid, ideal compressible fluid, perfect compressible fluid, inviscid compressible fluid, and barotropic fluid (Truesdell and Rajagopal, 2000, p. 44).

---

[63] In the literature of continuum mechanics, it is common to write $J=\det\mathbf{F}$, which is incorrect unless the physical components of the deformation gradient are used. For vectors $\mathbf{W}=W^{A}\frac{\partial}{\partial X^{A}}\in T_{X}\mathcal{B}$ and $\mathbf{w}=w^{a}\frac{\partial}{\partial x^{a}}\in T_{x}\mathcal{S}$, the physical components are defined as $\hat{w}^{a}=\sqrt{g_{aa}}\,w^{a}$ (no summation on a) and $\hat{W}^{A}=\sqrt{G_{AA}}\,W^{A}$ (no summation on A) (Truesdell, 1953). The physical components of deformation gradient $\hat{F}^{a}{}_{A}$ are defined such that $\hat{w}^{a}=\hat{F}^{a}{}_{A}\,\hat{W}^{A}$. This implies that $\hat{F}^{a}{}_{A}=\sqrt{g_{aa}}\,\frac{1}{\sqrt{G_{AA}}}\,F^{a}{}_{A}$ (no summation). In a coordinate chart $\{X^{A}\}$ the Riemannian material volume element is written as $\boldsymbol{\mu}_{\mathbf{G}}=\sqrt{\det\mathbf{G}}\;dX^{1}\wedge dX^{2}\wedge dX^{3}$. Similarly, the Riemannian volume element in the current configuration with respect to a coordinate chart $\{x^{a}\}$ has the following coordinate representation: $\boldsymbol{\mu}_{\mathbf{g}}=\sqrt{\det\mathbf{g}}\;dx^{1}\wedge dx^{2}\wedge dx^{3}$. The Jacobian relates the deformed and undeformed Riemannian volume forms as $\varphi^{*}\boldsymbol{\mu}_{\mathbf{g}}=J\,\boldsymbol{\mu}_{\mathbf{G}}$. Note that $\varphi^{*}(dx^{1}\wedge dx^{2}\wedge dx^{3})=\det\mathbf{F}\,dX^{1}\wedge dX^{2}\wedge dX^{3}$. Thus

$$\varphi^{*}\boldsymbol{\mu}_{\mathbf{g}}=\sqrt{\det\mathbf{g}}\;\varphi^{*}(dx^{1}\wedge dx^{2}\wedge dx^{3})=\sqrt{\det\mathbf{g}}\;\det\mathbf{F}\,dX^{1}\wedge dX^{2}\wedge dX^{3}=J\;\sqrt{\det\mathbf{G}}\;dX^{1}\wedge dX^{2}\wedge dX^{3}\,.\tag{D.1}$$

Hence, $J=\sqrt{\frac{\det\mathbf{g}}{\det\mathbf{G}}}\det\mathbf{F}$. Using the explicit form of the physical deformation gradient

$$\hat{\mathbf{F}}=\begin{bmatrix}\frac{\sqrt{g_{11}}}{\sqrt{G_{11}}}F^{1}{}_{1} & \frac{\sqrt{g_{11}}}{\sqrt{G_{22}}}F^{1}{}_{2} & \frac{\sqrt{g_{11}}}{\sqrt{G_{33}}}F^{1}{}_{3}\\ \frac{\sqrt{g_{22}}}{\sqrt{G_{11}}}F^{2}{}_{1} & \frac{\sqrt{g_{22}}}{\sqrt{G_{22}}}F^{2}{}_{2} & \frac{\sqrt{g_{22}}}{\sqrt{G_{33}}}F^{2}{}_{3}\\ \frac{\sqrt{g_{33}}}{\sqrt{G_{11}}}F^{3}{}_{1} & \frac{\sqrt{g_{33}}}{\sqrt{G_{22}}}F^{3}{}_{2} & \frac{\sqrt{g_{33}}}{\sqrt{G_{33}}}F^{3}{}_{3}\end{bmatrix},\tag{D.2}$$

we see that $\det\hat{\mathbf{F}}=\frac{\sqrt{g_{11}g_{22}g_{33}}}{\sqrt{G_{11}G_{22}G_{33}}}\det\mathbf{F}$. If $\{X^{A}\}$ and $\{x^{a}\}$ are orthogonal curvilinear coordinates, e.g., cylindrical and spherical coordinates, $\sqrt{g_{11}g_{22}g_{33}}=\det\mathbf{g}$ and $\sqrt{G_{11}G_{22}G_{33}}=\det\mathbf{G}$, and hence $J=\det\hat{\mathbf{F}}$.

[64] A similar constitutive relation for thermoelastic fluids has been proposed in (Ateshian and Shim, 2022).

References

Abeyaratne, R., Knowles, J.K., 1993. A continuum model of a thermoelastic solid capable of undergoing phase transitions. J. Mech. Phys. Solids 41 (3), 541–571.

Abeyaratne, R., Puntel, E., Recrosi, F., Tomassetti, G., 2022a. Surface accretion of a pre-stretched half-space: Biot's problem revisited. J. Mech. Phys. Solids 167, 104958.

Abeyaratne, R., Puntel, E., Tomassetti, G., 2022b. On the stability of surface growth: The effect of a compliant surrounding medium. J. Elasticity 1–25.

Ateshian, G.A., Shim, J.J., 2022. Continuum thermodynamics of the phase transformation of thermoelastic fluids. arXiv preprint arXiv:2207.14158.

Bachmann, J., Obst, P., Knorr, L., Schmölzer, S., Fruhmann, G., Witt, G., Osswald, T., Wudy, K., Hinrichsen, O., 2021. Cavity vat photopolymerisation for additive manufacturing of polymer-composite 3D objects. Commun. Mater. 2 (1), 107.

Bažant, Z.P., Hauggaard, A.B., Baweja, S., Ulm, F.-J., 1997. Microprestress-solidification theory for concrete creep. I: Aging and drying effects. J. Eng. Mech. 123 (11), 1188–1194.

Bico, J., Reyssat, É., Roman, B., 2018. Elastocapillarity: When surface tension deforms elastic solids. Annu. Rev. Fluid Mech. 50, 629–659.

Binder, K., 1987. Theory of first-order phase transitions. Rep. Progr. Phys. 50 (7), 783.

Brown, C., Goodman, L., 1963. Gravitational stresses in accreted bodies. In: Proceedings of the Royal Society of London A, Vol. 276, No. 1367. The Royal Society, pp. 571–576.

Budak, B., Vasil'ev, F., Uspenskii, A., 1965. Difference methods for solving certain boundary value problems of stefan type. Chislennye metody v gazovoi dinamike 139–183.

Buffett, B.A., Huppert, H.E., Lister, J.R., Woods, A.W., 1992. Analytical model for solidification of the earth's core. Nature 356 (6367), 329–331.

Buffett, B.A., Huppert, H.E., Lister, J.R., Woods, A.W., 1996. On the thermal evolution of the earth's core. J. Geophys. Res. Solid Earth 101 (B4), 7989–8006.

Buffett, B.A., Mathews, P., Herring, T., Shapiro, I., 1993. Forced nutations of the earth: contributions prom the effects of ellipticity and rotation on the elastic deformations. J. Geophys. Res. Solid Earth 98 (B12), 21659–21676.

Camacho, C., Neto, A.L., 2013. Geometric Theory of Foliations. Springer Science & Business Media.

Carslaw, H., Jaeger, J., 1959. Conduction of Heat in Solids. Clarendon Press, Oxford.

Chambre, P., 1956. On the dynamics of phase growth. Quart. J. Mech. Appl. Math. 9 (2), 224–233.

Chan, C., Tan, F., 2006. Solidification inside a sphere—An experimental study. Int. Commun. Heat Mass Transfer 33 (3), 335–341.

Coleman, B.D., Noll, W., 1963. The thermodynamics of elastic materials with heat conduction and viscosity. Arch. Ration. Mech. Anal. 13 (1), 167–178.

Coussy, O., 2005. Poromechanics of freezing materials. J. Mech. Phys. Solids 53 (8), 1689–1718.

Crank, J., 1984. Free and Moving Boundary Problems. Oxford University Press.

Crank, J., Gupta, R.S., 1972. A moving boundary problem arising from the diffusion of oxygen in absorbing tissue. IMA J. Appl. Math. 10 (1), 19–33.

Danilyuk, I.I., 1985. On the stefan problem. Russian Math. Surveys 40 (5), 157.

DebRoy, T., Wei, H., Zuback, J., Mukherjee, T., Elmer, J., Milewski, J., Beese, A.M., Wilson-Heid, A.d., De, A., Zhang, W., 2018. Additive manufacturing of metallic components–process, structure and properties. Prog. Mater. Sci. 92, 112–224.

Deore, B., Sampson, K.L., Lacelle, T., Kredentser, N., Lefebvre, J., Young, L.S., Hyland, J., Amaya, R.E., Tanha, J., Malenfant, P.R., et al., 2021. Direct printing of functional 3D objects using polymerization-induced phase separation. Nature Commun. 12 (1), 55.

Douglas, J., 1957. A uniqueness theorem for the solution of a stefan problem. Proc. Amer. Math. Soc. 8 (2), 402–408.

Douglas, Jr., J., Gallie, Jr., T., 1955. On the numerical integration of a parabolic differential equation subject to a moving boundary condition. Duke Math. J. 22, 557–571.

Doyle, T.C., Ericksen, J.L., 1956. Nonlinear elasticity. Adv. Appl. Mech. 4, 53–115.

Eckart, C., 1948. The thermodynamics of irreversible processes. IV. The theory of elasticity and anelasticity. Phys. Rev. 73 (4), 373–382.

Elahinia, M., Moghaddam, N.S., Andani, M.T., Amerinatanzi, A., Bimber, B.A., Hamilton, R.F., 2016. Fabrication of NiTi through additive manufacturing: A review. Prog. Mater. Sci. 83, 630–663.

Epstein, M., 2010. Kinetics of boundary growth. Mech. Res. Commun. 37 (5), 453–457.

Evans, G.W., et al., 1951. A note on the existence of a solution to a problem of stefan. Quart. Appl. Math. 9 (2), 185–193.

Fasano, A., Primicerio, M., 1979. Free boundary problems for nonlinear parabolic equations with nonlinear free boundary conditions. J. Math. Anal. Appl. 72 (1), 247–273.

Fedosejevs, C.S., Schneider, M.F., 2022. Sharp, localized phase transitions in single neuronal cells. Proc. Natl. Acad. Sci. 119 (8), e2117521119.

Fekry, M., 2023. Thermal stresses in growing thermoviscoelastic cylinder and their evolution in the course of selective laser melting processing. Z. Ang. Math. Mech. 103 (2), e202100519.

Ganghoffer, J.-F., Goda, I., 2018. A combined accretion and surface growth model in the framework of irreversible thermodynamics. Internat. J. Engrg. Sci. 127, 53–79.

Ghosh, K., Lopez-Pamies, O., 2022. Elastomers filled with liquid inclusions: Theory, numerical implementation, and some basic results. J. Mech. Phys. Solids 166, 104930.

Gough, J., 1805. A description of a property of caoutchouc, or Indian rubber. Memor. Literacy Philos. Soc. Manchester 1, 288–295.

Gupta, S.C., 2017. The Classical Stefan Problem: Basic Concepts, Modelling and Analysis with Quasi-Analytical Solutions and Methods, vol. 45, Elsevier.

Gurtin, M.E., Fried, E., Anand, L., 2010. The Mechanics and Thermodynamics of Continua. Cambridge University Press.

Gurtin, M.E., Ian Murdoch, A., 1975. A continuum theory of elastic material surfaces. Arch. Rational Mech. Anal. 57, 291–323.

Heinlein, M., Mukherjee, S., Richmond, O., 1986. A boundary element method analysis of temperature fields and stresses during solidification. Acta Mech. 59 (1–2), 59–81.

Hill, J.M., Kucera, A., 1983. Freezing a saturated liquid inside a sphere. Int. J. Heat Mass Transfer 26 (11), 1631–1637.

Hodge, N., Papadopoulos, P., 2010. A continuum theory of surface growth. Proc. R. Soc. A: Math. Phys. Eng. Sci. 466 (2123), 3135–3152.

Holzapfel, G.A., 2002. Nonlinear Solid Mechanics: A Continuum Approach for Engineering Science. Kluwer Academic Publishers Dordrecht.

Holzapfel, G.A., Simo, J., 1996. Entropy elasticity of isotropic rubber-like solids at finite strains. Comput. Methods Appl. Mech. Engrg. 132 (1–2), 17–44.

Horvay, G., 1962. Freezing into an undercooled melt accompanied by density change. In: Proc. of the 4 US National Congres of Appl. Mech., Univ. California. pp. 1315–1325.

Isayev, A., Crouthamel, D., 1984. Residual stress development in the injection molding of polymers. Polym.-Plast. Technol. Eng. 22 (2), 177–232.

Jaeger, G., 1998. The ehrenfest classification of phase transitions: Introduction and evolution. Arch. Hist. Exact Sci. 53, 51–81.

Jiang, H., Wang, S., Huang, Y., He, X., Cui, H., Zhu, X., Zheng, Y., 2015. Phase transition of spindle-associated protein regulate spindle apparatus assembly. Cell 163 (1), 108–122.

Joule, J.P., 1859. On some thermo-dynamic properties of solids. Philos. Trans. R. Soc. Lond. (149), 91–131.

Klingbeil, N.W., Beuth, J.L., Chin, R., Amon, C., 2002. Residual stress-induced warping in direct metal solid freeform fabrication. Int. J. Mech. Sci. 44 (1), 57–77.

Kondo, K., 1949. A proposal of a new theory concerning the yielding of materials based on Riemannian geometry. J. Japan Soc. Aeronaut. Eng. 2 (8), 29–31.

Kou, S., 2015. A criterion for cracking during solidification. Acta Mater. 88, 366–374.

Kumar, A., Dean, L.M., Yourdkhani, M., Guo, A., BenVau, C., Sottos, N.R., Geubelle, P.H., 2022. Surface pattern formation induced by oscillatory loading of frontally polymerized gels. J. Mech. Phys. Solids 168, 105055.

Kumar, A., Gao, Y., Geubelle, P.H., 2021. Analytical estimates of front velocity in the frontal polymerization of thermoset polymers and composites. J. Polym. Sci. 59 (11), 1109–1118.
Labrosse, S., Hernlund, J., Coltice, N., 2007. A crystallizing dense magma ocean at the base of the earth's mantle. Nature 450 (7171), 866–869.
Labrosse, S., Poirier, J.-P., Le Mouël, J.-L., 1997. On cooling of the earth's core. Phys. Earth Planet. Inter. 99 (1–2), 1–17.
Lamé, G., Clapeyron, B., 1831. Mémoire sur la solidification par refroidissement d'un globe liquide. In: Ann. Chimie Phys.. 47, (1831), pp. 250–256.
Landau, L., 1936. The theory of phase transitions. Nature 138 (3498), 840–841.
Li, X., Cohen, T., 2024. Mechanical forces quench frontal polymerization: Experiments and theory. J. Mech. Phys. Solids 183, 105517.
London, A., Seban, R., 1943. Rate of ice formation. Trans. Am. Soc. Mech. Eng. 65 (7), 771–778.
Lotkin, M., 1960. The calculation of heat flow in melting solids. Quart. Appl. Math. 18 (1), 79–85.
Lubarda, V.A., 2004. Constitutive theories based on the multiplicative decomposition of deformation gradient: Thermoelasticity, elastoplasticity, and biomechanics. Appl. Mech. Rev. 57 (2), 95–108.
Lychev, S.A., Fekry, M., 2023a. Evaluation of residual stresses in additively produced thermoelastic cylinder. Part I. Thermal fields. Mech. Adv. Mater. Struct. 30 (10), 1975–1990.
Lychev, S.A., Fekry, M., 2023b. Evaluation of residual stresses in additively produced thermoelastic cylinder. Part II. Residual stresses. Mech. Adv. Mater. Struct. 30 (10), 1991–2000.
Marsden, J., Hughes, T., 1983. Mathematical Foundations of Elasticity. Dover.
Mazur, P., 1970. Cryobiology: The freezing of biological systems: The responses of living cells to ice formation are of theoretical interest and practical concern. Science 168 (3934), 939–949.
McCue, S.W., King, J.R., Riley, D.S., 2003. Extinction behaviour for two–dimensional inward-solidification problems. Proc. R. Soc. London A 459 (2032), 977–999.
Melamed, V., 1958. Reduction of the stefan problem to a system of ordinary differential equations. Izv. Ac. Sci. USSR, Geophys, Set (7), 848–869.
Mercelis, P., Kruth, J.-P., 2006. Residual stresses in selective laser sintering and selective laser melting. Rapid Prototyp. J. 12 (5), 254–265.
Mukherjee, T., Manvatkar, V., De, A., DebRoy, T., 2017a. Mitigation of thermal distortion during additive manufacturing. Scr. Mater. 127, 79–83.
Mukherjee, T., Zhang, W., DebRoy, T., 2017b. An improved prediction of residual stresses and distortion in additive manufacturing. Comput. Mater. Sci. 126, 360–372.
Naghibzadeh, S.K., Walkington, N., Dayal, K., 2021. Surface growth in deformable solids using an Eulerian formulation. J. Mech. Phys. Solids 154, 104499.
Naghibzadeh, S.K., Walkington, N., Dayal, K., 2022. Accretion and ablation in deformable solids with an Eulerian description: Examples using the method of characteristics. Math. Mech. Solids 27 (6), 989–1010.
Ogden, R., 1992. On the thermoelastic modeling of rubberlike solids. J. Therm. Stresses 15 (4), 533–557.
Oleĭnik, O.A., 1960. A method of solution of the general stefan problem. In: Doklady Akademii Nauk, vol. 135, (no. 5), Russian Academy of Sciences, pp. 1054–1057.
O'Neill, K., 1983. Boundary integral equation solution of moving boundary phase change problems. Internat. J. Numer. Methods Engrg. 19 (12), 1825–1850.
Ozakin, A., Yavari, A., 2010. A geometric theory of thermal stresses. J. Math. Phys. 51, 032902.
Pedroso, R., Domoto, G., 1973a. Inward spherical solidification—solution by the method of strained coordinates. Int. J. Heat Mass Transfer 16 (5), 1037–1043.
Pedroso, R., Domoto, G., 1973b. State of stress during solidification with varying freezing pressure and temperature. J. Eng. Mater. Technol. 95 (4), 227–232.
Pielichowska, K., Pielichowski, K., 2014. Phase change materials for thermal energy storage. Prog. Mater. Sci. 65, 67–123.
Podio-Guidugli, P., Vergara Caffarelli, G., Virga, E., 1985. Cavitation and phase transition of hyperelastic fluids. In: Analysis and Thermomechanics: A Collection of Papers Dedicated To W. Noll on His Sixtieth Birthday. Springer, pp. 401–416.
Pradhan, S.P., Yavari, A., 2023. Accretion-ablation mechanics. Phil. Trans. R. Soc. A 20220373.
Rabin, Y., Steif, P., 1998. Thermal stresses in a freezing sphere and its application to cryobiology. J. Appl. Mech. 65 (2), 328–333.
Rejovitzky, E., Di Leo, C.V., Anand, L., 2015. A theory and a simulation capability for the growth of a solid electrolyte interphase layer at an anode particle in a li-ion battery. J. Mech. Phys. Solids 78, 210–230.
Richmond, O., Tien, R., 1971. Theory of thermal stresses and air-gap formation during the early stages of solidification in a rectangular mold. J. Mech. Phys. Solids 19 (5), 273–284.
Riley, D., Smith, F., Poots, G., 1974. The inward solidification of spheres and circular cylinders. Int. J. Heat Mass Transfer 17 (12), 1507–1516.
Rongved, L., 1954. Residual stress in glass spheres. (Ph.D. thesis). Columbia University..
Rubinsky, B., Cravalho, E.G., Mikic, B., 1980. Thermal stresses in frozen organs. Cryobiology 17 (1), 66–73.
Rubinstein, L., 1947. On the solution of stefan's problem. Bull. Acad. Sci. URSS. Sér. Géograph. Géophys.(Izvestia Akad. Nauk SSSR) 11, 37–54.
Rubinšteĭn, L., 1971. The Stefan Problem. American Mathematical Soc..
Rubinstein, L., 1979. The stefan problem: Comments on its present state. IMA J. Appl. Math. 24 (3), 259–277.
Sadik, S., Yavari, A., 2017a. Geometric nonlinear thermoelasticity and the time evolution of thermal stresses. Math. Mech. Solids 22 (7), 1546–1587.
Sadik, S., Yavari, A., 2017b. On the origins of the idea of the multiplicative decomposition of the deformation gradient. Math. Mech. Solids 22 (4), 771–772.
Sadik, S., Yavari, A., 2024. Nonlinear visco-anelasticity.
Shao, G., Hanaor, D.A., Shen, X., Gurlo, A., 2020. Freeze casting: From low-dimensional building blocks to aligned porous structures—a review of novel materials, methods, and applications. Adv. Mater. 32 (17), 1907176.
Shih, Y.-P., Chou, T.-C., 1971. Analytical solutions for freezing a saturated liquid inside or outside spheres. Chem. Eng. Sci. 26 (11), 1787–1793.
Simo, J., Marsden, J., 1984. Stress tensors, Riemannian metrics and the alternative descriptions in elasticity. In: Trends and Applications of Pure Mathematics To Mechanics. Springer, pp. 369–383.
Smith, A., Burns, J., Xiong, D., Dahn, J., 2011. Interpreting high precision coulometry results on li-ion cells. J. Electrochem. Soc. 158 (10), A1136.
Soward, A., 1980. A unified approach to stefan's problem for spheres and cylinders. Proc. R. Soc. London A 373 (1752), 131–147.
Sozio, F., Faghih Shojaei, M., Sadik, S., Yavari, A., 2020. Nonlinear mechanics of thermoelastic accretion. Z. Ang. Math. Phys. 71, 1–24.
Sozio, F., Yavari, A., 2017. Nonlinear mechanics of surface growth for cylindrical and spherical elastic bodies. J. Mech. Phys. Solids 98, 12–48.
Sozio, F., Yavari, A., 2019. Nonlinear mechanics of accretion. J. Nonlinear Sci. 29 (4), 1813–1863.
Stanley, H.E., 1971. Phase Transitions and Critical Phenomena, vol. 7, Clarendon Press, Oxford.
Stefan, J., 1891. Über die theorie der eisbildung, insbesondere über die eisbildung im polarmeere. Ann. Phys., Lpz. 278 (2), 269–286.
Stewartson, K., Waechter, R., 1976. On stefan's problem for spheres. Proc. R. Soc. London A 348 (1655), 415–426.
Stojanović, R., 1969. On the stress relation in non-linear thermoelasticity. Int. J. Non-Linear Mech. 4 (3), 217–233.
Stojanović, R., Djurić, S., Vujošević, L., 1964. On finite thermal deformations. Arch. Mech. Stosow. 1 (16), 103–108.
Tao, L.C., 1967. Generalized numerical solutions of freezing a saturated liquid in cylinders and spheres. AIChE J. 13 (1), 165–169.
Tien, R., Koump, V., 1969. Thermal stresses during solidification on basis of elastic model. J. Appl. Mech. 36 (4), 763–767.
Tomassetti, G., Cohen, T., Abeyaratne, R., 2016. Steady accretion of an elastic body on a hard spherical surface and the notion of a four-dimensional reference space. J. Mech. Phys. Solids 96, 333–352.
Truesdell, C., 1953. The physical components of vectors and tensors. Z. Ang. Math. Mech. 33 (10–11), 345–356.
Truesdell, C., Noll, W., 2004. In: Antman, S. (Ed.), The Non-Linear Field Theories of Mechanics, third ed. Springer.
Truesdell, C., Rajagopal, K.R., 2000. An Introduction to the Mechanics of Fluids. Springer Science & Business Media.
Truskinovsky, L., Zurlo, G., 2019. Nonlinear elasticity of incompatible surface growth. Phys. Rev. E 99 (5), 053001.

Visintin, A., 2008. Introduction to stefan-type problems. Handbook Differ. Equ. Evolut. Equ. 4, 377–484.
Vuik, C., 1993. Some historical notes about the Stefan problem. Delft University of Technology, Faculty of Technical Mathematics and Informatics.
Wang, C.-C., Truesdell, C., 1973. Introduction to Rational Elasticity, vol. 1, Springer Science & Business Media.
Weiner, J., Boley, B., 1963. Elasto-plastic thermal stresses in a solidifying body. J. Mech. Phys. Solids 11 (3), 145–154.
Withers, P.J., Bhadeshia, H., 2001a. Residual stress. Part 1–measurement techniques. Mater. Sci. Technol. 17 (4), 355–365.
Withers, P.J., Bhadeshia, H., 2001b. Residual stress. Part 2–nature and origins. Mater. Sci. Technol. 17 (4), 366–375.
Wuttig, M., Bhaskaran, H., Taubner, T., 2017. Phase-change materials for non-volatile photonic applications. Nat. Photonics 11 (8), 465–476.
Yang, W., Zhiwei, J., 2009. Injection moulding of polymers. Adv. Polymer Process. 175–203.
Yavari, A., 2010. A geometric theory of growth mechanics. J. Nonlinear Sci. 20 (6), 781–830.
Yavari, A., Marsden, J.E., Ortiz, M., 2006. On spatial and material covariant balance laws in elasticity. J. Math. Phys. 47 (4).
Yavari, A., Pradhan, S.P., 2022. Accretion mechanics of nonlinear elastic circular cylindrical bars under finite torsion. J. Elasticity 1–32.
Yavari, A., Safa, Y., Soleiman Fallah, A., 2023. Finite extension of accreting nonlinear elastic solid circular cylinders. Contin. Mech. Thermodyn. 1–17.
Yavari, A., Sozio, F., 2023. On the direct and reverse multiplicative decompositions of deformation gradient in nonlinear anisotropic anelasticity. J. Mech. Phys. Solids 170, 105101.
Zabaras, N., Mukherjee, S., 1987. An analysis of solidification problems by the boundary element method. Internat. J. Numer. Methods Engrg. 24 (10), 1879–1900.
Zabaras, N., Ruan, Y., Richmond, O., 1990. Front tracking thermomechanical model for hypoelastic-viscoplastic behavior in a solidifying body. Comput. Methods Appl. Mech. Engrg. 81 (3), 333–364.
Zabaras, N., Ruan, Y., Richmond, O., 1991. On the calculation of deformations and stresses during axially symmetric solidification. J. Appl. Mech. 58 (4), 865–871.
Zarek, M., Layani, M., Cooperstein, I., Sachyani, E., Cohn, D., Magdassi, S., 2016. 3D printing of shape memory polymers for flexible electronic devices. Adv. Mater. 28 (22), 4449–4454.
Zurlo, G., Truskinovsky, L., 2017. Printing non-euclidean solids. Phys. Rev. Lett. 119 (4), 048001.
Zurlo, G., Truskinovsky, L., 2018. Inelastic surface growth. Mech. Res. Commun. 93, 174–179.